AFAPL-TR-70-79
Volume I

THREE-DIMENSIONAL NOZZLE DESIGN FOR MAXIMUM THRUST

VOLUME I. THEORETICAL DEVELOPMENT AND RESULTS

Lynn E. Snyder and H. Doyle Thompson

FOREWORD

The present study is part of the program "An Analytical Study of the Exhaust Expansion System (Scramjet Scientific Technology)" being conducted by the Jet Propulsion Center, Purdue University, under United States Air Force Contract No. F33615-67-C-1068, BPSN 7(63 301206 6205214). The Air Force program monitor was Lt. Gary J. Jungwirth of the Air Force Aero Propulsion Laboratory. This report presents a procedure for designing three-dimensional nozzles for maximum thrust.

The work of Dr. Victor H. Ransom and Professors H. Doyle Thompson and Joe D. Hoffman in developing a computer program for analysis of three-dimensional supersonic flow fields is acknowledged. Stimulating discussions of the problem with Professor Hoffman and Drs. Ransom and Gearold R. Johnson at the Jet Propulsion Center, Purdue University are also acknowledged.

This report was submitted by the authors on 28 October 1970.

Gary J. Jungwirth
1st Lt., USAF
Project Engineer
Ramjet Technology Branch
Ramjet Engine Division
AF Aero Propulsion Laboratory

ABSTRACT

The problem of designing three-dimensional (nonaxisymmetric) supersonic nozzles which produce the maximum axial thrust for a prescribed upstream flow field, mass flow rate, exit lip shape and position, and ambient pressure has been formulated and numerically solved. The formulation was written to consider a three-dimensional, supersonic, isoenergetic, homentropic flow of a perfect gas. The axial thrust and mass flow rate were written as integrals over a control surface which was constrained to pass through the exit lip of the nozzle. The functional to be maximized was formed by summing the integral equation for the axial thrust and the integral equation for the mass flow rate times a Lagrange multiplier. The fixed length and fixed ambient pressure constraints were imposed by substitution into the variational problem.

The set of partial differential equations and the algebraic equations which resulted from setting the first variation of the functional equal to zero were numerically solved. For a particular set of initial conditions the numerical solution technique generates the characteristic surface which passes through the exit of the resulting optimal nozzle, the position of the exit lip, the magnitude of the axial thrust, and the ambient pressure for which the nozzle is an optimal.

The numerical solution technique was programmed for the CDC 6500 computer. The results for nine sample cases are presented. The results confirm that the three-dimensional optimal nozzles designed using this technique are significantly better than other three-dimensional nozzles that have identical initial conditions and have comparable overall dimensions. Furthermore, the results show that two-dimensional or axisymmetric methods are not adequate for designing three-dimensional optimum nozzles.

TABLE OF CONTENTS

	Page
SECTION I. INTRODUCTION	1
1. Introductory Remarks	1
2. State of the Art Evaluation	2
3. Scope and Method of Approach	6
SECTION II. THEORETICAL DEVELOPMENT	9
1. Formulation of the Optimization Problem	12
a. Geometrical Relationships	12
b. Gas Dynamic Model	13
c. Functional to be Maximized	14
2. Derivation of the Optimization Equations	17
a. Application of the Calculus of Variations	17
b. Equations Which Define Optimal Control Surfaces	20
c. Transversality Equation	22
d. Corner Line Conditions	26
3. Compatibility of the Control Surface and the Kernel	28
4. Special Case of Axisymmetric Flow	28
SECTION III. NUMERICAL DEVELOPMENT	30
1. Three-Dimensional Kernel Region	31
2. Initial Value Line	32
3. Control Surface	34
4. Nozzle Exit Lip	37
SECTION IV. RESULTS	39
1. Introduction	39
2. Case A	41
a. Optimal Nozzle 1	41
b. Optimal Nozzle 2	43
c. Optimal Nozzle 3	45
3. Case B	45
a. Optimal Nozzle 4	45
b. Optimal Nozzle 5	46
c. Optimal Nozzle 6	46
4. Case C	46
a. Optimal Nozzle 7	47
b. Optimal Nozzle 8	47
c. Optimal Nozzle 9	47

Page

SECTION V. SUMMARY 72

APPENDIX A: DERIVATION OF GEOMETRICAL RELATIONSHIPS. 74

APPENDIX B: DYNAMICS AND THERMODYNAMICS OF THE FLOW. 81

APPENDIX C: DERIVATION OF THE INTEGRAL THRUST AND MASS FLOW RATE EQUATIONS 86

APPENDIX D: APPLICATION OF THE CALCULUS OF VARIATIONS. 91

APPENDIX E: DERIVATION OF THE EQUATIONS FOR AN OPTIMAL CONTROL SURFACE. 96

APPENDIX F: DERIVATION OF THE TRANSVERSALITY EQUATION. 104

APPENDIX G: DERIVATION OF THE CORNER LINE CONDITIONS 112

APPENDIX H: PROOF THAT THE OPTIMAL CONTROL SURFACES ARE WAVE SURFACES. 115

APPENDIX I: THE AXISYMMETRIC SOLUTION. 125

APPENDIX J: DETAILS OF THE CONSTRUCTION OF INITIAL VALUE LINES . 133

APPENDIX K: DETAILS OF THE CONSTRUCTION OF OPTIMAL CONTROL SURFACES 141

APPENDIX L: DETAILS OF THE CONSTRUCTION OF OPTIMAL NOZZLE EXIT LIPS. 155

LIST OF REFERENCES. 161

LIST OF ILLUSTRATIONS

Figure		Page
1.	Axisymmetric Nozzle Geometry	3
2.	Three-Dimensional Nozzle Geometry	10
3.	Extremal Surface	18
4.	Control Surface Projection on the r,ϕ-Plane	24
5.	Plane of Symmetry Views of Optimal Nozzle 1	48
6.	Initial Value Line for Optimal Nozzle 1	49
7.	Control Surface for Optimal Nozzle 1	50
8.	Exit Lip for Optimal Nozzle 1	51
9.	Projection on the r,ϕ-Plane of Optimal Nozzle 1	52
10.	Summary for Optimal Nozzle 1	53
11.	Plane of Symmetry Views of Optimal Nozzle 2	54
12.	Initial Value Line for Optimal Nozzle 2	55
13.	Control Surface for Optimal Nozzle 2	56
14.	Exit Lip for Optimal Nozzle 2	57
15.	Projection on the r,ϕ-Plane of Optimal Nozzle 2	58
16.	Summary for Optimal Nozzle 2	59
17.	Plane of Symmetry Views of Optimal Nozzle 3	60
18.	Initial Value Line for Optimal Nozzle 3	61
19.	Control Surface for Optimal Nozzle 3	62
20.	Exit Lip for Optimal Nozzle 3	63
21.	Projection on the r,ϕ-Plane of Optimal Nozzle 3	64

Figure Page

22. Summary for Optimal Nozzle 3 65

23. Summary for Optimal Nozzle 4 66

24. Summary for Optimal Nozzle 5 67

25. Summary for Optimal Nozzle 6 68

26. Summary for Optimal Nozzle 7 69

27. Summary for Optimal Nozzle 8 70

28. Summary for Optimal Nozzle 9 71

Appendix
Figures

29. Three-Dimensional Nozzle 75

30. Unit Vector Normal to the Control Surface. 77

31. Velocity Vector. 79

32. Control Surface. 87

33. Extremal Surface 92

34. Control Surface Projection on the r,ϕ-Plane. 106

35. Annular Surface for Deriving Transversality Equation 110

36. Characteristic Surfaces. 117

37. Coordinate System for Wave Surfaces. 119

38. Axisymmetric Nozzle Geometry 129

39. Lines of Constant λ_2 137

40. Initial Value Line 140

41. Mesh Point Network 148

42. Overall Mesh Point Network 154

43. Solution for Optimal Exit Lip. 160

LIST OF NOMENCLATURE

English Symbols

A	area
A'	coefficient defined by Eq. (378)
a	sound speed
a_1, a_2	coefficients defined by Eqs. (283) and (284)
B	projection of the boundary of the extremal surface onto the r,ϕ-plane
B'	coefficient defined by Eq. (379)
b_1, b_2	coefficients defined by Eqs. (285) and (286)
C'	coefficient defined by Eq. (380)
C_i	coefficients defined by Eqs. (274) through (280)
C_f	thrust coefficient
c_i	coefficients defined by Eqs. (369) through (371)
D_i	coefficients defined by Eqs. (339) through (345)
$D_{8,9}$	coefficients defined by Eqs. (350) and (351)
$D_{10,11}$	coefficients defined by Eqs. (396) and (397)
F	fundamental function
F'	function parametrically defining the control surface
f	function describing the control surface
G_i	coefficients defined by Eqs. (290) through (296)
H_i	coefficients defined by Eqs. (353) through (357)
$H_{10,11}$	coefficients defined by Eqs. (398) and (399)

h	specific enthalpy
I	functional to be maximized
$\bar{i}_r$	unit vector in the radial direction
$\bar{i}_\phi$	unit vector in the tangential direction
$\bar{i}_z$	unit vector in the axial direction
K	coefficient defined by Eq. (144)
$K_{1,2,3}$	constants
$\bar{L}$	unit vector along a bicharacteristic on a wave surface
L_r	radial component of unit vector $\bar{L}$
L_ϕ	tangential component of unit vector $\bar{L}$
L_z	axial component of unit vector $\bar{L}$
M	Mach number
$\bar{m}$	outer unit normal to a wave surface
$\dot{m}$	mass flow rate
$\bar{N}$	unit vector on a wave surface normal to the bicharacteristic direction
N_r	radial component of unit vector $\bar{N}$
N_ϕ	tangential component of unit vector $\bar{N}$
N_z	axial component of unit vector $\bar{N}$
n	number of dependent variables
$\bar{n}$	outer unit normal to the control surface
n_r	radial component of unit normal $\bar{n}$
n_ϕ	tangential component of unit normal $\bar{n}$
n_z	axial component of unit normal $\bar{n}$
p	pressure
p_k	partial derivative of z_k with respect to ϕ
Q	coefficient defined by Eq. (145)

$Q_{1,2}$	denote points on the exit lip
q_k	partial derivative of z_k with respect to r
R	gas constant
R_K	coefficients defined by Eq. (146) (k = 1,,n)
r	coordinate in cylindrical coordinate system
$\dot{r}$	symbol representing $dr/d\phi$
S	projected area of extremal surface on $r\phi$-plane
$S_{1,2}$	subregions of region S
s	specific entropy
T	temperature
t	time
$\overline{V}$	velocity vector
V	magnitude of the velocity
V_r	radial component of the velocity vector $\overline{V}$
V_ϕ	tangential component of the velocity vector $\overline{V}$
V_z	axial component of the velocity vector $\overline{V}$
W_k	coefficient defined by Eq. (143)
X	coefficient defined by Eq. (141)
x	coordinate in cartesian coordinate system
Y	coefficient defined by Eq. (142)
y	coordinate in cartesian coordinate system
z	axial coordinate in cylindrical and cartesian coordinate system
z_k	dependent variables (k = 1,···,n)

Greek Symbols

α	angle partially defining the direction of the unit outer normal to the control surface

β	angle partially defining the direction of the unit outer normal to the control surface
Γ_e	exit lip of the nozzle (i.e., the outer boundary of the control surface)
γ	ratio of specific heat capacities
δ	variational operator
ε	variational parameter
η	angle relating bicharacteristic direction to cylindrical coordinate system
θ	angle partially defining the direction of the velocity vector
λ	slope of the characteristic direction for a set of hyperbolic partial differential equations
λ_2	Lagrange multiplier
λ_3	constant of integration
μ	Mach angle
ξ	angle defined by Eq. (91)
π	ratio of the circumference to the diameter of a circle
ρ	density
Σ	indicates a summation
σ	extremal surface
$\sigma_{1,2}$	functions used in method of characteristics solution
τ	boundary of the extremal surface
ϕ	angular coordinate of cylindrical coordinate system
ϕ'	angle used in axisymmetric solution given by Eq. (315)
ψ	angle partially defining the direction of the velocity vector

Subscripts

a	ambient conditions

CE	between points C and E
c.s.	control surface
E	evaluated at point E
e	nozzle exit lip
IE	between points I and E
IF	between points I and F
IVL	initial value line
i	initial value line
ideal	ideal (perfect) nozzle
k	variable index
n	counter for number of iterations
o	stagnation conditions
p_k	partial derivative with respect to p_k
q_k	partial derivative with respect to q_k
r	partial derivative with respect to r
s	constant entropy
T	total or entire quantity
ϕ	partial derivative with respect to ϕ
$\partial f/\partial r$	partial derivative with respect to $\partial f/\partial r$
$\partial f/\partial \phi$	partial derivative with respect to $\partial f/\partial \phi$
1,2,3	points 1, 2 and 3 in numerical solution technique
I	denotes right running characteristics
II	denotes left running characteristics

Operators

∂	partial derivative operator
d	total derivative operator

δ	variational operator with no restrictions on independent variables
$\tilde{\delta}$	variational operator where independent variables held fixed
$(\overline{})$	vector
$\cdot$	scalar product
∇	del operator
$\nabla \times (\ )$	curl
D/Dt	substantial derivative
$\lvert\ \rvert$	absolute value, scalar magnitude
x	vector or cross product

SECTION I
INTRODUCTION

1. INTRODUCTORY REMARKS

Applications of the calculus of variations occur in several fields of engineering, such as flight mechanics, fluid dynamics, optimal control and system optimization. The theory of the calculus of variations has been of great interest in the professional journals devoted to applied mathematics, but it is only in the last fifteen years that the theory has been applied to engineering problems. It is the application of the calculus of variations to the problem of designing three-dimensional nozzle contours which deliver maximum axial thrust that is treated here.

At present, there are several applications which can benefit from the use of three-dimensional nozzles. These include three-dimensional nozzles for rocket engines having nonsymmetric exit area constraints and three-dimensional nozzles for airbreathing propulsion systems where a high degree of integration of engine and vehicle structure is required. With the ability to apply the calculus of variations to the design of three-dimensional nozzles it is possible to determine the maximum thrust which can be delivered by a three-dimensional nozzle with specific geometrical constraints, compare the performance of optimal three-dimensional nozzles with that of nonoptimally designed three-dimensional nozzles, and eliminate costly analytical and experimental parametric studies to determine optimal nozzle contours.

The objective of the present research is the development of a method to design three-dimensional, supersonic thrust nozzles to produce the maximum axial thrust for specific design constraints. The need for such a sophisticated design procedure is established by the critical dependence of several advanced mission systems on the propulsion system performance and thus on the thrust nozzle performance. For such systems as

advanced airbreathing propulsion units (e.g. ramjets and scramjets) and rocket engines, a small change in engine efficiency is magnified many times in determining the overall system performance. For example, NASA's Office of Advanced Research and Technology has estimated that for the space shuttle a one per cent degradation in specific impulse will reduce the cargo payload by 20 per cent where a payload of 50,000 pounds is being sought (25). Furthermore, the final version of many of these advanced systems will almost certainly require an integration of the engine with the airframe and will result in a three-dimensional thrust nozzle.

The techniques which are necessary in the design of maximum thrust, axisymmetric, supersonic nozzles are well developed. The axisymmetric optimization problem has been solved for a variety of flow assumptions and geometrical constraints. The technique necessary to design maximum thrust, fixed length, axisymmetric nozzles with irrotational flow is in use in many propulsion companies. Analyses which permit more involved flow models and which allow for more general geometrical constraints do exist for optimized axisymmetric nozzles. While these methods for axisymmetric and two-dimensional nozzles have become fairly well developed, equivalent methods for three-dimensional nozzles are in their infancy. Although formulations exist which deal with the design of maximum thrust three-dimensional nozzles, no numerical solutions have existed until now.

2. STATE OF THE ART EVALUATION

The concept of designing nozzle contours by applying variational calculus techniques was introduced in 1955 by Guderley and Hantsch (1) for nozzles with axisymmetric, supersonic, homentropic flow. Until then only empirical investigations of the problem of designing maximum thrust nozzles had been carried out. The principal idea of Guderley and Hantsch was the introduction of a characteristic surface as a control surface for computing the thrust, the mass flow rate and the length of the nozzle. Figure 1 illustrates the general nozzle geometry employed in the thrust nozzle optimization. The entire optimization problem is formulated along the control surface IE, and the thrust across this

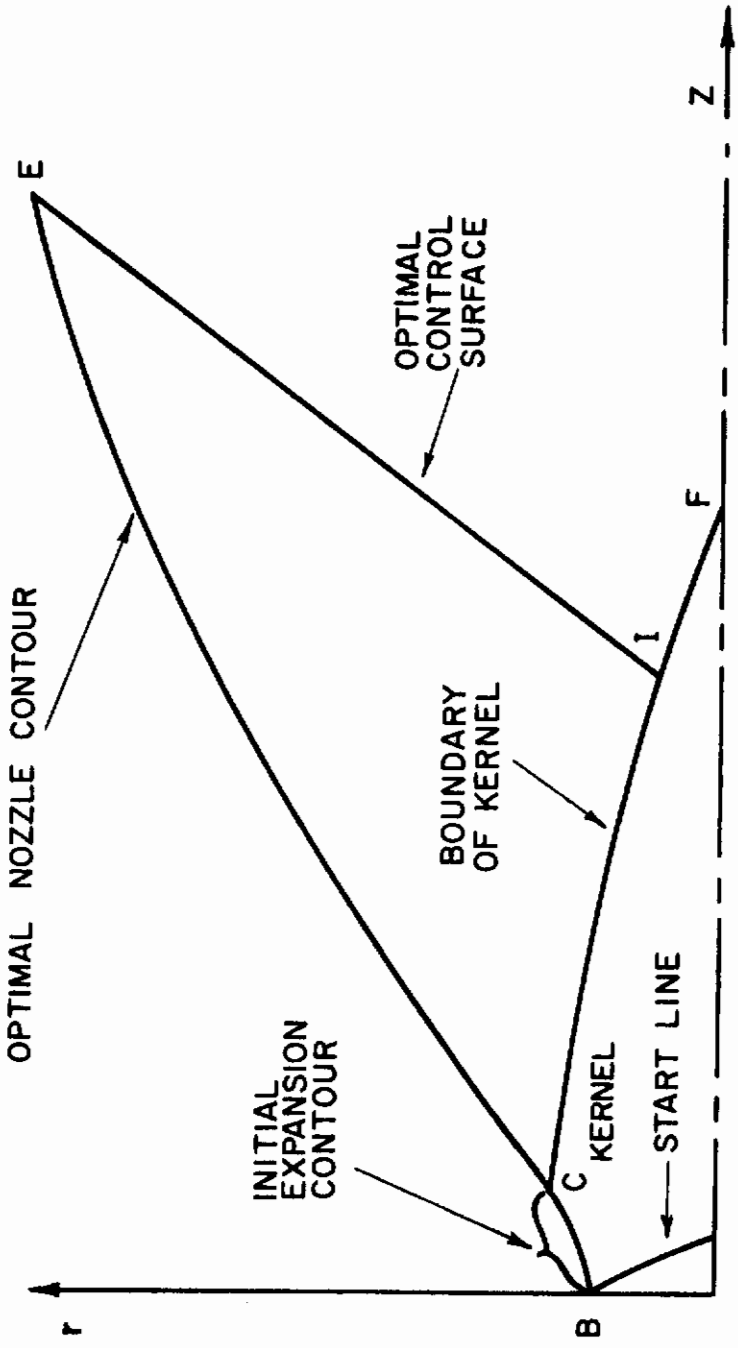

FIGURE 1. AXISYMMETRIC NOZZLE GEOMETRY

control surface is maximized for a fixed value of nozzle length and constant mass flow rate.

The condition that the control surface is a characteristic surface in reality imposes two constraints on the control surface. First, the condition forces the control surface to be everywhere tangent to a characteristic (wave) surface of the flow, and second, it forces the compatibility equation for a characteristic (wave) surface to be satisfied on the control surface.

In 1958 Rao (2) considered the same problem and demonstrated that it is not necessary to impose specifically the constraint that the control surface be a characteristic surface. He found that the control surface becomes a characteristic surface when a maximum thrust nozzle is designed under the constraints of fixed length and constant mass flow rate. Rao's formulation and solution technique has proven to be much easier to apply than that of Guderley and Hantsch, and Rao's technique is currently used by engineers in the design of supersonic thrust nozzles.

The differences between the formulations in Refs. (1) and (2) were analyzed by Guderley (3), who extended the development to include isentropic flows with constant total enthalpy and constant entropy along a streamline but with entropy variations between streamlines. Guderley showed that the two formulations in Refs. (1) and (2) were both valid and yield the same result.

In the above three analyses, the variables on the control surface are functions of only one independent variable, and only the fixed length problem is treated. The problem of obtaining the contour which produces the maximum thrust for a general geometrical constraint on the shape of the nozzle wall was formulated by Guderley and Armitage (4, 5). Their formulation results in a variational problem in two independent variables.

Recently, several more general nozzle optimization problems for axisymmetric and two-dimensional nozzles have been treated. Hoffman (6) extended the Guderley and Armitage (4, 5) formulation to treat a general gas mixture in chemical nonequilibrium. Scofield, Thompson and Hoffman (7) developed a design technique and computer program for the

design of maximum thrust nozzle contours including boundary layer effects for irrotational flow fields. The formulations of (6) and (7) were combined and extended by Hoffman, Scofield and Thompson (8) to include a general gas mixture in chemical nonequilibrium, a simple dissociating gas in chemical nonequilibrium, and a general gas mixture whose composition is either frozen or in chemical equilibrium, all including boundary layer effects. The design technique and computer program for the formulation in (8) was developed by Scofield and Hoffman (9). Shmyglevskii (26) considered both irrotational and rotational nozzle flows but restricted his investigations to geometrical models with prescribed endpoints, thus omitting from consideration constraints such as fixed surface area and arc length. Kraiko et al. (27) developed the design equations for maximum thrust nozzles for both irrotational and nonequilibrium flows.

The theory of the calculus of variations has also been applied to the design of maximum thrust plug nozzles. Rao (10) applied the variational technique to the problem of generating maximum thrust plug nozzles for axisymmetric, homentropic flow. Rao's formulation for plug nozzles is similar to the work in Refs. (1) through (3) in that the optimization equations are functions of only one independent variable. Humphreys, Thompson and Hoffman (11) formulated the maximum thrust plug nozzle problem in two independent variables so that geometrical constraints could be imposed on the optimization. Johnson (12) formulated the maximum thrust plug nozzle problem with variable inlet geometry and developed the numerical technique and computer program to solve the resulting equations.

In 1965 Thompson and Murthy (13) formulated the problem of designing maximum thrust, three-dimensional nozzles. Their formulation for the three-dimensional optimization case is analogous to Rao's (2) approach to the axisymmetric optimization case in that they formulated the problem in terms of variables on a control surface which passes through the exit of the nozzle. Thus, the three-dimensional optimization problem reduces to a variational problem in two independent variables. Borisov (14) has also formulated the three-dimensional optimization problem for fixed exit conditions. Borisov's formulation is analogous to the formulation of

Guderley and Armitage (4, 5) for axisymmetric nozzles in that his formulation includes the flow region bounded by the kernel and the control surface. Thus, Borisov's formulation results in a variational problem in three independent variables. Up until this time, no numerical technique for the design of a maximum thrust, three-dimensional nozzle has been presented.

In general, the development of the procedures to design optimal three-dimensional nozzles has proceeded relatively slowly. This is not due to lack of interest but is rather a result of the extreme complexity of the problem and the need to develop the analytical techniques required to implement a numerical procedure. For example, in addition to the requirement for a relatively large and fast computer, the design procedure for optimal three-dimensional nozzles requires the ability to numerically analyze supersonic, three-dimensional flow fields. Ransom, Hoffman and Thompson (15) have presented a comprehensive review of the methods available for computing three-dimensional, supersonic flows. Their survey indicates that prior to 1969 no practical and accurate numerical method existed to calculate internal, three-dimensional, supersonic flows. In Refs. (15) and (23), Ransom, Hoffman and Thompson develop a numerical algorithm and associated computer program for the analysis of internal, three-dimensional, supersonic flow. In general, the numerical algorithm and computer program have been demonstrated to be highly satisfactory; however, for the design of optimal three-dimensional nozzles the numerical algorithm and computer program are too specialized and require modification to solve the entire three-dimensional design problem. The computer program (23) was utilized in this research to analyze the three-dimensional kernel flow.

3. SCOPE AND METHOD OF APPROACH

In this research the variational problem is formulated in a manner similar to that presented by Thompson and Murthy (13); however, the present formulation possesses several important differences. The most important difference is that no differential constraint is introduced into the fundamental function to specifically prevent the existence of

Beltrami flow (24) on the control surface (in all the numerical cases presented in this report, an irrotational kernel is used to generate irrotational flow on the control surface).

The problem is formulated as a variational problem for the three-dimensional, supersonic, isoenergetic, homentropic flow of a perfect gas. The quantity to be maximized is the axial thrust of the nozzle which is written as a surface integral over a control surface. The initial flow conditions, the mass flow rate, and the nozzle length are held fixed. The control surface passes through the exit lip of the nozzle and intersects the kernel region, where the kernel region is that portion of the flow field that can be determined from the prescribed initial conditions.

The integral thrust expression is maximized by applying the calculus of variations to obtain a set of design equations (two partial differential equations and three algebraic relations) which relate the flow variables on an optimal control surface. Boundary conditions corresponding to the fixed length constraint are also obtained from the variational solution.

The uniqueness of the solution is established by proving that an optimal control surface is a characteristic surface, a result which assures a unique matching of the flow in the kernel with the flow across the control surface. When the flow is constrained to be axially symmetric, the solution reduces to the well known result obtained by Rao (2).

The design equations are solved numerically. An overall solution procedure is developed which is conceptually similar to the method discussed in Ref. (21) for axisymmetric optimum nozzles. The procedure has the advantages that optimal solutions are obtained by a straightforward calculation and that to match specific boundary conditions the iterations are between optimal nozzles.

In this research the main emphasis is to establish:

1) that the three-dimensional optimization procedure can be implemented,
2) that the three-dimensional optimization will produce a significantly better thrust nozzle than other, heretofore

arbitrary, design procedures for three-dimensional nozzles, and

3) how the optimized three-dimensional nozzles differ from the nozzles that have resulted from applying approximate two-dimensional methods.

Once the control surface for an optimal nozzle has been determined, the corresponding optimal nozzle contour can be found by computing the three-dimensional flow field between the kernel and the control surface (using the three-dimensional method of characteristics) and then following the streamlines from the exit lip back to their origin. This final part of the design procedure relies on the theory developed in Refs. (15) and (23); however, that part of the procedure is not part of this research. The exit contour, the axial thrust and the exit flow properties can be determined and compared for whole families of optimal nozzles without having to complete the contour determination.

The method presented by Borisov (14) was studied and found to be too complex to be used in the initial attempt to solve the three-dimensional nozzle design problem. The Borisov formulation does offer some advantages and is worthy of further consideration when better methods become available to analyze systems of quasi-linear, first order, hyperbolic, partial differential equations in three independent space variables.

SECTION II
THEORETICAL DEVELOPMENT

The problem of designing optimal, three-dimensional, supersonic nozzles to be discussed in this work concerns only the determination of the supersonic portion of the nozzle contour downstream of a specified initial expansion contour. The theoretical development of this optimization problem is presented in this section.

Figure 2 shows a schematic representation of a general three-dimensional nozzle with supersonic flow. The zone of influence of the initial expansion contour of the nozzle is referred to as the kernel. The properties of the supersonic flow in the kernel are completely determined by the upstream conditions in a totally supersonic region of the flow and by a prescribed initial expansion contour. The flow properties in the kernel are determined by applying the three-dimensional method of characteristics analysis described in Refs. (15) and (23). The initial flow conditions and initial contour are specified as part of the problem, and they act as initial conditions for the mathematical optimization problem.

The formulation of the maximum thrust, three-dimensional design problem is based on considering the flow across a three-dimensional control surface which is constrained to pass through the exit lip of the nozzle contour and to intersect the boundary of the three-dimensional kernel. The intersection of the control surface and the outer surface of the kernel is referred to as the initial value line since the flow properties along this intersection serve as initial conditions for the calculation of the control surface. The flow across the control surface is restricted to steady, inviscid, isoenergetic, homentropic flow. The shape of the control surface and the flow properties on the control surface are described in terms of four dependent variables V, θ, ψ and f which are functions of two independent variables r and ϕ. The variables

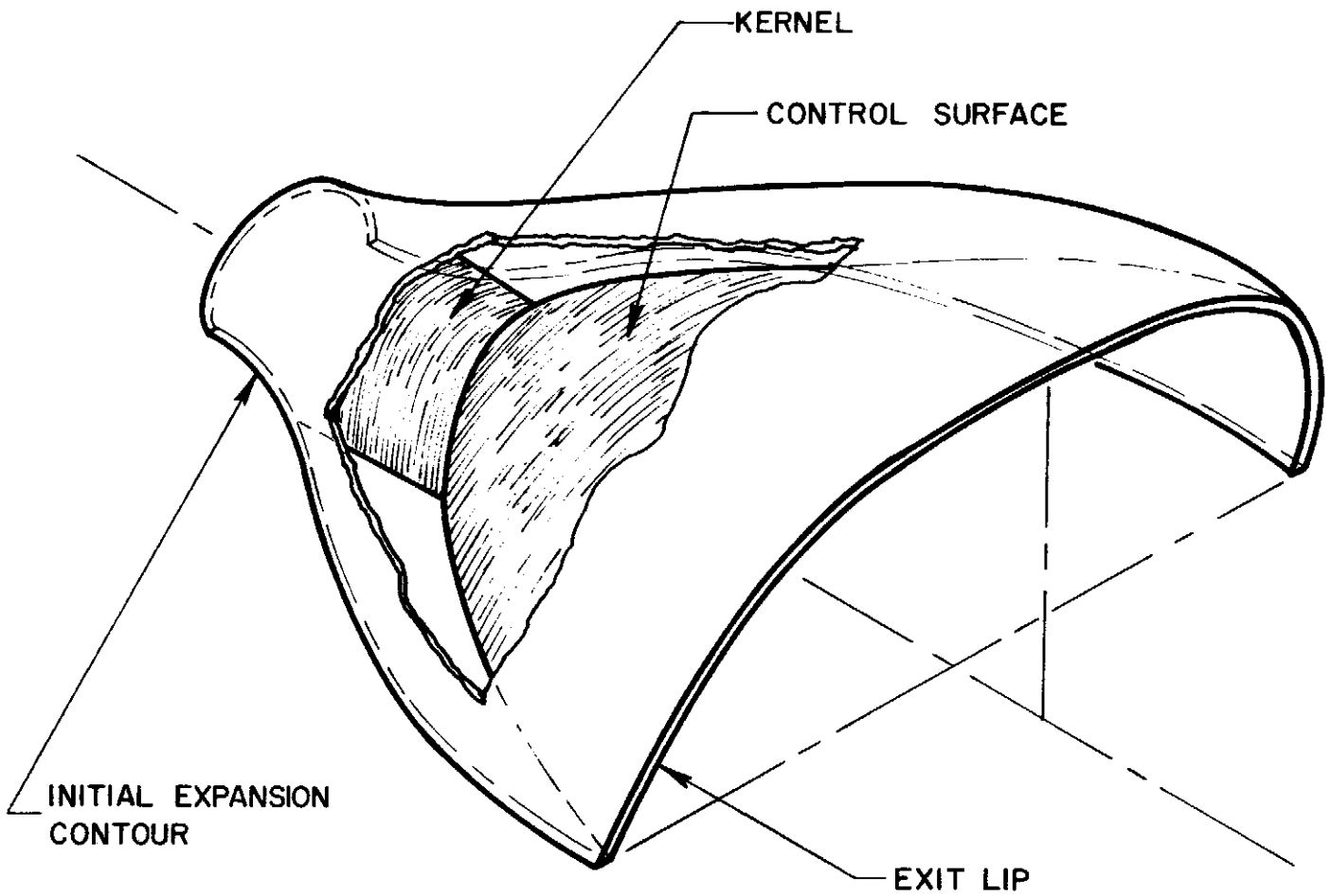

FIGURE 2. THREE-DIMENSIONAL NOZZLE GEOMETRY

V, θ and ψ describe the magnitude and direction of the velocity vector $\overline{V}$ while the function f defines the axial position of any point on the control surface.

The axial thrust is expressed in terms of the four dependent variables as an integral equation over the control surface. The mass flow rate through the control surface is also written in terms of the dependent variables as an integral equation over the control surface. The mass flow rate is constrained to be a constant quantity by multiplying the surface integral expression for the mass flow rate by a constant Lagrange multiplier and adding the total expression to the surface integral expression for the axial thrust. This linear combination of terms is the functional I to be maximized.

A necessary condition for maximum thrust with a constant mass flow rate requires that the first variation of the functional I vanishes identically for every admissible distribution of variations of the variables in the problem. The restrictions on the thermodynamics of the flow and the fixed length constraint are imposed by substitution into the expression for the first variation of I.

In the analysis, arbitrary and independent variations in the four dependent variables V, θ, ψ and f are allowed on the control surface. When the first variation of the functional I is required to vanish identically, sufficient equations result to solve for the dependent variables on the extremal control surface (It is assumed that a maximum exists and that the solution will be for a maximum thrust nozzle and not a minimum thrust nozzle.). The fixed length constraint is introduced into the analysis by not allowing variations in the axial position of the exit lip. By allowing variations in the radius of the exit lip, an equation is derived which relates the variables along the outer boundary of the control surface (i.e., the nozzle exit lip). At this point in the development, the equations which result from requiring the first variation of the functional I to vanish identically are used to prove that the extremal control surface and the kernel flow are compatible. Finally, at the end of this section, it is shown that the optimization equations derived for the three-dimensional case reduce to the equations derived in Refs. (2) and (3) under the assumption of axisymmetric flow.

1. FORMULATION OF THE OPTIMIZATION PROBLEM

A. Geometrical Relationships

A cylindrical coordinate system is used throughout this work as the spatial reference. The z-axis is oriented in the direction that the thrust is to be maximized. Since the control surface is a three-dimensional surface, it is convenient to transform the problem to the two-dimensional $r\phi$-plane. The transformation corresponds physically to projecting the control surface onto the $r\phi$-plane. On the control surface, the four dependent variables V, θ, ψ and f are only functions of the two independent variables r and ϕ.

As stated above, the velocity vector $\overline{V}$ at any point in a three-dimensional nozzle flow, and specifically at a point on the control surface, is uniquely determined by its magnitude and two spherical angles θ and ψ. The direction cosines of $\overline{V}$ are as follows:

$$V_r = V \sin\theta \cos\psi$$

$$V_\phi = V \sin\theta \sin\psi \qquad (1)$$

$$V_z = V \cos\theta$$

The control surface is described by the equation

$$z = f(r,\phi) \qquad (2)$$

where the function $f(r,\phi)$ is to be determined from the analysis. The control surface shape is also known if at every point on the control surface the direction of the unit outer normal to the control surface is known. The unit outer normal $\overline{n}$ is uniquely specified by two spherical angles α and β. The direction cosines of the unit outer normal to the control surface are as follows:

$$n_r = \sin\beta \cos\alpha$$

$$n_\phi = \sin\beta \sin\alpha \qquad (3)$$

$$n_z = \cos\beta$$

Although the angles α and β will appear in the integral expressions for the thrust and mass flow rate across the control surface, it should be emphasized that the shape of the control surface is defined by the single dependent variable f. The angles α and β are related to f by the following equations:

$$\frac{\partial f}{\partial r} = - \tan\beta \cos\alpha \qquad (4)$$

$$\frac{\partial f}{\partial \phi} = - r \tan\beta \sin\alpha \qquad (5)$$

where $\partial f/\partial r$ and $\partial f/\partial \phi$ are related through the mathematical relationship

$$df = (\partial f/\partial r)dr + (\partial f/\partial \phi)d\phi \qquad (6)$$

If the values of $\alpha(r,\phi)$ and $\beta(r,\phi)$ are known, then Eqs. (4), (5) and (6) can be combined with the proper initial conditions to solve for $f(r,\phi)$. If $f(r,\phi)$ is known, then Eqs. (4) and (5) can be used to solve for $\alpha(r,\phi)$ and $\beta(r,\phi)$. A more complete discussion of the geometrical relations involved in this three-dimensional nozzle optimization problem is given in Appendix A.

B. Gas Dynamic Model

The supersonic motion of most compressible fluids encountered in propulsion systems can be accurately described by means of the governing equations for the motion of an ideal fluid. The major assumptions which constitute the gas dynamic model are: 1) continuum, 2) inviscid, 3) steady, 4) isoenergetic (i.e., constant stagnation enthalpy h_o

throughout the flow) and 5) homentropic flow (i.e., constant entropy throughout the flow). In this work the fluid is assumed to be a perfect gas. Other equations of state could be treated and the basic approach would be unchanged.

Under these assumptions, it is possible to show that the pressure p, density ρ, sound speed a, and Mach angle μ are functions of the magnitude of the velocity and the stagnation conditions. Thus, the following differential relationships are valid throughout the flow:

$$dp = - \rho V dV \tag{7}$$

$$d\rho = - \rho V / a^2 dV \tag{8}$$

$$da = - \left(\frac{\gamma - 1}{2}\right) \frac{V}{a} dV \tag{9}$$

$$d\mu = \frac{- \left(\frac{\gamma - 1}{2} + \sin^2 \mu\right)}{V \sin\mu \cos\mu} dV \tag{10}$$

In the formulation of the optimization problem the gas dynamic model constraint is introduced by eliminating derivatives of pressure, density, sound speed and Mach angle in the variational equations by substitution from Eqs. (7) through (10).

The existence of shock waves has been implicitly excluded in the flow model by the homentropic flow assumption. The flow in the kernel is assumed to satisfy the gas dynamic model since the kernel flow serves as an initial condition on the calculation of the control surface. A more complete discussion of the gas dynamic model is given in Appendix B.

C. Functional to be Maximized

The thrust expression to be maximized is written as the sum of the pressure differential and the momentum flux across the control surface. The pressure differential is the difference in the pressure acting on the outside of the nozzle wall and that acting on the control surface. It

is assumed that a constant and uniform ambient pressure acts on the outer surface of the nozzle wall. For a given nozzle, the only portion of the thrust which enters the variational problem is that part generated by the flow passing through the control surface. The magnitude of the axial thrust produced by the flow not passing through the control surface T_{IVL} is a constant for a given kernel and specified initial value line.

The total axial thrust T is given by the following equation:

$$T = T_{IVL} + \int_0^{2\pi} \int_{r_i(\phi)}^{r_e(\phi)} \left(r(p-p_a) - r\rho V^2 \frac{\cos\theta \sin\xi}{\cos\beta} \right) dr d\phi \qquad (11)$$

where the angle ξ is defined by the vector relationship

$$\sin\xi = \frac{-(\bar{V} \cdot \bar{n})}{V} = \cos\beta \left(-\cos\theta + \sin\theta\cos\psi \frac{\partial f}{\partial r} + \frac{\sin\theta\sin\psi}{r} \frac{\partial f}{\partial \phi} \right) \qquad (12)$$

The limits of integration $r_i(\phi)$ and $r_e(\phi)$ refer to the radius of the initial value line and the nozzle exit lip, respectively.

The mass flow rate through the exit of the nozzle $\dot{m}_T$ is given by the following expression:

$$\dot{m}_T = \dot{m}_{IVL} + \dot{m}_{c.s.} \qquad (13)$$

where

$$\dot{m}_{c.s.} = \int_0^{2\pi} \int_{r_i(\phi)}^{r_e(\phi)} (-\rho V \sin\xi/\cos\beta) dr d\phi \qquad (14)$$

For a specified kernel and a specified initial value line $\dot{m}_T$ and $\dot{m}_{IVL}$ have constant values; therefore, from Eq. (13) the value of $\dot{m}_{c.s.}$ is a constant for a specified kernel and a specified initial value line.

To introduce the condition that $\dot{m}_{c.s.}$ has a constant value in the extremal problem, the expression

$$\int_0^{2\pi}\int_{r_i(\phi)}^{r_e(\phi)} (-\rho V \sin\varepsilon/\cos\beta)\,dr\,d\phi + \dot{m}_{IVL} - \dot{m}_T = 0 \qquad (15)$$

is multiplied by a constant Lagrange multiplier λ_2. The result is then added to the expression for the axial thrust as given in Eq. (11). Thus, the functional I to be maximized has the form

$$I = T + \lambda_2\left[\int_0^{2\pi}\int_{r_i(\phi)}^{r_e(\phi)} (-\rho V \sin\varepsilon/\cos\beta)\,dr\,d\phi + \dot{m}_{IVL} - \dot{m}_T\right] \qquad (16)$$

Equations (11), (12) and (16) can be combined and rearranged to obtain the following expression for I:

$$I = T_{IVL} + \lambda_2(\dot{m}_{IVL} - \dot{m}_T) + \int_0^{2\pi}\int_{r_i(\phi)}^{r_e(\phi)} F(r,\phi,V,p,\rho,\theta,\psi,\partial f/\partial\phi,\partial f/\partial r)\,dr\,d\phi \qquad (17)$$

where

$$F = r(p - p_a) - r\rho V(V\cos\theta + \lambda_2)\left(-\cos\theta + \sin\theta\cos\psi\,\frac{\partial f}{\partial r} + \frac{\sin\theta\,\sin\psi}{r}\,\frac{\partial f}{\partial\phi}\right) \qquad (18)$$

In the next section the calculus of variations will be applied to the fundamental function F given by Eq. (18) to determine the necessary conditions which must be satisfied for the total axial thrust to be a maximum for a constant mass flow rate, specified kernel and specified initial value line. A more detailed derivation of the integral equations

for the thrust and mass flow rate is given in Appendix C while a discussion of the method of Lagrange multipliers can be found in Ref. (17).

2. DERIVATION OF THE OPTIMIZATION EQUATIONS

A. Application of the Calculus of Variations

The application of the calculus of variations to the problem of determining the necessary conditions which must be satisfied in order to extremize an integral I of the form which appears in Eq. (17) is presented by Miele (18). A summary of the theory presented in Ref. (18) appears in Appendix D. The value of the functional I depends on the choice of the surface σ, defined by the n functions $z_k(r,\phi)$, whose projection on the $r\phi$-plane is the regions S_1 and S_2; it also depends on the geometry of the boundary line τ, defined by the n+1 functions $r = r(\phi)$ and $z_k = z_k(\phi)$, whose projection on the $r\phi$-plane is the contour B (see Figure 3). The purpose of this section is to determine the necessary conditions which must be satisfied by the n functions $z_k(r,\phi)$ and the n+1 functions, $r = r(\phi)$ and $z_k = z_k(\phi)$, in order to extremize the functional I.

For the surface σ to be an extremal surface, the set of functions $z_k(r,\phi)$ must be such that the first variation of the surface integral I vanishes identically for every admissible distribution of variations; that is,

$$\delta I = 0 \tag{19}$$

When an admissible surface σ is defined as any set of functions $z_k(r,\phi)$ which are continuous, whose derivatives are continuous everywhere except along a finite number of corner lines, and which satisfy the prescribed boundary conditions, the following extremal condition is obtained:

$$\delta I = \iint_{S_1} \sum_{k=1}^{n} \left(F_{z_k} - \frac{\partial}{\partial \phi}(F_{p_k}) - \frac{\partial}{\partial r}(F_{q_k}) \right) \tilde{\delta} z_k \, dr d\phi$$

$$+ \iint_{S_2} \sum_{k=1}^{n} \left(F_{z_k} - \frac{\partial}{\partial \phi}(F_{p_k}) - \frac{\partial}{\partial r}(F_{q_k}) \right) \tilde{\delta} z_k \, dr d\phi$$

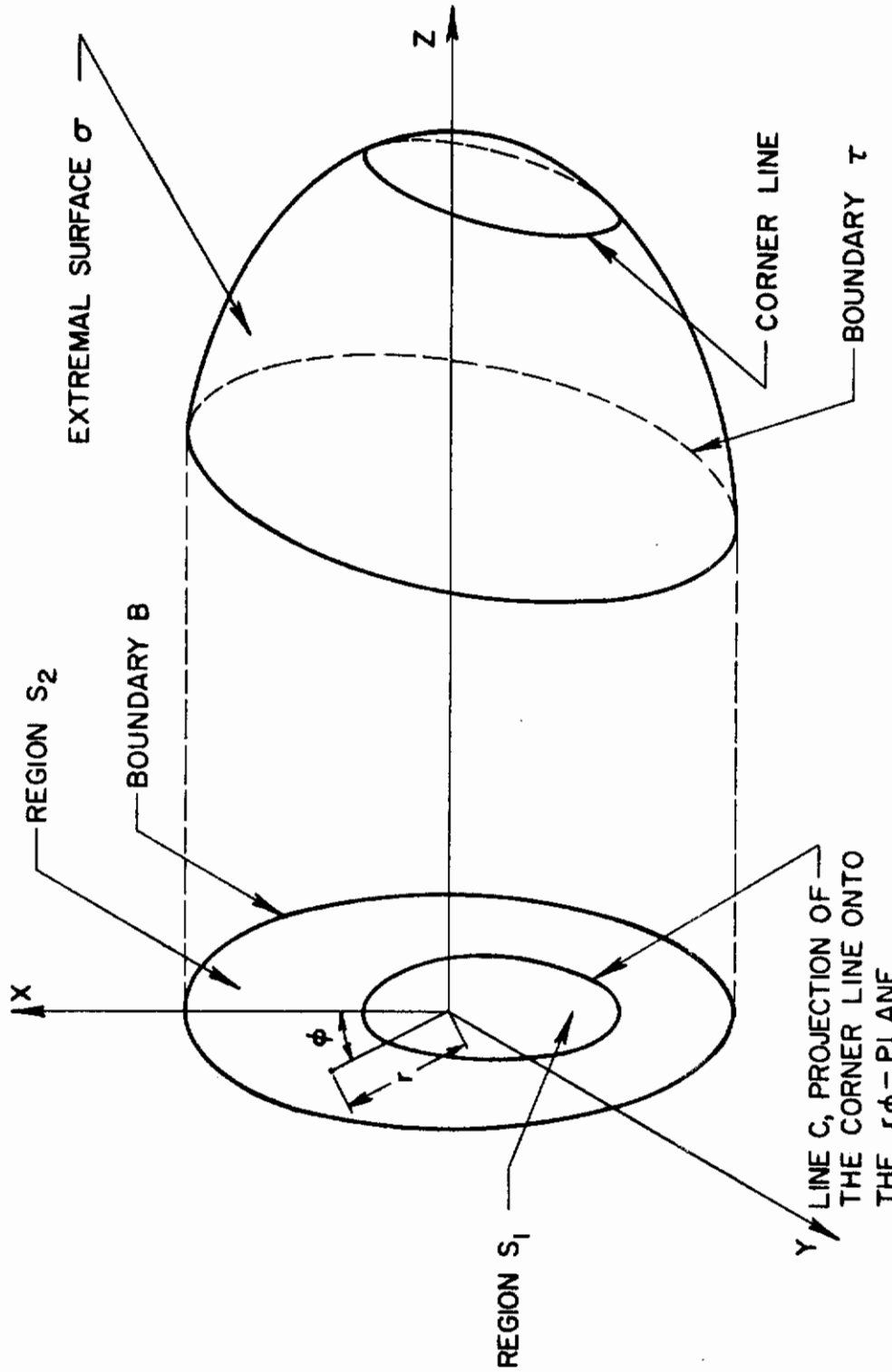

FIGURE 3. EXTREMAL SURFACE

$$+ \int_B (X\delta\phi + Y\delta r + \sum_{k=1}^{n} W_k \delta z_k) d\phi$$

$$- \int_C (\Delta K \delta\phi + \Delta Q \delta r + \sum_{k=1}^{n} \Delta R_k \delta z_k) d\phi = 0 \qquad (20)$$

which must be satisfied for every admissible distribution of variations. In Eq. (20) the functions p_k, q_k, X, Y, W_k, K, Q and R_k are given by the following expressions:

$$p_k = z_{k\phi} = \partial z_k / \partial \phi \qquad (k=1,..,n) \qquad (21)$$

$$q_k = z_{kr} = \partial z_k / \partial r \qquad (k=1,..,n) \qquad (22)$$

$$X = \sum_{k=1}^{n} p_k F_{q_k} + \dot{r}(F - \sum_{k=1}^{n} p_k F_{p_k}) \qquad (23)$$

$$Y = -(F - \sum_{k=1}^{n} q_k F_{q_k}) - \dot{r} \sum_{k=1}^{n} q_k F_{p_k} \qquad (24)$$

$$W_k = -F_{q_k} + \dot{r} F_{p_k} \qquad (k=1,...,n) \qquad (25)$$

$$K = \sum_{k=1}^{n} p_k F_{q_k} + \dot{r}(F - \sum_{k=1}^{n} p_k F_{p_k}) \qquad (26)$$

$$Q = -(F - \sum_{k=1}^{n} q_k F_{q_k}) - \dot{r} \sum_{k=1}^{n} q_k F_{p_k} \qquad (27)$$

$$R_k = -F_{q_k} + \dot{r} F_{p_k} \quad , \qquad (k=1,....,n) \qquad (28)$$

where F_{p_k} denotes the partial derivative of F with respect to p_k, and F_{q_k} denotes the partial derivative of F with respect to q_k. Equation (20)

is written with $\Delta(\cdots)$ denoting the difference in the quantity $(\cdots)$ evaluated on the outer side of the corner line and the same quantity evaluated on the inner side. The details of the derivation of Eq. (20) are shown in Appendix D.

B. Equations Which Define Optimal Control Surfaces

As shown in Eq. (17), the functional I to be maximized has the following form:

$$I = \text{constant} + \int_0^{2\pi} \int_{r_i(\phi)}^{r_e(\phi)} F(r,\phi, V,p,\rho,\theta,\psi, \frac{\partial f}{\partial r}, \frac{\partial f}{\partial \phi}) dr d\phi \qquad (29)$$

Since the constant term in Eq. (29) vanishes when variations in I are considered, the term can be dropped from further consideration. The functional in Eq. (29) matches the form of the generalized functional in Appendix D. As derived in Appendix B, the static pressure p and the density ρ are only functions of V and the constants p_o, h_o, R and γ; therefore, it is possible to write Eq. (29) in the following form:

$$I = \iint_S F(r,\phi,z_k,p_k,q_k) dr d\phi \qquad (30)$$

where

$$z_1 = V,\ z_2 = \theta,\ z_3 = \psi,\ z_4 = f \qquad (31)$$

$$p_1 = \partial V/\partial\phi,\ p_2 = \partial\theta/\partial\phi,\ p_3 = \partial\psi/\partial\phi,\ p_4 = \partial f/\partial\phi \qquad (32)$$

$$q_1 = \partial V/\partial r,\ q_2 = \partial\theta/\partial r,\ q_3 = \partial\psi/\partial r,\ q_4 = \partial f/\partial r \qquad (33)$$

The independent variables are r and ϕ while the z_k (k = 1, .., 4) represent the four dependent variables.

For arbitrary and independent variations of the four dependent variables V, θ, ψ and f, Eq. (20) can only be satisfied if the following four equations are valid in the regions S_1 and S_2:

$$F_{z_k} - \frac{\partial}{\partial \phi}(F_{p_k}) - \frac{\partial}{\partial r}(F_{q_k}) = 0 \qquad (k = 1,..,4) \tag{34}$$

These four equations are referred to as the Euler equations.

For the fundamental function F given by Eq. (18), the four Euler equations reduce to the following equations:

$$V\cos\theta + \lambda_2 = - V\sin\theta\tan\mu \tag{35}$$

$$\alpha = \psi \tag{36}$$

$$\beta = \theta + \mu + \pi/2 \tag{37}$$

$$\frac{\partial}{\partial \phi}(\rho V^2 \sin^2\theta\tan\mu\sin\psi) + \frac{\partial}{\partial r}(r\rho V^2 \sin^2\theta\tan\mu\cos\psi) = 0 \tag{38}$$

Thus, the application of the Euler equations yields expressions relating the variables on an optimal control surface.

The functional I is being maximized under the assumption that $V(r,\phi)$, $\theta(r,\phi)$, $\psi(r,\phi)$ and $f(r,\phi)$ are continuous and have continuous derivatives in regions S_1 and S_2. This requirement can be used to obtain a form of the geometrical relationships between α, β and f which can be combined with the Euler equations to obtain an additional relationship between V, θ and ψ in regions S_1 and S_2. This relationship results from equating the cross derivatives of $f(r,\phi)$ and is given as follows:

$$\frac{\partial}{\partial \phi}\left[\tan(\theta + \mu + \pi/2)\cos\psi\right] - \frac{\partial}{\partial r}\left[r\tan(\theta + \mu + \pi/2)\sin\psi\right] = 0 \tag{39}$$

The five equations, Eqs. (35) through (39), can be numerically solved for the five variables V, θ, ψ, α and β which describe an optimal control surface. The solution of these equations is discussed in Section III. A more detailed derivation of Eqs. (35) through (39) is given in Appendix E.

C. Transversality Equation

The transversality equation is a necessary condition that must be satisfied when variations of the dependent variables on the boundaries of the region S are considered. The transversality equation relates the values of the independent and dependent variables on the boundaries of the extremal surface and provides boundary conditions for the Euler equations. As shown in Appendix F, the following equation must be satisfied for every set of variations $\delta\phi$, δr and δz_k consistent with the conditions imposed on the location of the boundary line B:

$$\int_B (X\delta\phi + Y\delta r + \sum_{k=1}^{n} W_k \delta z_k) d\phi = 0 \tag{40}$$

where ϕ has been chosen as the independent variable of the line integral, and the terms X, Y and W_k are defined by Eqs. (23) through (25). For the fundamental function F presented in Eq. (18), Eqs. (40) and (23) through (25) reduce to the following equations:

$$\int_B (X\delta\phi + Y\delta r + W_4\delta f) d\phi = 0 \tag{41}$$

$$X = p_4 F_{q_4} + \dot{r}F - \dot{r}p_4 F_{p_4} \tag{42}$$

$$Y = -F + q_4 F_{q_4} - \dot{r}q_4 F_{p_4} \tag{43}$$

$$W_k = 0 \qquad (k = 1,2,3) \tag{44}$$

$$W_4 = - F_{q_4} + \dot{r} F_{p_4} \tag{45}$$

where $\dot{r} = dr/d\phi$ and

$$p_4 = \partial f/\partial \phi \tag{46}$$

$$q_4 = \partial f/\partial r \tag{47}$$

In this work the region S (which has two subregions S_1 and S_2) has an inner and an outer boundary. As shown in Figure 4, the projection of the initial value line on the $r\phi$-plane is the inner boundary, and the projection of the nozzle exit lip is the outer boundary.

Since the conditions on the initial value line are specified and fixed, no variations are allowed on the inner boundary of the region S. Hence, the three variations δf, δr and $\delta \phi$ are each identically zero when evaluated on the inner boundary of the region S. Therefore, Eq. (41) reduces to the following form:

$$\int_{\Gamma_e} (X \delta \phi_e + Y \delta r_e + W_4 \delta f_e) d\phi = 0 \tag{48}$$

where Γ_e denotes the outer boundary of the control surface (i.e., the nozzle exit lip). Before any additional information can be obtained from Eq. (48), it is necessary to determine how the variations δf_e, δr_e and $\delta \phi_e$ are related.

On the boundary Γ_e, ϕ_e is the sole independent variable, and the following expressions are valid:

$$\delta f_e = \tilde{\delta} f_e + \frac{\partial f_e}{\partial r_e} \partial r_e + \frac{\partial f_e}{\partial \phi_e} \delta \phi_e \tag{49}$$

$$\delta r_e = \tilde{\delta} r_e + \dot{r} \delta \phi_e \tag{50}$$

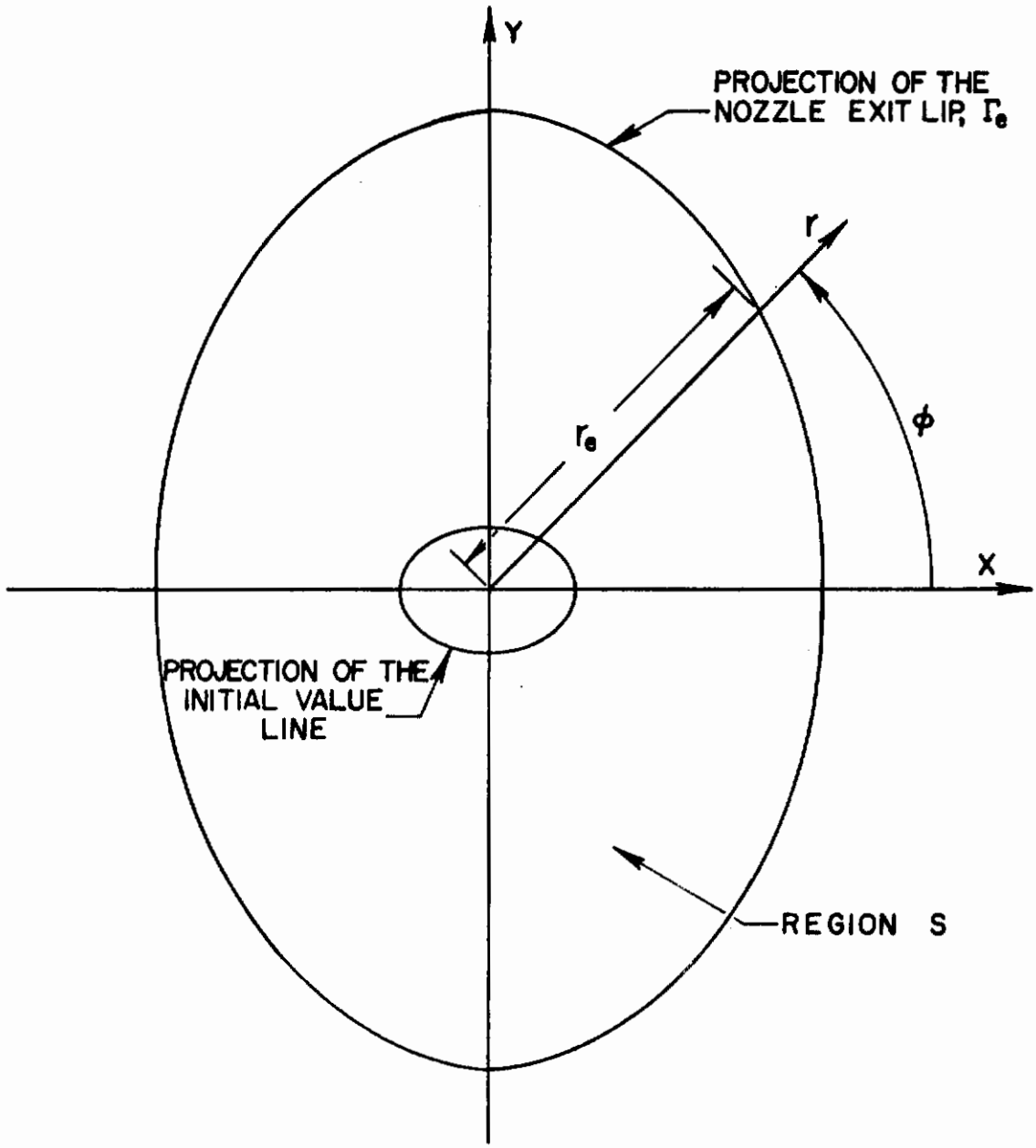

FIGURE 4. CONTROL SURFACE PROJECTION THE r,ϕ- PLANE

where $\tilde{\delta} f_e$ denotes variations of $f_e(\varepsilon, r_e, \phi_e)$ taken while holding the variables r_e and ϕ_e constant, δf_e denotes variations of $f_e(\varepsilon, r_e, \phi_e)$ with no restrictions on how r_e and ϕ_e can vary, $\tilde{\delta} r_e$ denotes variations of $r_e(\varepsilon, \phi_e)$ taken while holding the independent variable ϕ_e constant, and δr_e denotes variations of $r_e(\varepsilon, \phi_e)$ taken with no restrictions on how ϕ_e can vary. Forming the partial derivatives of F as indicated and substituting Eqs. (42) through (45), (49) and (50) into Eq. (48) yields the following equation:

$$\int_{\Gamma_e} \left\{ \left[r(p-p_a) - r\rho V(V\cos\theta + \lambda_2)\left(-\cos\theta + \sin\theta\cos\psi \frac{\partial f}{\partial r} + \frac{\sin\theta\sin\psi}{r} \frac{\partial f}{\partial \phi}\right)\right] \tilde{\delta} r_e \right.$$
$$\left. + \left[r\rho V \sin\theta (V\cos\theta + \lambda_2)(\cos\psi - \dot{r}\sin\psi/r) \right] \tilde{\delta} f_e \right\} d\phi = 0 \qquad (51)$$

Equation (51) is now evaluated consistent with the constraints on the problem.

The purpose of this research is to design three-dimensional nozzles which are designed for a fixed length (the length may vary with ϕ_e), have a constant mass flow rate, exhaust to a constant ambient pressure and produce the maximum axial thrust subject to these conditions. The constant mass flow rate constraint has already been imposed on the variational problem; however, the fixed length and constant ambient pressure constraints must be introduced into Eq. **(51)** in order for the constraints to be satisfied.

Since the length of the nozzle is fixed, the nozzle length f_e cannot be varied while applying the calculus of variations to maximize the thrust; therefore, the variation $\tilde{\delta} f_e$ is equal to zero. Since the exit radius r_e is allowed to seek its optimal value and satisfy the ambient pressure constraint, the variation $\tilde{\delta} r_e$ is arbitrary. There is an additional condition which must be true for the fixed length constraint to be satisfied. This condition is that in the variational problem while allowing for variations in r_e the following equations are valid: 1) $\partial f_e/\partial r_e = 0$ and, 2) $\partial f_e/\partial \phi_e = df_e/d\phi_e$. If this condition is not satisfied, the nozzle length f_e can change with variations in r_e. Thus,

in the variational problem, the variation $\tilde{\delta}r_e$ is arbitrary and independent, and the following three equations are substituted into Eq. (51) to enforce the fixed length constraint:

$$\tilde{\delta}f_e = 0 \tag{52}$$

$$\partial f_e/\partial r_e = 0 \tag{53}$$

$$\partial f_e/\partial \phi_e = df_e/d\phi_e \tag{54}$$

Substituting Eqs. (35) and (52) through (54) into Eq. (51), dividing by r_e and requiring that the variation $\tilde{\delta}r_e$ is arbitrary results in the following expression:

$$\left[(p-p_a) + \rho V^2 \sin\theta\tan\mu\left(-\cos\theta + \frac{\sin\theta\sin\psi}{r_e}\frac{df_e}{d\phi_e}\right)\right]\Bigg|_{\Gamma_e} = 0 \tag{55}$$

Equation (55) is the transversality equation for a fixed length, maximum thrust and constant mass flow rate nozzle where $r_e(\phi)$ has been allowed to seek its optimal value. The use of Eq. (55) to establish the location of the optimal exit lip on a generated optimal control surface is discussed in Section III. A more detailed discussion of the derivation of the transversality equation is presented in Appendix F.

D. Corner Line Conditions

An admissible extremal surface σ is defined as any set of functions $z_k(r,\phi)$ which are continuous everywhere except along a finite number of corner lines, and which satisfy the respective boundary conditions. The set of equations which govern the portion of an extremal surface where the derivatives are continuous and the transversality equation which must be satisfied along the outer boundary of an extremal surface have been presented. When a corner line is present on an extremal surface (i.e.,

the derivatives of the dependent variables z_k are discontinuous across a line on the extremal surface), a mathematical criterion is needed to join the subsurfaces of the extremal surface. This criterion is the Erdmann-Weirstrass corner condition.

The Erdmann-Weirstrass corner condition results from the following expression which must be satisfied in order for $\delta I = 0$:

$$\oint_C (\Delta K \delta\phi + \Delta Q \delta r + \sum_{k=1}^{4} \Delta R_k \delta z_k) d\phi = 0 \qquad (56)$$

where the line integral is along the corner lines on the extremal surface. In this work no restrictions are placed on the corner lines (i.e., the corner lines are free), and the six variations $\delta\phi$, δr and δz_k are independent and arbitrary along any corner line. From Eq. (56) it follows that at any point on a corner line the following six equations must be satisfied:

$$\Delta K = 0 \qquad (57)$$

$$\Delta Q = 0 \qquad (58)$$

$$\Delta R_k = 0 \qquad (k = 1,..,4) \qquad (59)$$

where K, Q and R_k are defined in Eqs. (26) through (28), and where the symbol $\Delta(\cdots)$ denotes the difference of the quantity $(\cdots)$ evaluated on the outer side of the corner line and the same quantity evaluated on the inner side. Equations (57) through (59) are the Erdmann-Weirstrass corner conditions for the case of the corner lines being free.

In Appendix G Eqs. (57) through (59) are evaluated for the fundamental function F given by Eq. (18), and it is shown that the corner line conditions for this problem are identically satisfied by the requirement that the dependent variables V, θ, ψ and f are continuous on the extremal surface. Therefore, no additional information is obtained from the

Erdmann-Weirstrass corner conditions.

3. COMPATIBILITY OF THE CONTROL SURFACE AND THE KERNEL

At this point there is no assurance that the equations which have been derived to describe the dependent variables V, θ, ψ and f will produce flow properties on the control surface which can be matched with the given flow in the kernel. If it can be shown that the control surface has the properties of a wave surface in a homentropic, isoenergetic, supersonic flow, then the matching of the flows is assured.

The necessary and sufficient conditions for a surface to be a wave surface are discussed in Appendix H. Briefly, the surface must be oriented in a direction tangent to a wave surface of the flow, and the variation of the flow properties along the surface must satisfy the compatibility equation that applies along wave surfaces in the flow. It can be shown that an optimal control surface is indeed tangent everywhere to a wave surface in the flow and that Eqs. (35) through (38) can be combined to derive the compatibility equation which must be satisfied along wave surfaces in the flow. Thus, the compatibility of the flow on the control surface with the flow in the kernel is assured. For details on the derivation of these conditions, see Appendix H.

4. SPECIAL CASE OF AXISYMMETRIC FLOW

If the six equations, Eqs. (35) through (39) and Eq. (55), correctly describe the control surface for a maximum thrust, fixed length, constant mass flow rate nozzle, then for an axisymmetric flow these equations will be compatible with the axisymmetric optimization equations as derived by Rao (2) and Guderley (3). For an axisymmetric flow $\psi \equiv 0$ and $\partial(\ )/\partial\phi \equiv 0$. Under these conditions, Eqs. (35) through (39) reduce to the following three equations:

$$\frac{V\cos(\theta - \mu)}{\cos\mu} = -\lambda_2 \tag{60}$$

$$\phi' = \theta + \mu \tag{61}$$

$$r\rho V^2 \sin^2\theta \tan\mu = -\lambda_3 \tag{62}$$

where $\phi' \equiv \beta - \pi/2$ and λ_3 is a constant. If the condition that $\psi \equiv 0$ is substituted into Eq. (55), the transversality equation can be rewritten as follows:

$$\left[(p - p_a) - \rho V^2 \sin\theta \cos\theta \tan\mu\right]\Big|_{\Gamma_e} = 0 \tag{63}$$

Equations (60) through (63) are identical to the equations which were derived by Rao (2) and Guderley (3). Thus, for axisymmetric flow the optimization equations for the three-dimensional problem reduce to the corresponding equations for the equivalent axisymmetric problem. For more details of the axisymmetric nozzle optimization analysis consult Appendix I.

SECTION III
NUMERICAL DEVELOPMENT

In this section the numerical solution procedure used to solve the design equations derived in Section II is presented. When these equations are solved using initial conditions obtained from a specified three-dimensional kernel, the solution yields the following information for a maximum thrust nozzle: 1) the position of the control surface, 2) the flow properties on the control surface, 3) the shape of the exit lip of the nozzle, 4) the thrust produced by the optimal nozzle and 5) the ambient pressure for which the nozzle is optimally designed. The design parameters which affect the features of maximum thrust nozzles are the initial contour, the initial value surface, and the position of the initial value line.

Before the numerical solution procedure used in this research is presented in detail some general comments should be made. There are several design procedures which could be used to design optimal three-dimensional nozzles. The possible approaches can be separated into the following two cases: 1) solve the problem as a two point boundary value problem and 2) solve the problem as an initial value problem. To solve the problem as a two point boundary value problem, conditions are specified on both the inner and outer boundary of the control surface (e.g., the flow in the kernel could be specified along with the desired shape of the exit lip, the desired nozzle length and the desired ambient pressure). When the problem is solved as a two point boundary value problem, a number of iterations are necessary before an optimal control surface is generated which satisfies the conditions at both boundaries. Treating the problem as an initial value problem makes it possible to calculate an optimal control surface with no iterations and then iterate between optimal solutions to match specific boundary conditions. Both

approaches are valid; however, they differ in complexity. In this research the problem is solved as an initial value problem since this is the most straightforward approach. The overall algorithm used in this approach is now presented.

The overall numerical algorithm consists of four basic steps which are discussed separately in this section. The four steps are listed below:

1) For a specified initial contour and starting surface in supersonic flow calculate the resulting flow field (kernel).
2) Determine the shape of an initial value line in the generated flow field which satisfies the design equations presented in Section II.
3) Use the conditions along the initial value line as initial conditions, and solve for the corresponding optimal control surface.
4) Determine the nozzle exit lip which corresponds to the optimal control surface which has been generated.

The above four steps are discussed in more detail on the following pages.

1. THREE-DIMENSIONAL KERNEL REGION

For a specified initial contour and starting conditions in a supersonic portion of the flow, the flow in the kernel can be calculated. Later in this section it will be shown that to obtain an optimal, three-dimensional nozzle, it is necessary to start with a three-dimensional kernel; therefore, all discussions concerning the kernel will be for three-dimensional flow fields.

In this work the theoretical development and associated computer program presented in Refs. (15) and (23) are used to analyze the flow in the kernel. The three-dimensional, supersonic, steady flow analysis is based on a method of characteristics numerical scheme which has second order accuracy. The computer program may be applied to analyze non-isoenergetic and nonhomentropic flows of a calorically perfect gas or homentropic flows of a real gas in chemical equilibrium. In this work

the flow on the noncharacteristic starting surface is restricted to an isoenergetic, homentropic flow of a perfect gas. Hence, the flow throughout the kernel is isoenergetic and homentropic since shocks waves are not treated by the flow analysis program, and the flow is assumed to be inviscid.

The procedure to generate a three-dimensional kernel is as follows: 1) specify an initial expansion contour which extends from a planar starting surface to a station which is downstream of the region where the initial value line will be located, 2) specify supersonic flow conditions on a planar starting surface which is normal to the z-axis and 3) utilize the three-dimensional flow analysis program to calculate the flow field downstream of the initial value surface. A planar starting surface is necessary since the integration process in the analysis program takes place between a series of planes parallel to the starting surface. Hence, more of the flow field than just that in the kernel is calculated. In fact, the extent of the kernel is not known until the initial value line in the three-dimensional flow has been constructed. To obtain a three-dimensional flow in the kernel it is possible to specify a three-dimensional contour, specify a three-dimensional flow on the starting surface or do both.

Since the flow field in the kernel will directly affect the contour of the particular maximum thrust nozzle that is generated, the initial expansion contour and starting surface should be chosen with care. When the numerical results are presented in Section IV, it will become clearer what defines a reasonable contour and starting surface. A more detailed discussion of the calculation of the flow in three-dimensional nozzles is presented in Appendix J.

2. INITIAL VALUE LINE

An initial value line is defined as the intersection of the boundary of the kernel with the optimal control surface. However, at this point in the numerical development the extent of the kernel has not been determined. Once the position of an allowable initial value line is determined, the extent of the kernel can be determined, and the control

surface corresponding to the particular initial value can be numerically determined.

Since an initial value line is the inner boundary of an optimal control surface, not only must the conditions along an initial value line match the conditions in the kernel, but they must also satisfy the set of design equations that define an optimal control surface (i.e., Eqs. (35) through (39)). Therefore, the following equations must be satisfied along an initial value line:

$$V\cos\theta + \lambda_2 = - V\sin\theta \tan\mu \tag{64}$$

$$\alpha = \psi \tag{65}$$

$$\beta = \theta + \mu + \pi/2 \tag{66}$$

$$df = (\partial f/\partial r)dr + (\partial f/\partial \phi)d\phi \tag{67}$$

where λ_2 is a constant and

$$\partial f/\partial r = - \tan\beta\cos\alpha \tag{68}$$

$$\partial f/\partial \phi = - r\tan\beta\sin\alpha \tag{69}$$

Equations (38) and (39) do not specify any conditions that can be evaluated along an initial value line; therefore, they are not included in the above set of equations. For Eq. (64) to be satisfied along an initial value line, the values of V, θ and μ at all points along the initial value line must be such that

$$- V(\cos\theta + \sin\theta\tan\mu) = \lambda_2 \tag{70}$$

where λ_2 has the same constant value at all points. By substituting Eqs.

(65), (66), (68) and (69) into Eq. (67), Eq. (67) can be rewritten in the following form:

$$df = - \tan(\theta + \mu + \pi/2)(\cos\psi dr + r\sin\psi d\phi) \tag{71}$$

By choosing an initial value line to satisfy Eqs. (70) and (71), the initial value line will be compatible with the optimal control surface.

For a specified initial contour and starting surface the specification of the position of one point which must lie on the initial value line and the application of Eqs. (70) and (71) are sufficient to determine a unique initial value line in the generated flow field. The details concerning the manner in which Eqs. (70) and (71) are applied are presented in Appendix J.

Before continuing it should be noted that, in general, in an axisymmetric flow field, Eqs. (70) and (71) are only satisfied along axisymmetric curves in the flow. Only an optimal axisymmetric nozzle can be designed from an initial value line along which r, z, M, θ and ψ are constant. Therefore, in general, it is necessary to have a three-dimensional kernel to be able to design an optimal three-dimensional nozzle.

3. CONTROL SURFACE

The equations which govern the shape of the control surface and the flow variables on the control surface were derived in Section II. Three of the equations, Eqs. (35), (38) and (39), are written in such a form that they contain only three of the dependent variables $V(r,\phi)$, $\theta(r,\phi)$ and $\psi(r,\phi)$. Equations (35), (38) and (39) can be solved numerically for these three dependent variables where the initial value line serves as the inner boundary to the control surface and gives initial conditions for the solution.

If Eq. (35) is differentiated, solved for the quantity $d\theta/dV$, and combined with the following two equations which are derived in Appendix B,

$$d\mu = - 1/\left[M(M^2 - 1)^{1/2}\right] dM \tag{72}$$

$$dM = \left[1 + (\gamma-1)M^2/2\right]/a \; dV \tag{73}$$

then the following equation is obtained:

$$d\theta = \frac{\left[\frac{(M^2-1)^{1/2}\cos\theta + \sin\theta}{M(1 + (\gamma-1)M^2/2)}\right] - \frac{M\sin\theta}{(M^2-1)}}{\left[(M^2 - 1)^{1/2}\sin\theta - \cos\theta\right]} dM \tag{74}$$

If Eqs. (38) and (39) are expanded and Eqs. (72) through (74) are used to eliminate derivatives of ρ, V, and θ, Eqs. (38) and (39) can be rewritten in the following form:

$$D_8 \frac{\partial M}{\partial r} + D_9 \frac{\partial M}{r\partial \phi} + D_5 \frac{\partial \psi}{\partial r} + D_6 \frac{\partial \psi}{r\partial \phi} + D_7 = 0 \tag{75}$$

$$H_1 \frac{\partial M}{\partial r} + H_2 \frac{\partial M}{\partial \phi} + H_5 \frac{\partial \psi}{\partial r} + H_6 \frac{\partial \psi}{r\partial \phi} + H_7 = 0 \tag{76}$$

The coefficients in Eqs. (75) and (76) are functions of the Mach number M and the flow angles θ and ψ. The expressions for the coefficients are given in Appendix K.

In order to numerically solve the set of first order, quasi-linear, partial differential equations given by Eqs. (74) through (76), it is necessary to determine the nature of the set of equations. By putting Eqs. (75) and (76) into a form suitable for solution by the method of characteristics, it can be shown numerically that the slopes of the characteristic directions of the equations are real in the domain of interest. Thus, the partial differential equations are hyperbolic, and a marching numerical scheme can be used for their solution.

To solve the hyperbolic set of equations, the two partial differential equations, Eqs. (75) and (76), are put into characteristic form by using the theory of the method of characteristics. Thus, the two partial

differential equations are replaced by two ordinary differential equations called compatibility equations. Each of the compatibility equations is valid along a characteristic direction. The equations for the slopes of the characteristic directions are obtained by the application of the method of characteristics.

The two ordinary differential compatibility equations, in combination with the equations for the characteristic directions and Eq. (74), are solved by expressing these five equations in finite difference form and employing a modified Euler numerical solution scheme. The details of the equations, procedures and mesh used in the solution are presented in Appendix K.

With the values of the variables $V(r,\phi)$, $\theta(r,\phi)$ and $\psi(r,\phi)$ known on the control surface for a specified initial value line, Eq. (71) is solved for $f(r,\phi)$ by expressing the differential equation in the following form:

$$f_2 = f_1 - (r_2 - r_1)\left[\tan(\theta + \mu + \pi/2)\cos\psi\right]\Big|_{\text{average}} - (\phi_2 - \phi_1)\left[r\tan(\theta + \mu + \pi/2)\sin\psi\right]\Big|_{\text{average}} \qquad (77)$$

where the averages are between points 1 and 2. Equation (77) is applied between mesh points on the control surface using the initial value line as an initial condition.

For a specified kernel and initial value line the solution for the control surface is continued radially outward to a radius such that the exit lip of the nozzle will lie inside the outer boundary of the solution surface. Since the position of the nozzle exit lip corresponding to the specified kernel and initial value line is not known beforehand, the point at which to stop constructing the control surface depends on the amount of mass flow crossing the control surface. More about the procedure at this point in the solution is presented in Appendix K.

4. NOZZLE EXIT LIP

The equation which must be satisfied along the exit lip of an optimal fixed length nozzle has the following form:

$$\left[(p-p_a) + \rho V^2 \sin\theta\tan\mu\left(-\cos\theta + \frac{\sin\theta\sin\psi}{r_e}\frac{df_e}{d\phi_e}\right)\right]\Bigg|_{\Gamma_e} = 0 \qquad (78)$$

Equation (78) is used to determine the shape of the exit lip of an optimal nozzle after the control surface has been constructed. It should also be noted that the optimal exit lip must also satisfy Eq. (13) so that the constant mass flow rate constraint is satisfied.

To apply Eq. (78) the equation is rewritten as the following finite difference equation:

$$f_{2_e} = f_{1_e} + \left[\frac{r\rho V^2 \sin\theta\cos\theta\tan\mu - r(p-p_a)}{\rho V^2 \sin^2\theta\tan\mu\sin\psi}\right]\Bigg|_{\text{average}} (\phi_2 - \phi_1) \qquad (79)$$

For a known control surface $V(r,\phi)$, $\theta(r,\phi)$, $\psi(r,\phi)$, $p(r,\phi)$, $\rho(r,\phi)$ and $f(r,\phi)$ are available to use in Eq. (79). If one point on a known control surface is assumed to lie on the exit lip corresponding to the control surface, a second point on the exit lip can be determined by picking a ϕ_2 and iterating until a f_{2_e} is found which satisfies Eq. (79). This process can be continued around the exit lip until an entire curve on the control surface has been constructed. Since Eq. (79) contains the quantity p_a, it is necessary to assume a value for p_a when the first point on the exit lip is picked. Unless the correct value of p_a is chosen, the curve which is generated using Eq. (79) will not be a closed curve. Thus, an iterative process is necessary to determine the value of p_a which yields a closed curve.

Once a closed curve has been generated on an optimal control surface, then the mass flow rate through the portion of the control surface

bounded by the initial value line and the exit lip is calculated. Since the total mass flow rate which passes through the nozzle and the mass flow rate which passes through the exit of the nozzle interior to the initial value line can be calculated, the required value of $\dot{m}_{c.s.}$ is known.

If the first complete exit lip which is generated does not satisfy the mass flow rate constraint, a new first point for another exit lip and another p_a value are chosen. If the calculated value of $\dot{m}_{c.s.}$ is less than the required value, the new first point is chosen to be at a larger radius than the original first point, and vice versa. The correct value of p_a for the new point is determined as explained above, and a second candidate exit lip is generated. This process is continued until a closed curve on the control surface is found which allows the correct mass flow rate to pass across the control surface and satisfies Eq. (79). The details on the numerical solution for the optimal exit lip are presented in Appendix L.

SECTION IV
THREE-DIMENSIONAL OPTIMAL NOZZLE RESULTS

In this section results are presented for nine optimal nozzles which have been numerically generated using the theory presented in Sections I, II and III. Solutions for three different initial expansion contours are presented to illustrate the general capabilities of the technique and to illustrate general trends which have been observed. The cases presented are not necessarily directed toward any specific applications but are representative of the types of nozzles which might be considered for either rocket, ramjet or scramjet nozzles.

1. INTRODUCTION

The optimal control surfaces for several maximum thrust, three-dimensional nozzles have been generated numerically in the course of this research. The primary results for nine of these optimal nozzles are discussed in this section and are illustrated in Figures 5 through 28. In each case the kernel region was computed for a prescribed set of initial conditions (i.e. a prescribed initial expansion contour and a prescribed start condition) using the three-dimensional method of characteristics program described in Refs. (15) and (23). In each case a circular initial expansion contour was specified with parallel uniform flow of Mach number 1.05 at the throat. Also, it was assumed that two planes of symmetry exist. This is not essential to the general optimization procedure, but it does permit a considerable reduction in computational time while investigating the salient features of the method.

The nine optimal nozzles are divided into three sets of three nozzles each. Each set of nozzles has been designed using a different initial expansion contour. The three sets of initial expansion contours differ in their throat radii and their radii of curvature, but all sets have initial expansion contours which are elliptical in cross section.

In this work the term throat is used to denote the cross section of the nozzle where the starting conditions are specified. Since the nozzle contour is not specified upstream of the throat, it is not known that the throat section is actually a minimum area section. Thus, the results are not restricted to converging-diverging nozzles.

Since no convenient dimension exists to nondimensionalize the length and radius of three-dimensional nozzles, the actual dimensions are shown in inches. Of course, all dimensions can be scaled upward or downward.

The thrust coefficients of the optimal three-dimensional nozzles are nondimensionalized with respect to the thrust coefficient of the ideal (perfect) nozzle designed for the same ambient pressure, stagnation pressure and specific heat ratio. For an ideal nozzle $C_{f_{ideal}}$ is given by the following equation:

$$C_{f_{ideal}} = \left[\frac{2\gamma^2}{\gamma-1}\left(\frac{2}{\gamma+1}\right)^{(\gamma+1)/(\gamma-1)}\left(1 - (p_a/p_o)^{(\gamma-1)/\gamma}\right)\right]^{1/2} \qquad (80)$$

The pressure ratio for which the three-dimensional nozzles are optimally designed are expressed as dimensionless ratios of the form (p_o/p_a) where p_o is the stagnation pressure and p_a is the ambient pressure. The values of (p_o/p_a) range from 11.1 to 470.0 for the nine nozzles shown in this report.

As each optimal nozzle is discussed, it should be remembered that each nozzle produces the maximum axial thrust for the following set of conditions: 1) starting flow conditions, 2) initial expansion contour, 3) length, exit lip shape and flow conditions along the exit lip and 4) ambient pressure. Therefore, each of the nozzles discussed here is optimally designed for a unique set of conditions. It should also be pointed out that the determination of the actual optimal nozzle contour is not a part of this research; however, many important features of optimal three-dimensional nozzles can be determined without knowing the entire nozzle contour.

The flow is irrotational on each starting surface since the flow is uniform and parallel; therefore, the flow on an optimal control surface generated using an initial value line in this irrotational flow field must also be irrotational. In each of the nine cases presented here it has been numerically shown that the flow on the optimal control surface is irrotational.

The results for the nine sample optimal nozzles are now presented. As discussed above, the nine nozzles are divided into three sets of three nozzles each. These three sets are referred to as Case A, Case B and Case C, and the sets of nozzles differ in their throat shapes and their throat radius of curvature. For convenience Figures 5 through 28 are grouped together at the end of this section.

2. CASE A

The three optimal nozzles in Case A were designed from a kernel region produced by an initial expansion contour with a radius of curvature of one inch and an elliptical throat cross section with a major diameter equal to four inches and a minor diameter equal to two inches. In each case a different amount of the initial expansion contour is a part of the optimal contour since the extent of the kernel is different for each of the three optimal nozzles.

A. Optimal Nozzle 1

Figure 5 shows the intersection of optimal nozzle 1 with the two planes of symmetry (i.e., the $\phi = 0°$ and $\phi = 90°$ planes). The figure shows the initial expansion contour, the extent of the kernel, and the optimal control surface. As shown in Figure 5 the optimal nozzle does not end in a plane or have a constant exit radius.

Figure 6 shows the values of r, z, M, θ and ψ along the initial value line for $0° \leq \phi \leq 90°$. As shown in the figure, the initial value line lies very nearly in a plane; however, the radius of the initial value line is a strong function of the polar angle ϕ. Also, the values of M, θ and ψ vary in a smooth fashion along the initial value line. The values of the flow angle ψ($-11.6° \leq \psi \leq 0.0°$) along the initial

value line illustrate that the flow is indeed three-dimensional.

Figure 7 shows the values of the flow variables M, θ and ψ on the optimal control surface. The values of M, θ and ψ are shown as functions of radius along the ϕ = 0°, 45° and 90° planes. As shown the Mach number on the control surface increases with radius while the flow angle θ on the control surface decreases with radius. A very interesting result is shown by the plot of $\psi(45°)$ as a function of radius (The flow angle ψ is identically equal to zero on the two planes of symmetry.). In the ϕ = 45° plane the value of ψ on the control surface very rapidly decreases in absolute value from 11.6° to 0.0° and then slowly increases in absolute value to reach a value of 1.25° at the exit lip. This indicates that the flow on the control surface near the initial value line has a cross flow component in the counterclockwise direction (facing the positive z direction), while on the control surface near the exit lip the flow has a cross flow component in the clockwise direction.

Figure 8 shows the values of r, z, M, θ and ψ along the exit lip of optimal nozzle 1. As shown the radius of the exit lip varies from 4.6 inches to 2.8 inches, and the nozzle does not end in a plane (9.2 inches $\leq$ length $\leq$ 13.8 inches). The figure also shows that the Mach number is constant along the exit lip, while the flow angle θ varies slightly from a mean value. Also along the exit lip the flow angle ψ varies as a function of ϕ($-.30 \leq \psi \leq 1.25°$).

Figure 9 shows the projections of the throat, the initial value line, and the exit lip on the r,ϕ-plane. An interesting and unexpected result is illustrated in this figure. Figure 9 shows that the maximum thrust nozzle corresponding to the elliptical initial flow (throat) has an exit lip which has a generally elliptical projection on the r,ϕ-plane but with the orientation of the ellipse rotated by 90 degrees. Figure 10 summarizes portions of the results presented in Figures 5 through 9 by presenting the results in tabular form.

The nozzle illustrated in Figures 5 through 10 is optimally designed for a pressure ratio of $(p_o/p_a) = 49.7$. Also the ratio $C_f/C_{f_{ideal}}$ is equal to 0.996 where the perfect nozzle is designed for the same pressure ratio.

To further evaluate the performance of this maximum thrust, three-dimensional nozzle a three-dimensional comparison nozzle was designed and analyzed using the three-dimensional flow analysis program described in Refs. (15) and (23). The starting flow conditions and initial expansion contour for the comparison nozzle were identical to those of optimal nozzle 1. The length and exit radius of the comparison nozzle was chosen so that the comparison nozzle was not overexpanded for a pressure ratio of $(p_o/p_a) = 49.7$. The comparison nozzle was 12.8 inches long and had an exit radius of 5.0 inches. For this three-dimensional nozzle $C_f/C_{f_{ideal}} = 0.940$ when the nozzle is operating at an ambient pressure such that $(p_o/p_a) = 49.7$. Similar results were obtained for other comparison three-dimensional nozzles which were designed with overall dimensions similar to nozzle 1. Since the flow analysis program (23) is not written to handle free pressure boundaries, only three-dimensional nozzles for which the exit lip was in a plane were analyzed.

B. Optimal Nozzle 2

Figure 11 shows the intersection of optimal nozzle 2 with the two planes of symmetry. The figure shows the initial expansion contour, the extent of the kernel, and the optimal control surface. As shown in Figure 11 optimal nozzle 2 does not end in a plane, and its exit radius is a function of the polar angle ϕ. By comparing Figure 11 to Figure 5 it can be seen that the initial value line for nozzle 2 is farther downstream and at a larger radius than the initial value line for nozzle 1.

Figure 12 shows the values of r, z, M, θ and ψ along the initial value line of optimal nozzle 2. As was the case with nozzle 1, the values of r, z, M, θ and ψ vary along the initial value line. By comparing the initial value line of nozzle 2 with the initial value line of nozzle 1, it is seen that the initial value line of nozzle 2 is in a region of higher Mach number, higher divergence angle θ and lower absolute value of the flow angle ψ. Thus, the equations which define the optimal control surface have different initial conditions in the two cases.

Figure 13 shows the values of the flow variables M, θ and ψ on the optimal control surface of optimal nozzle 2. As shown, the Mach number

increases with radius while the flow angle θ decreases with radius. Again the angle $\psi(45°)$ decreases in absolute value, passes through zero and then slowly increases to a value of 2.09°. This variation of ψ is similar to that observed in Figure 7; however, for optimal nozzle 2 $\partial^2\psi(45°)/\partial^2 r > 0$ on the control surface near the initial value line, while for optimal nozzle 1 $\partial^2\psi(45°)/\partial^2 r < 0$ on the control surface near the initial value line.

Figure 14 shows the values of r, z, M, θ and ψ along the exit lip. The radius of the exit lip varies from 5.80 inches to 3.88 inches. The value of the Mach number is constant, while the flow angle θ varies slightly ($7.94° \leq \theta \leq 8.14°$). Also, along the exit lip $-0.30° \leq \psi \leq 2.09°$.

Figure 15 shows the projections of the throat, the initial value line and the exit lip on the rϕ-plane. Again the results show that the maximum thrust nozzle corresponding to the elliptical initial flow (throat) has an exit lip which has a generally elliptical projection on the rϕ-plane but with the orientation of the ellipse rotated by 90°. Figure 15 also shows that the projection of the exit lip of optimal nozzle 2 is more nearly rectangular than that of optimal nozzle 1. It is also interesting to note that the exit lip dips in slightly near both planes of symmetry. Figure 16 summarizes portions of the information presented in Figures 11 through 15.

Optimal nozzle 2 is designed to operate at a pressure ratio of $(p_o/p_a) = 170.0$. Thus, if both nozzle 1 and nozzle 2 are operated for identical stagnation pressures, nozzle 2 is optimally designed for a lower ambient pressure. The performance of optimal nozzle 2 is such that $C_f/C_{f_{ideal}} = 0.984$ where the comparison perfect nozzle is also designed for a pressure ratio of $(p_o/p_a) = 170.0$.

To further evaluate the performance of this optimally designed three-dimensional nozzle, a comparison three-dimensional nozzle was analyzed. The starting flow conditions and initial expansion contour for the comparison nozzle were identical to those of nozzle 2. The comparison nozzle was 12.33 inches long and had a circular exit lip with a radius of 6.45 inches. For this three-dimensional nozzle $C_f/C_{f_{ideal}} = 0.958$ when the nozzle is operated at a pressure ratio of $(p_o/p_a) = 170.0$.

C. Optimal Nozzle 3

Figures 17 through 22 present the numerical results for optimal nozzle 3. Nozzle 3 has the same throat region as nozzles 1 and 2; however, the extent of the kernel is different. The initial value line of nozzle 3 is farther downstream than the initial value line of either nozzle 1 or nozzle 2. Also, optimal nozzle 3 is longer and has a larger projected exit area than either optimal nozzle 1 or optimal nozzle 2.

The results are generally similar to the results presented for nozzles 1 and 2, but there are some differences. As shown in Figures 20 through 22, the variations of r, z, M, θ and ψ along the exit lip do not vary in as smooth a manner as is the case with nozzles 1 and 2. These variations result from the more irregular variations in r, z, M, θ and ψ along the initial value line (see Figure 18).

Optimal nozzle 3 is designed to operate at a pressure ratio of 314.0. The thrust performance of the nozzle is such that $C_f/C_{f_{ideal}} = 0.993$. A comparison three-dimensional nozzle with a length of 20.0 inches and an exit radius of 7.0 inches was analyzed and for this comparison nozzle $C_f/C_{f_{ideal}} = 0.960$ when evaluated at a pressure ratio of $(p_o/p_a) = 314.0$.

3. CASE B

The three optimal nozzles in Case B were generated from a kernel region produced by an initial expansion contour with a radius of curvature of 1.2 inches in the $\phi = 0°$ plane of symmetry and a radius of curvature of 1.0 inch in the $\phi = 90°$ plane of symmetry. The throat of each of the nozzles has an elliptical cross section with a minor diameter of 2.0 inches in the $\phi = 0°$ plane and a major diameter of 2.4 inches in the $\phi = 90°$ plane. The rest of the initial expansion contour for $0° < \phi < 90°$ is composed of a smooth transition section. Therefore, the initial expansion contours of the nozzles in Case B are less axisymmetric than the initial expansion contours used in Case A.

A. Optimal Nozzle 4

Figure 23 summarizes the numerical results for optimal nozzle 4. The projection on the rϕ-plane of the throat, the initial value line and the

exit lip are shown for one quadrant of the nozzle. In the table the values of z, θ, M and ψ along the initial value line and along the exit lip are tabulated as functions of the polar angle ϕ.

As shown in Figure 23 optimal nozzle 4 has a three-dimensional shape, but it is less axisymmetric than the nozzles in Case A. Nozzle 4 is optimally designed for pressure ratio of $(p_o/p_a) = 21.55$. The overall performance of the nozzle is such that $C_f/C_{f_{ideal}} = 0.991$.

B. Optimal Nozzle 5

Figure 24 summarizes the numerical results for optimal nozzle 5. Nozzle 5 was generated using an initial value line which is at a larger radius and is farther downstream than the initial value line for nozzle 4. The result is that nozzle 5 is a longer nozzle with a larger exit radius and is designed for a higher pressure ratio ($(p_o/p_a) = 66.6$). As with the previous four optimal nozzles, optimal nozzle 5 has a projected exit lip which is generally elliptical in shape, but the orientation of the major axis is rotated 90° from the major axis of the throat. For optimal nozzle 5, $C_f/C_{f_{ideal}} = 0.974$.

C. Optimal Nozzle 6

Figure 25 summarizes the numerical results for optimal nozzle 6 (note that different scales are used in the plots on Figures 23 through 25). Nozzle 6 is the most symmetric nozzle presented up to point, and it was generated using the most symmetric initial value line that has been presented. Nozzle 6 is optimally designed for a pressure ratio of $(p_o/p_a) = 470.0$, and has a performance such that $C_f/C_{f_{ideal}} = 0.997$.

4. CASE C

The three optimal nozzles in Case C were generated from a kernel region produced by an initial expansion contour with a radius of curvature of 0.5 inches in the $\phi = 0°$ plane of symmetry and a radius of curvature of 1.0 inches in the $\phi = 90°$ plane of symmetry. The throat of each of the nozzles has a circular cross section with a 1.0 inch

radius. The rest of the initial expansion contour is composed of a smooth transition section along which the radius of curvature varies from 0.5 inches to 1.0 inch.

A. Optimal Nozzle 7

Figure 26 summarizes the numerical results for optimal nozzle 7. The exit radius of optimal nozzle 7 varies from 1.40 inches to 1.61 inches while the length varies from 2.75 inches to 3.07 inches. This nozzle is optimally designed for a pressure ratio of $(p_o/p_a) = 11.1$ and has a performance such that $C_f/C_{f_{ideal}} = 0.998$.

B. Optimal Nozzle 8

Figure 27 summarizes the numerical results for optimal nozzle 8. The initial value line for nozzle 8 is in nearly the same $r\phi$-plane as the initial value line for nozzle 7, but it has a larger radius. The result of the two different initial value lines is that nozzle 8 has a larger projected area than nozzle 7, but nozzle 8 is shorter than nozzle 7.

Nozzle 8 is optimally designed for a pressure ratio of $(p_o/p_a) = 19.6$. Its thrust performance is such that $C_f/C_{f_{ideal}} = 0.982$.

C. Optimal Nozzle 9

Figure 28 summarizes the numerical results for optimal nozzle 9. The initial value line for nozzle 9 is in nearly the same $r\phi$-plane as the initial value lines for nozzle 8 and 9, but it is at a larger radius than either of the other two initial value lines. Also the values of M and θ are higher on the initial value line for nozzle 9 than on the initial value lines for nozzles 7 or 8. The result is that nozzle 9 has the greatest projected exit area, the shortest length and the highest design pressure ratio ($(p_o/p_a) = 29.8$). The thrust coefficient ratio for optimal nozzle 9 is $C_f/C_{f_{ideal}} = 0.963$.

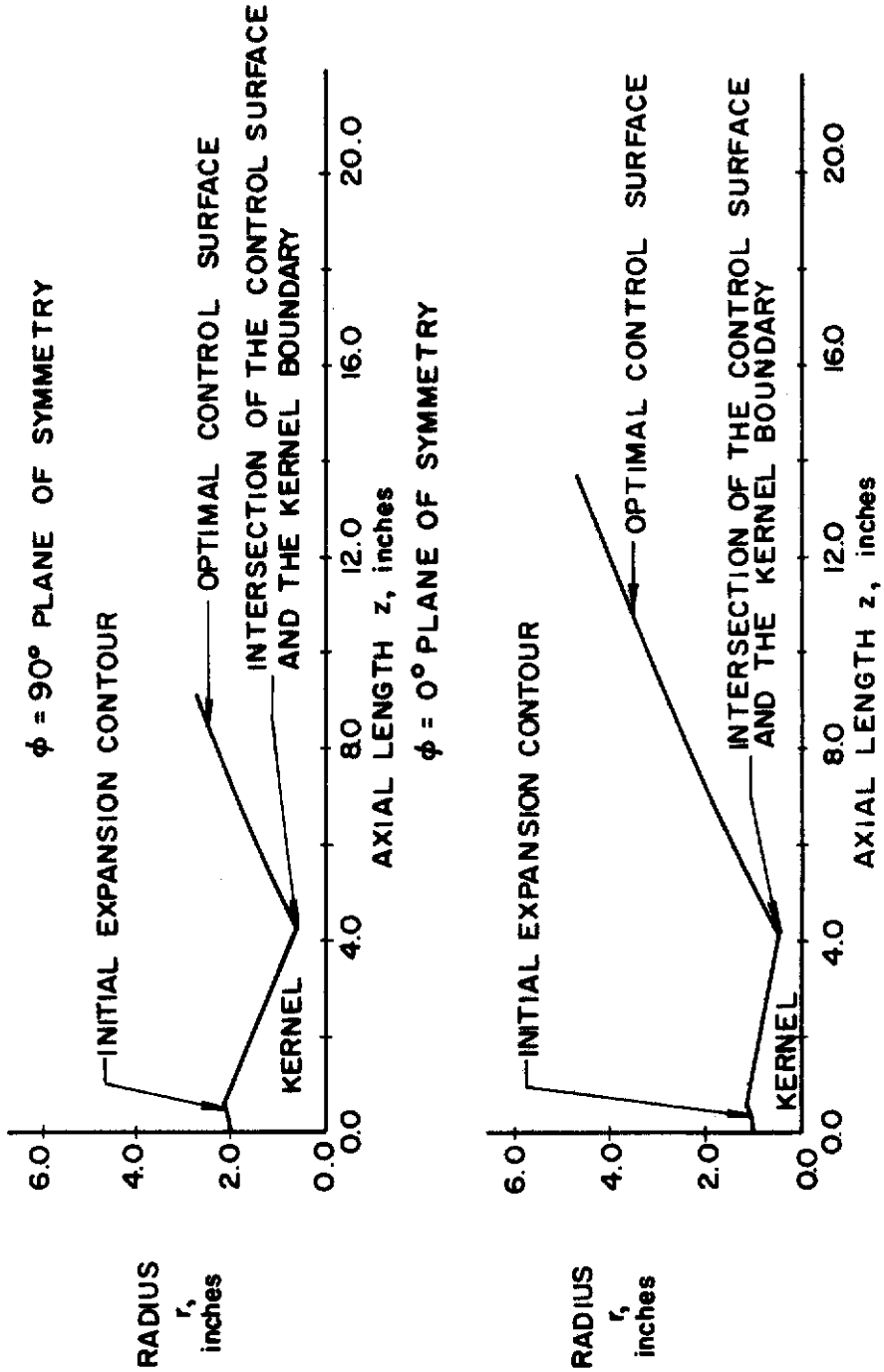

FIGURE 5. PLANE OF SYMMETRY VIEWS OF OPTIMAL NOZZLE I

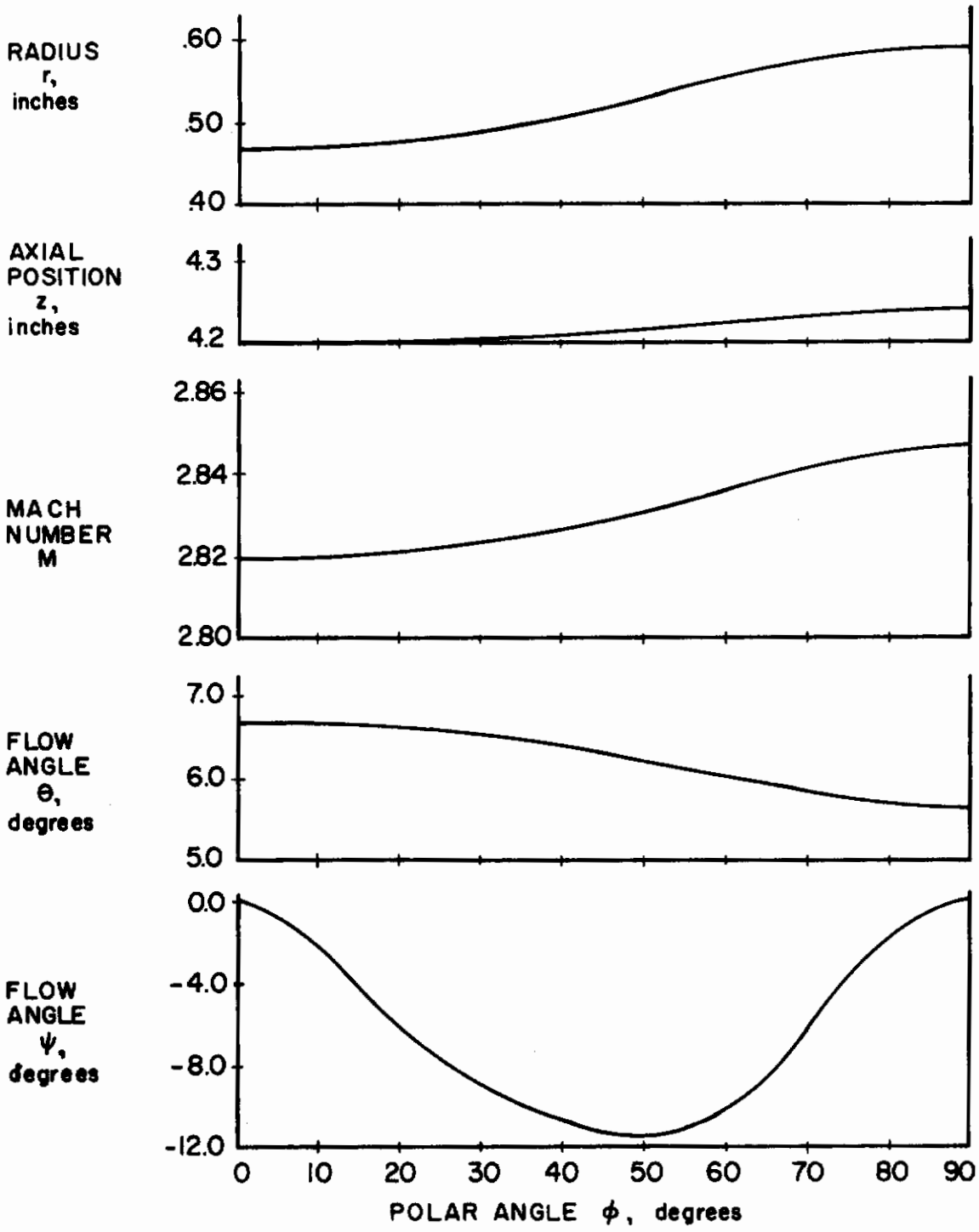

FIGURE 6. INITIAL VALUE LINE FOR OPTIMAL NOZZLE I

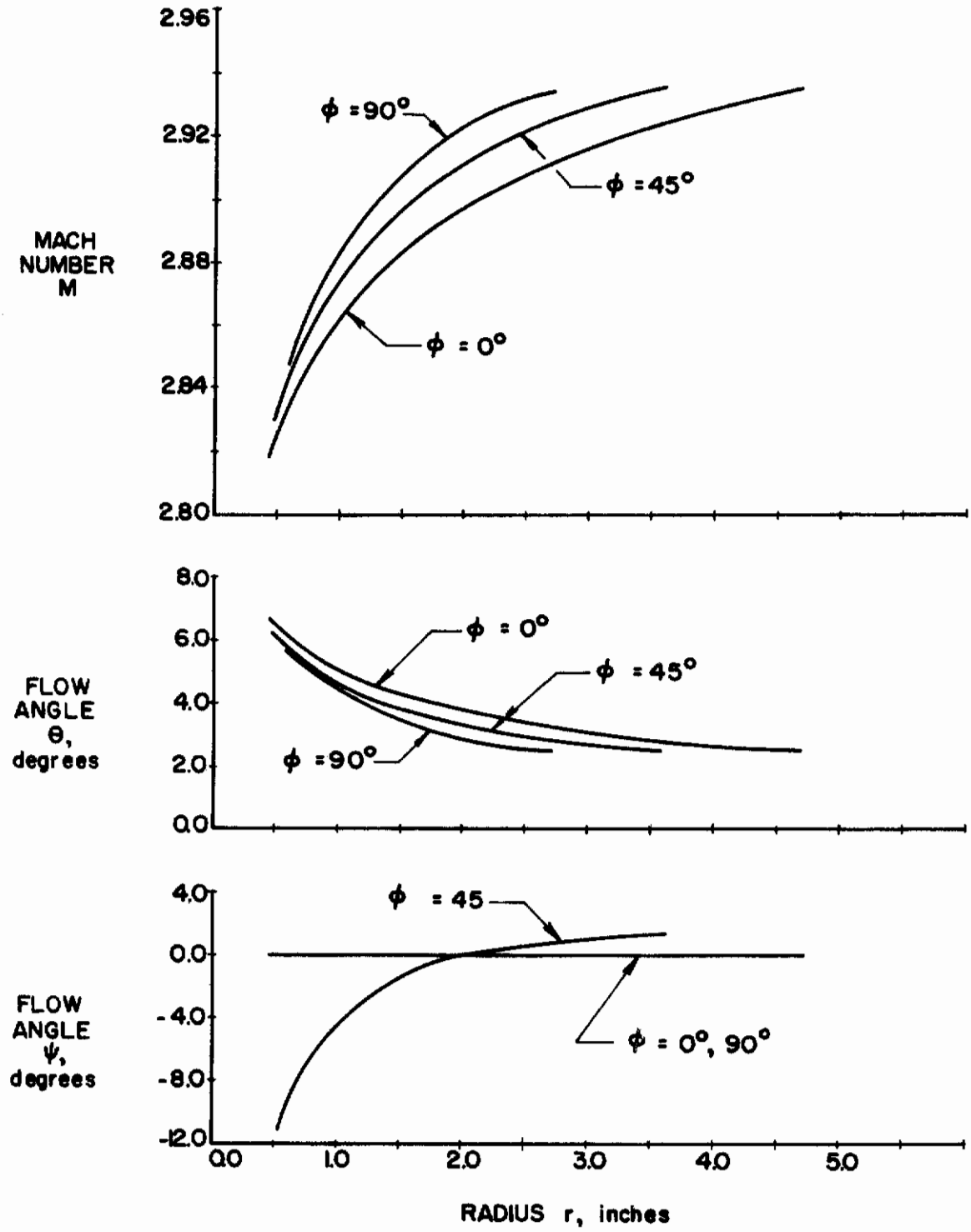

FIGURE 7. CONTROL SURFACE FOR OPTIMAL NOZZLE I

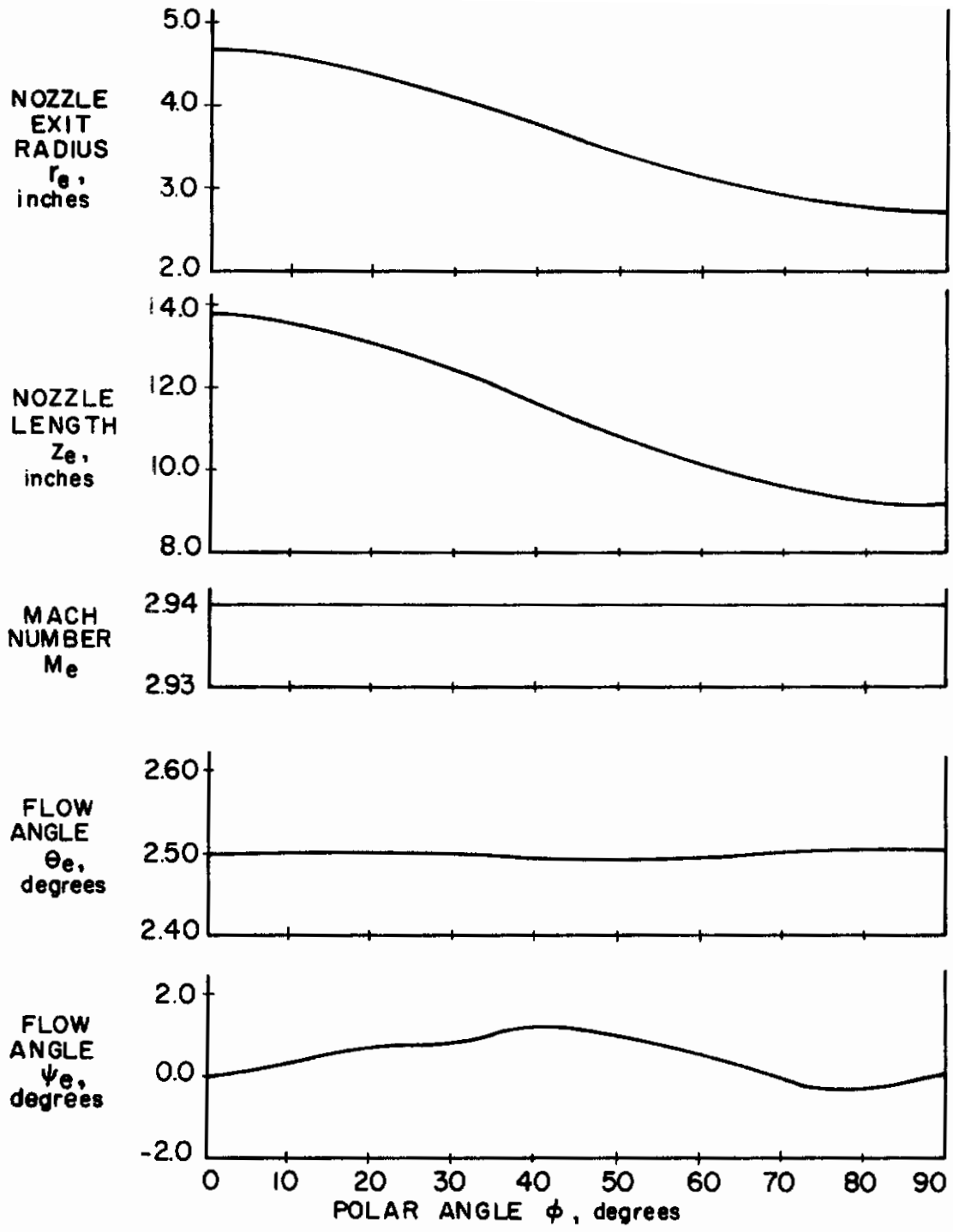

FIGURE 8. EXIT LIP FOR OPTIMAL NOZZLE I

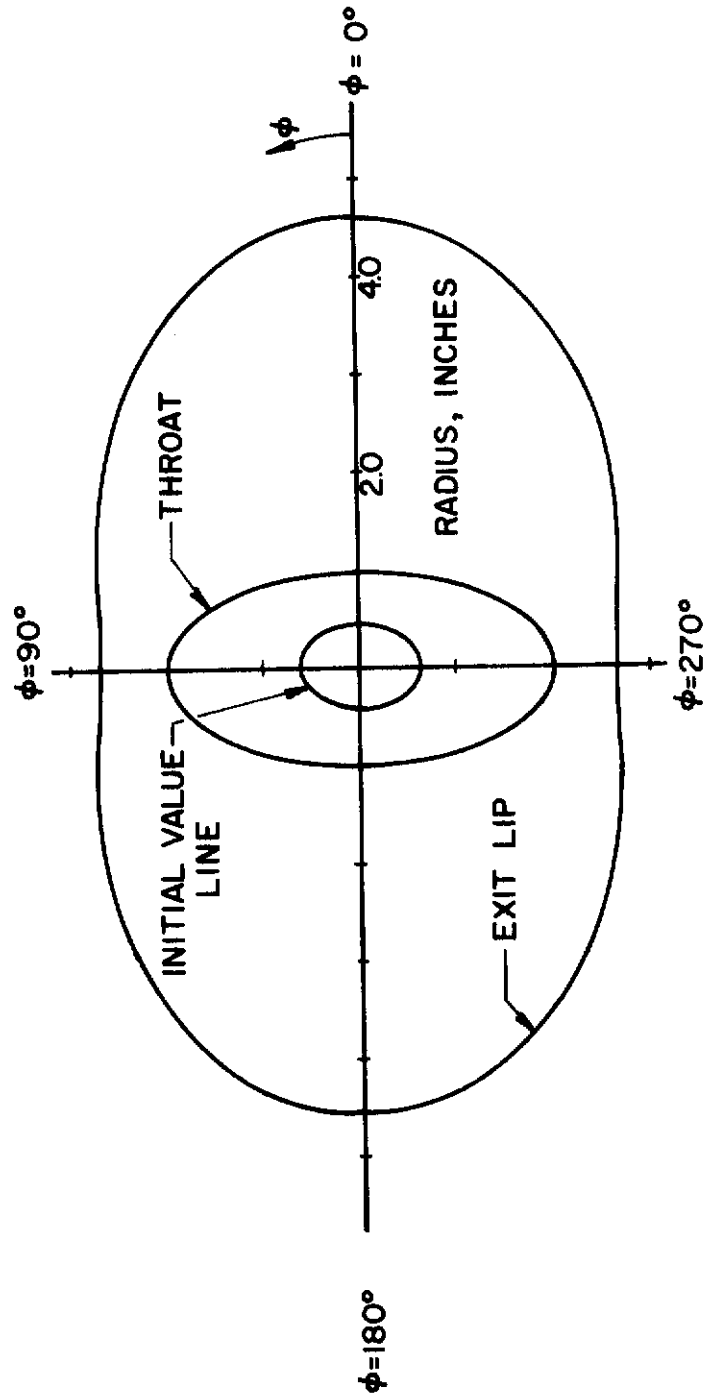

FIGURE 9. PROJECTION ON THE r,φ-PLANE OF OPTIMAL NOZZLE I

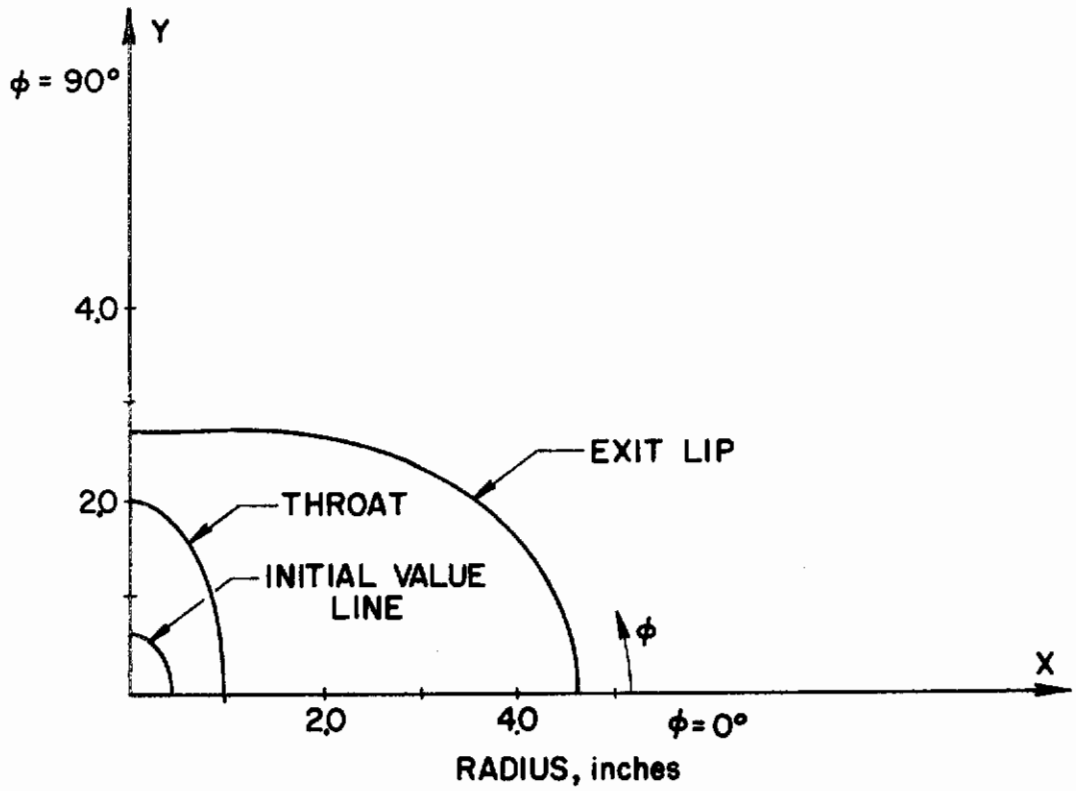

ϕ	Z_{IVL}	θ_{IVL}	M_{IVL}	ψ_{IVL}	Z_e	θ_e	M_e	ψ_e
0.0°	4.20"	6.65°	2.82	0.00°	13.8"	2.50°	2.94	0.00°
15.0	4.20	6.62	2.82	- 3.85	13.3	2.50	2.94	0.52
30.0	4.21	6.52	2.82	- 8.94	12.3	2.49	2.94	0.80
45.0	4.21	6.30	2.83	-11.43	11.3	2.49	2.94	1.25
60.0	4.22	6.05	2.84	-10.26	10.1	2.50	2.94	0.46
75.0	4.24	5.76	2.84	- 3.61	9.4	2.50	2.94	-0.30
90.0	4.24	5.66	2.84	0.00	9.2	2.50	2.94	0.00

FIGURE 10. SUMMARY FOR OPTIMAL NOZZLE 1

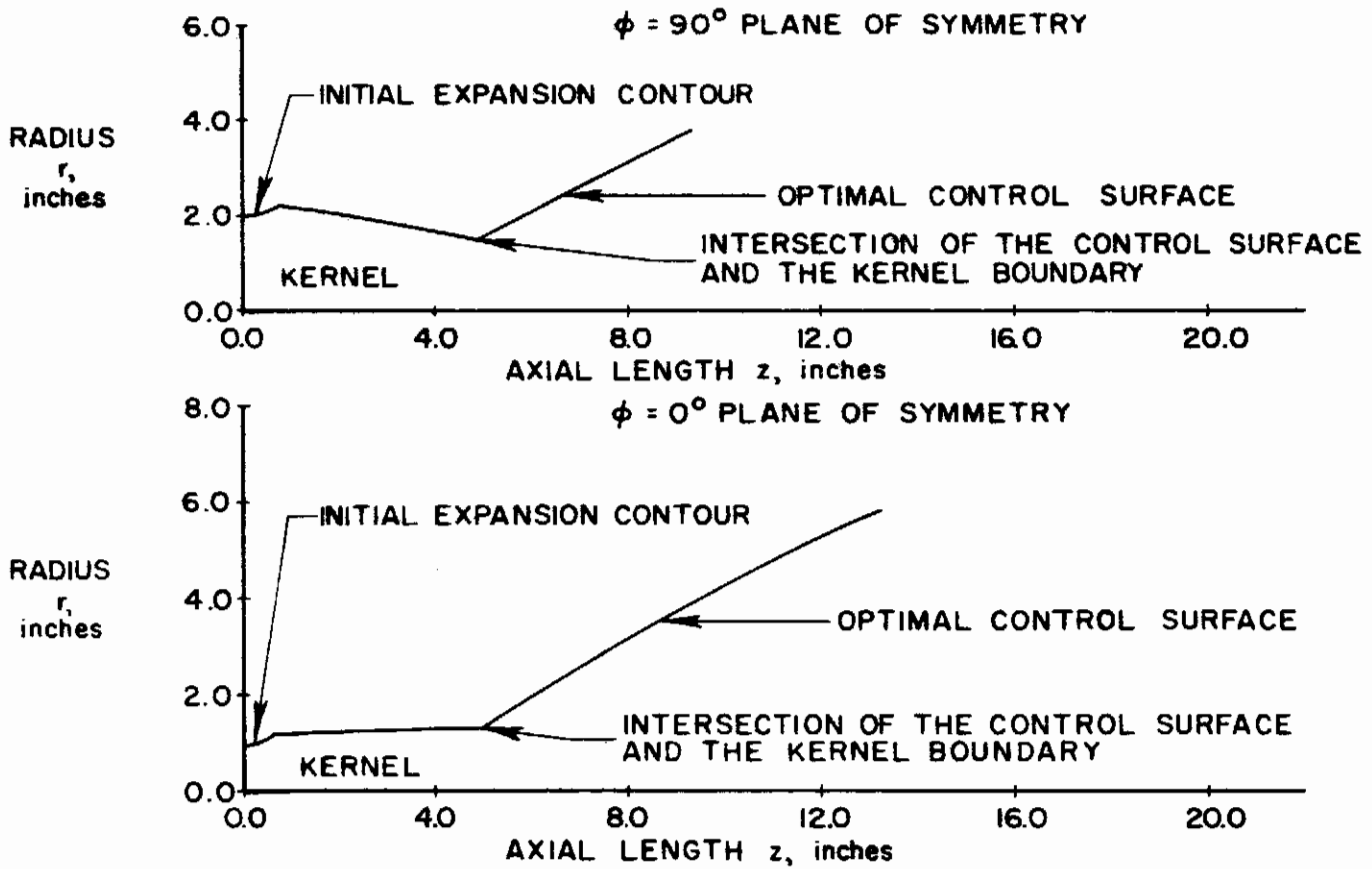

FIGURE II. PLANE OF SYMMETRY VIEWS OF OPTIMAL NOZZLE 2

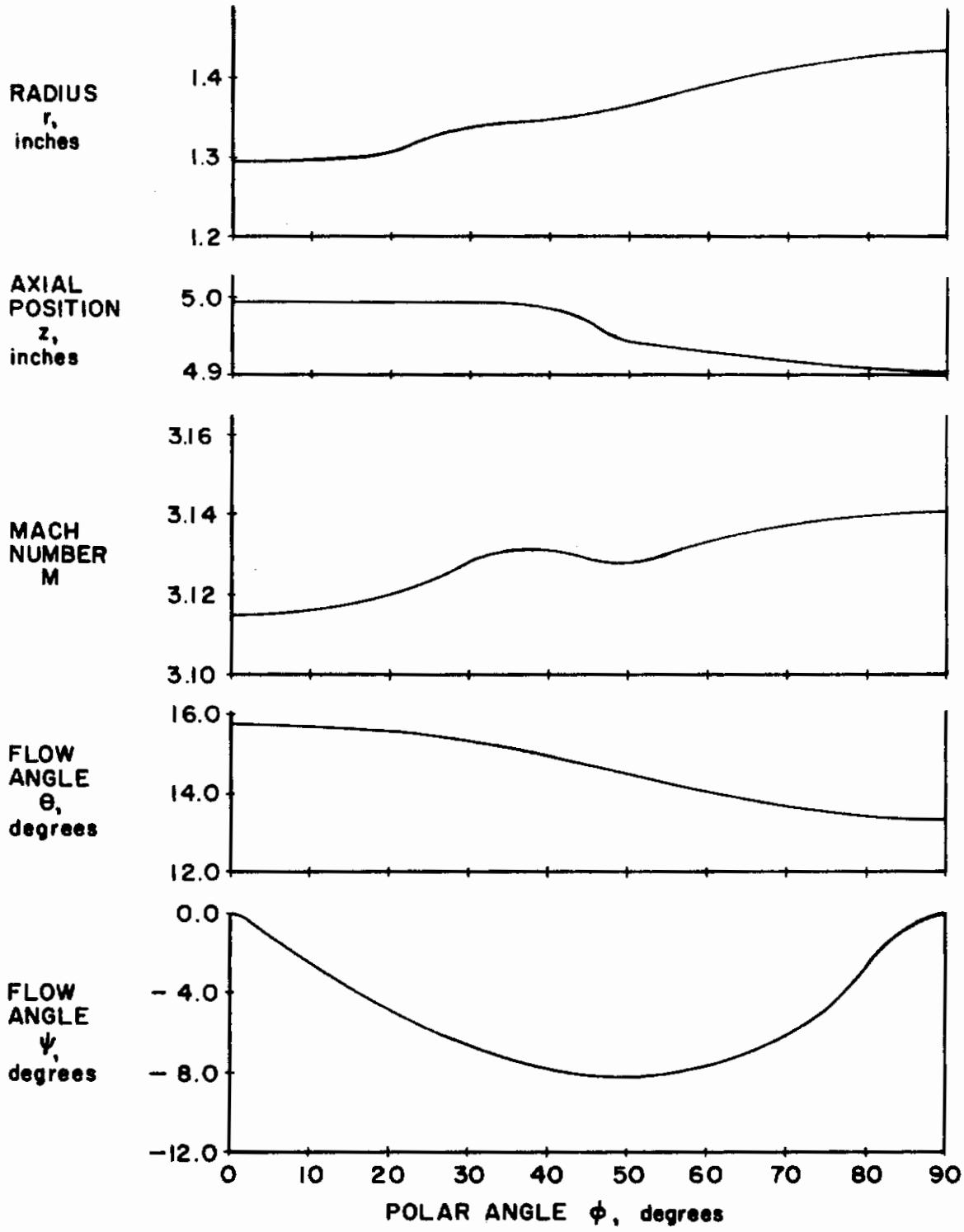

FIGURE 12. INITIAL VALUE LINE FOR OPTIMAL NOZZLE 2

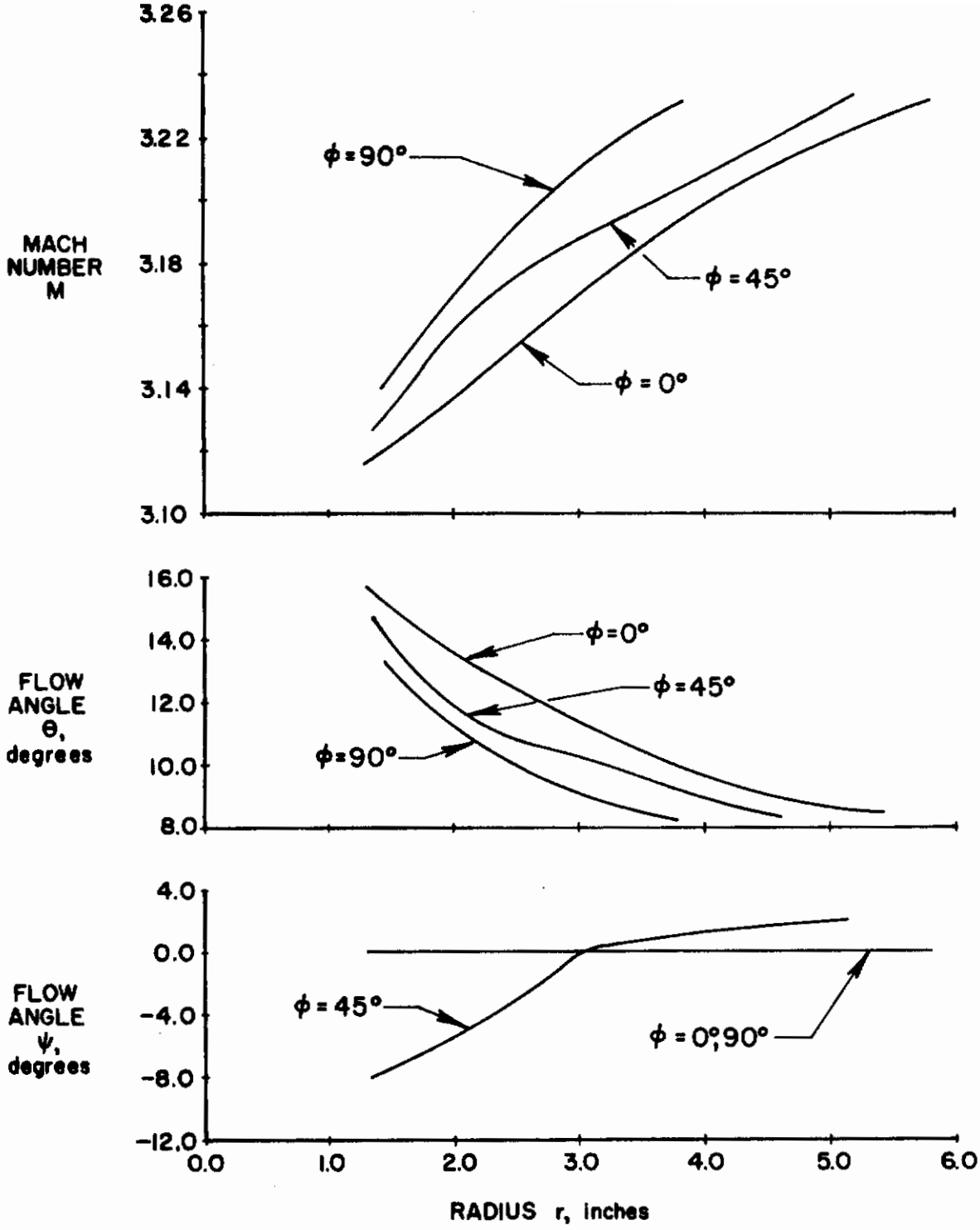

FIGURE 13. CONTROL SURFACE FOR OPTIMAL NOZZLE 2

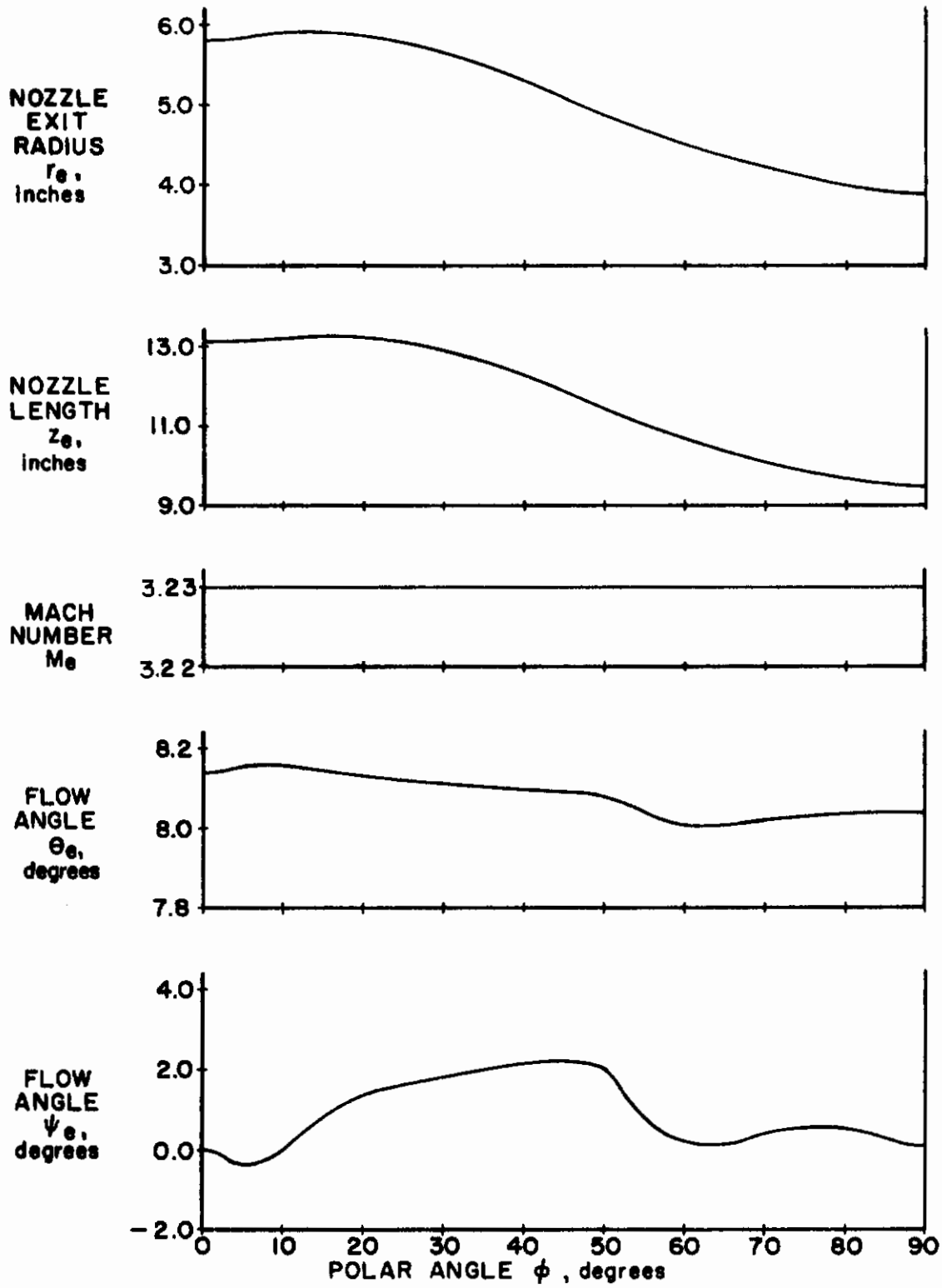

FIGURE 14. EXIT LIP FOR OPTIMAL NOZZLE 2

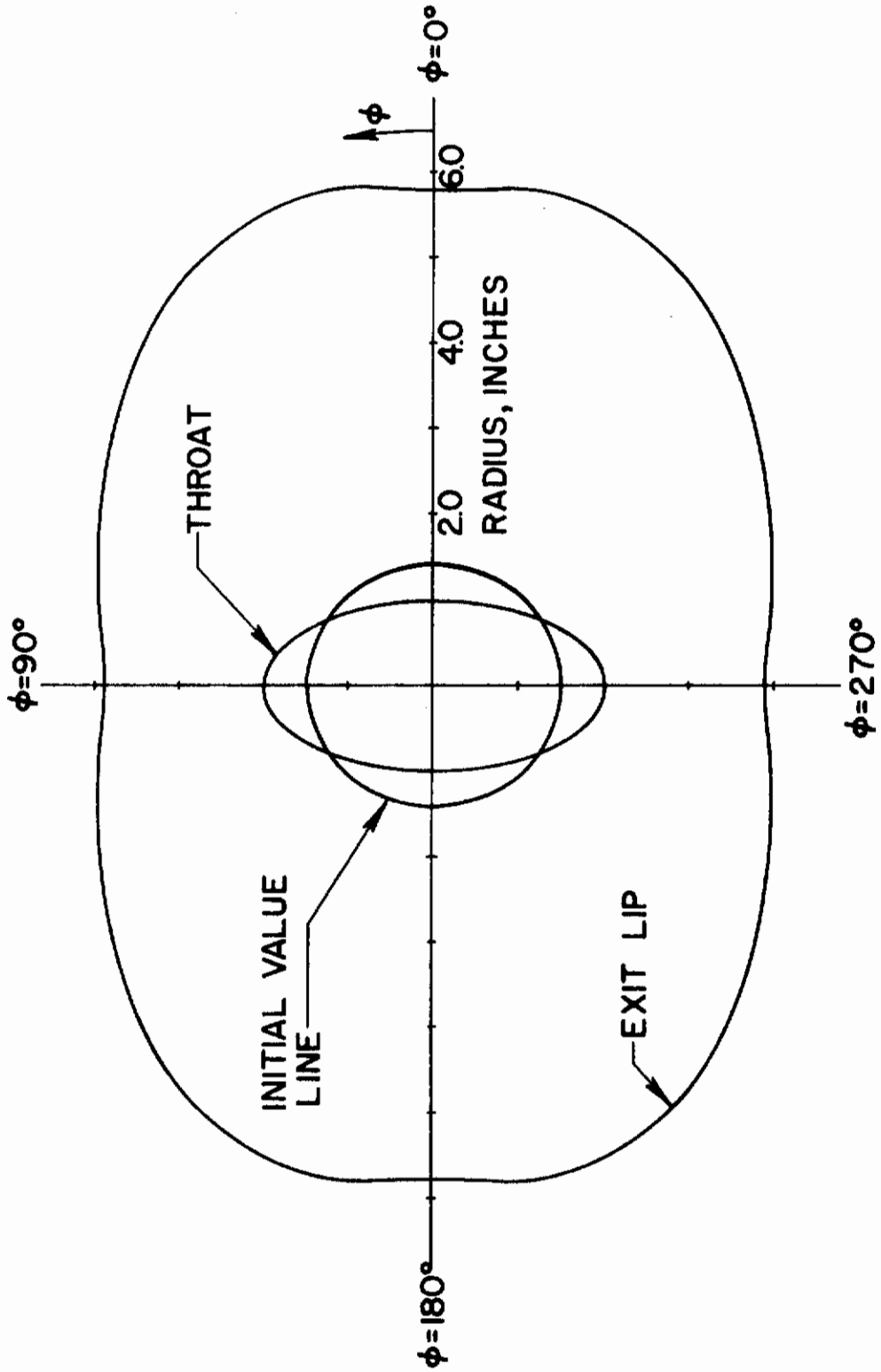

FIGURE 15. PROJECTION ON THE r,φ-PLANE OF OPTIMAL NOZZLE 2

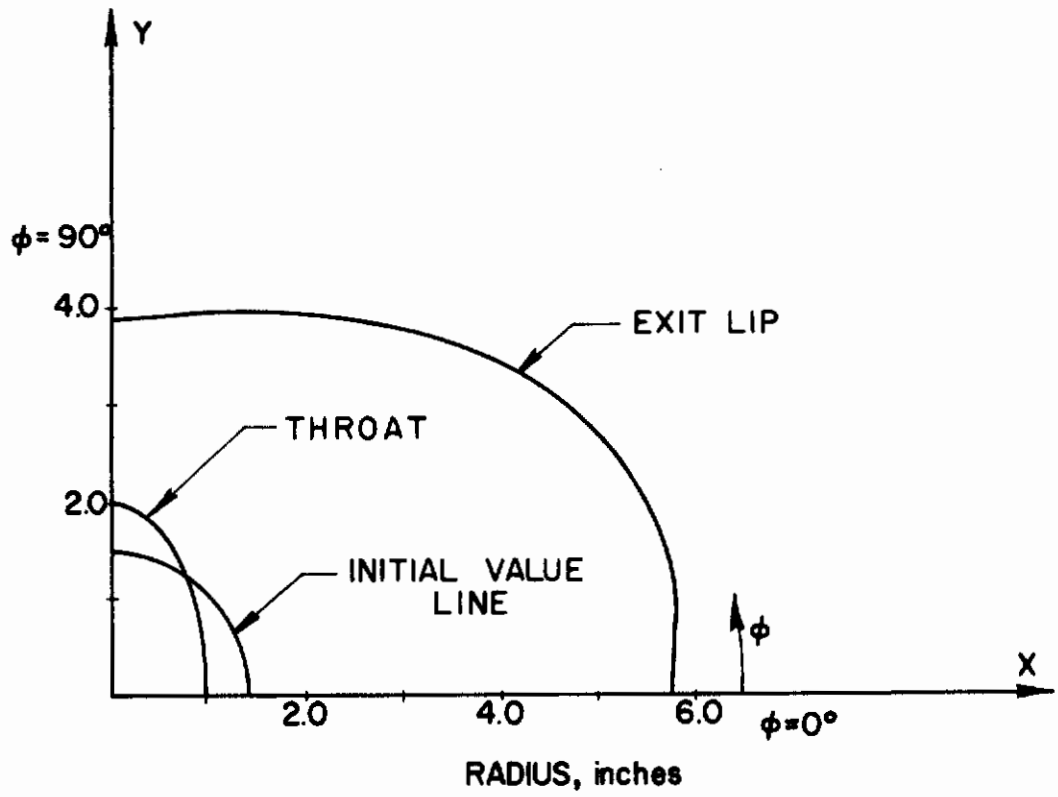

ϕ	Z_{IVL}	θ_{IVL}	M_{IVL}	ψ_{IVL}	Z_e	θ_e	M_e	ψ_e
0.0°	4.99"	15.70°	3.12	0.00°	13.1"	8.14°	3.23	0.00°
15.0	4.99	15.56	3.12	-3.83	13.3	8.14	3.23	0.87
30.0	4.99	15.35	3.13	-6.49	12.8	8.11	3.23	1.77
45.0	4.95	14.62	3.13	-8.15	11.9	8.07	3.23	2.09
60.0	4.93	14.02	3.13	-7.61	10.6	7.94	3.23	0.12
75.0	4.91	13.52	3.14	-5.06	9.9	8.13	3.23	0.67
90.0	4.91	13.26	3.14	0.00	9.5	8.14	3.23	0.00

FIGURE 16. SUMMARY FOR OPTIMAL NOZZLE 2

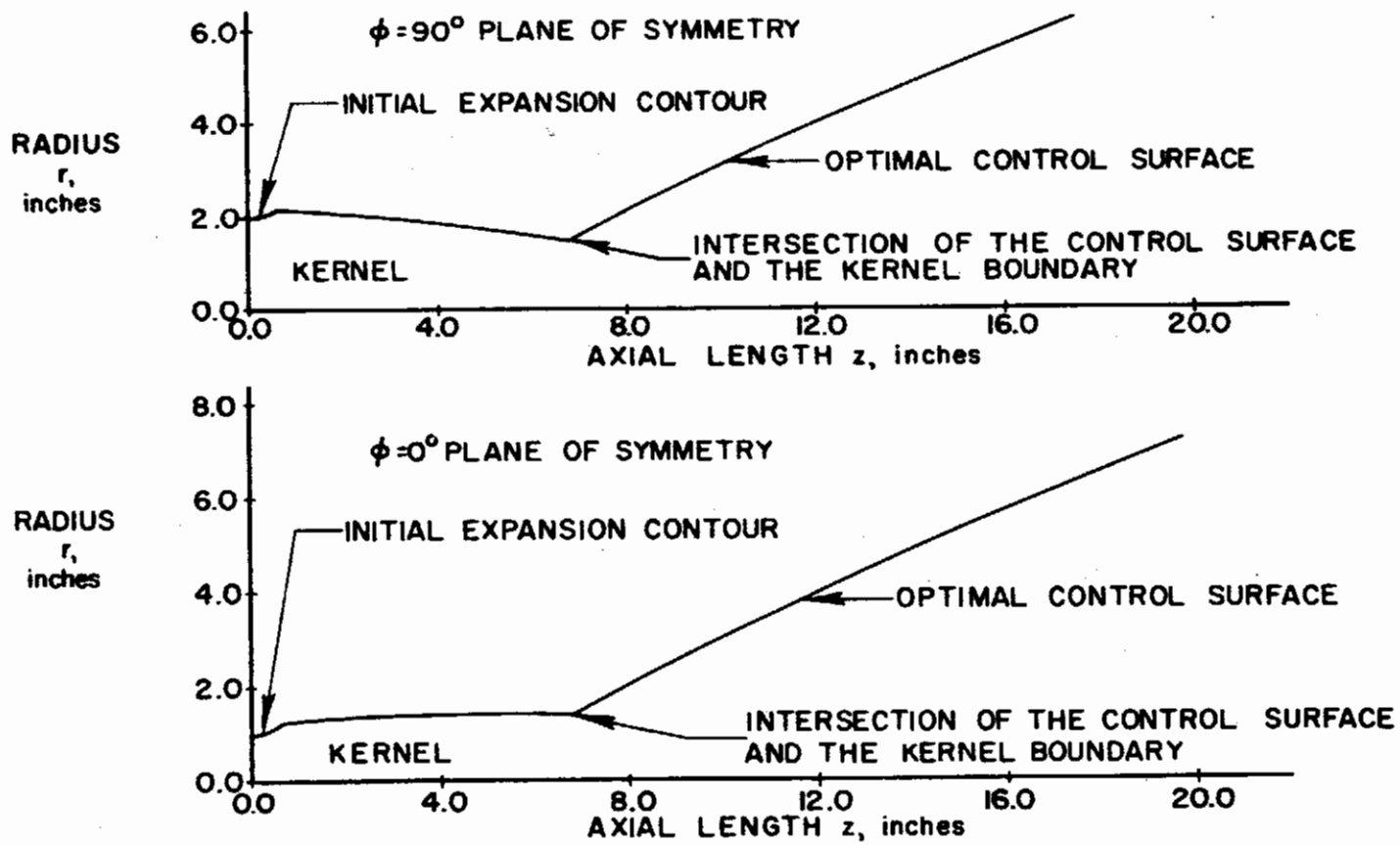

FIGURE 17. PLANE OF SYMMETRY VIEWS OF OPTIMAL NOZZLE 3

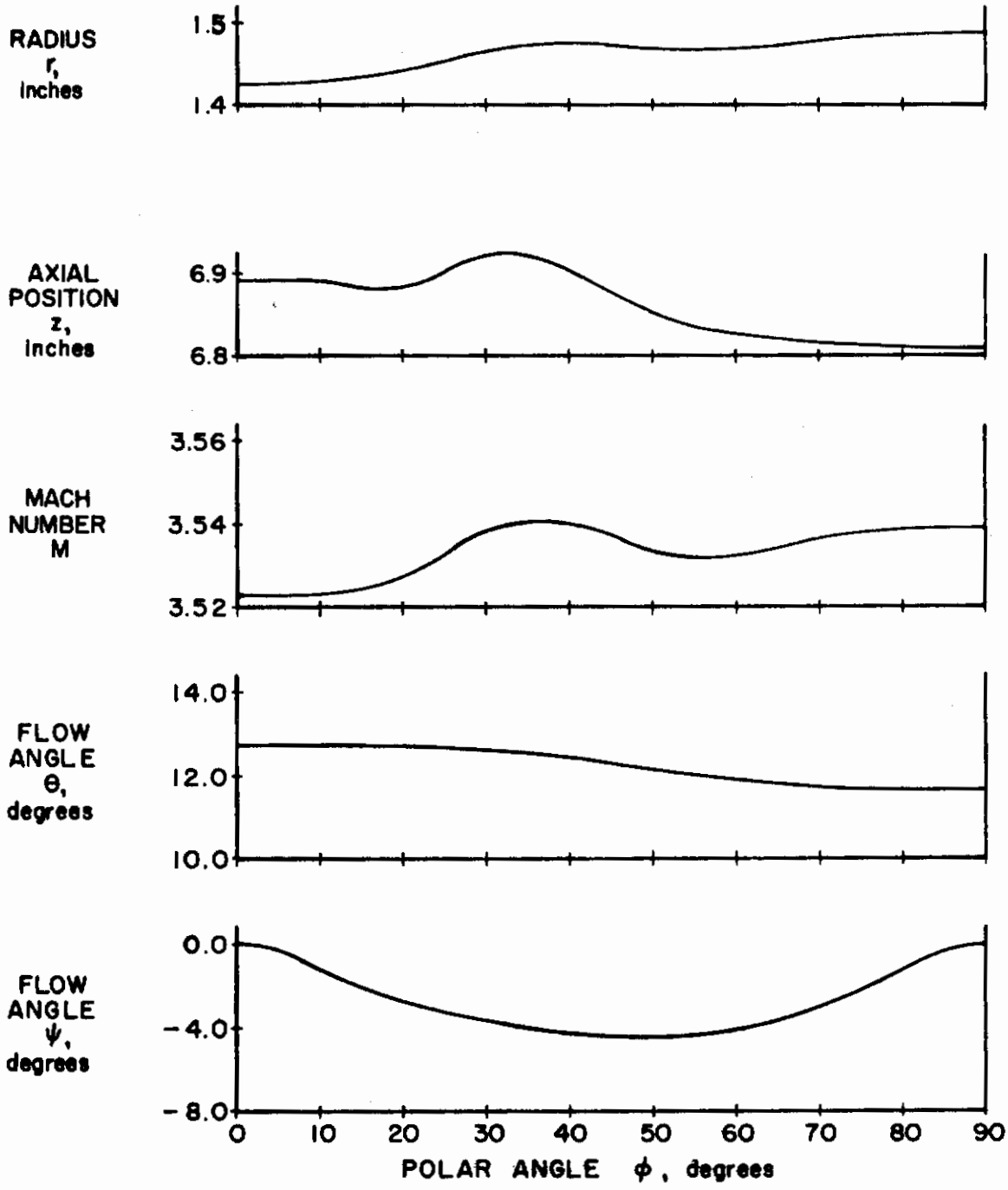

FIGURE 18. INITIAL VALUE LINE FOR OPTIMAL NOZZLE 3

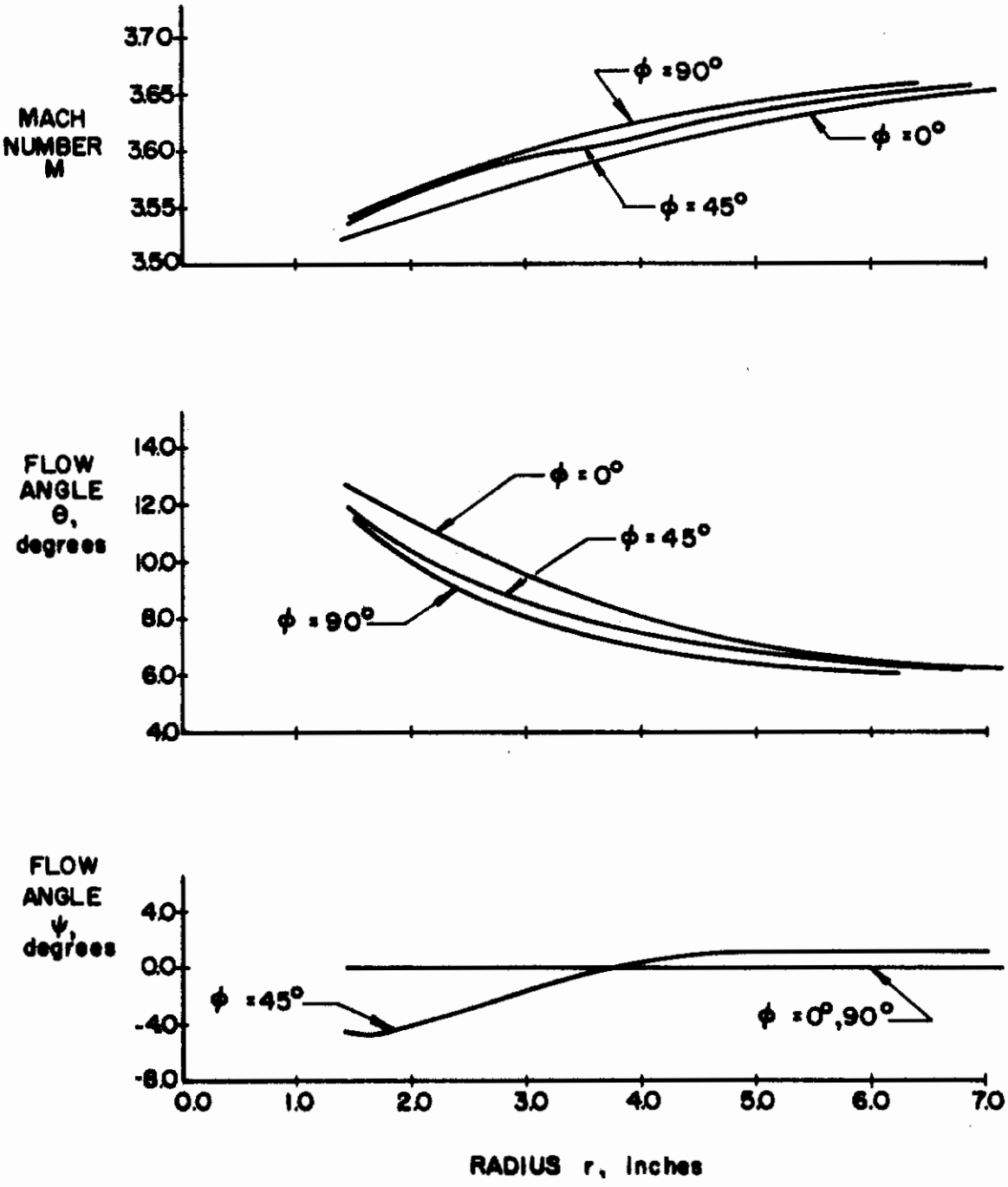

FIGURE 19. CONTROL SURFACE FOR OPTIMAL NOZZLE 3

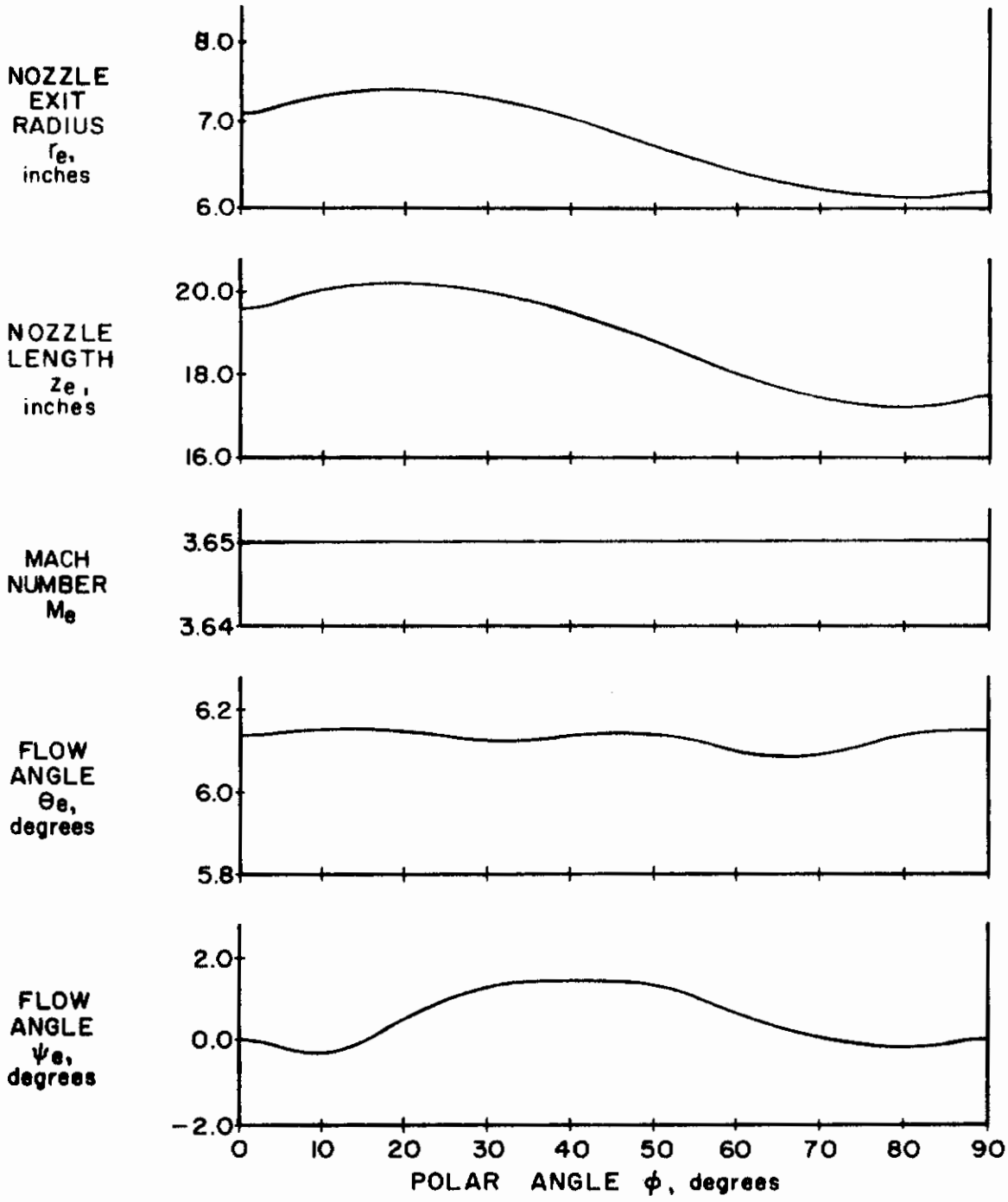

FIGURE 20. EXIT LIP FOR OPTIMAL NOZZLE 3

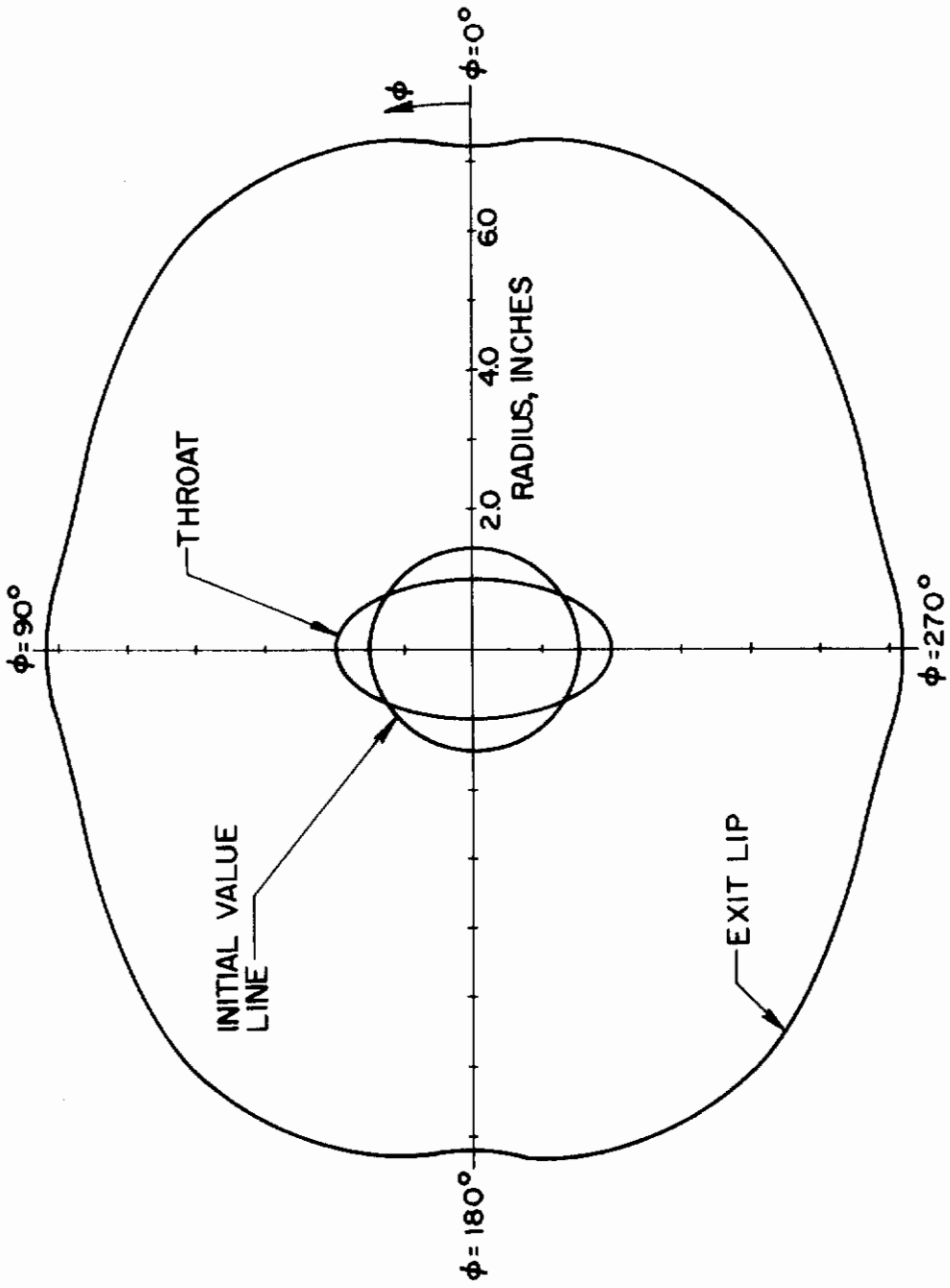

FIGURE 21. PROJECTION ON THE r,φ-PLANE OF OPTIMAL NOZZLE 3

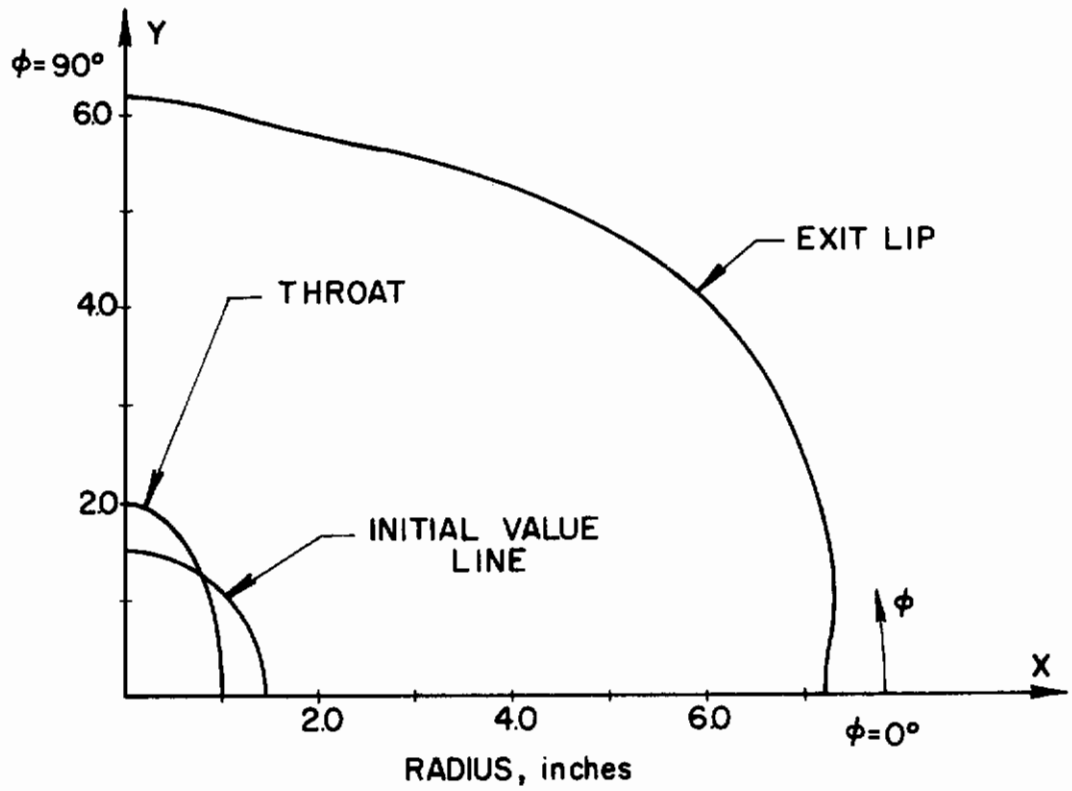

ϕ	Z_{IVL}	θ_{IVL}	M_{IVL}	ψ_{IVL}	Z_e	θ_e	M_e	ψ_e
0.0°	6.89"	12.74°	3.52	0.00°	19.6"	6.14°	3.65	0.00°
15.0	6.88	12.65	3.52	-2.16	20.2	6.17	3.65	0.10
30.0	6.93	12.62	3.54	-3.50	20.1	6.12	3.65	1.29
45.0	6.87	12.25	3.54	-4.22	19.1	6.12	3.65	1.45
60.0	6.82	11.90	3.53	-4.03	18.0	6.10	3.65	0.57
75.0	6.81	11.70	3.54	-1.89	17.1	6.14	3.65	-0.25
90.0	6.80	11.60	3.54	0.00	17.4	6.14	3.65	0.00

FIGURE 22 SUMMARY FOR OPTIMAL NOZZLE 3

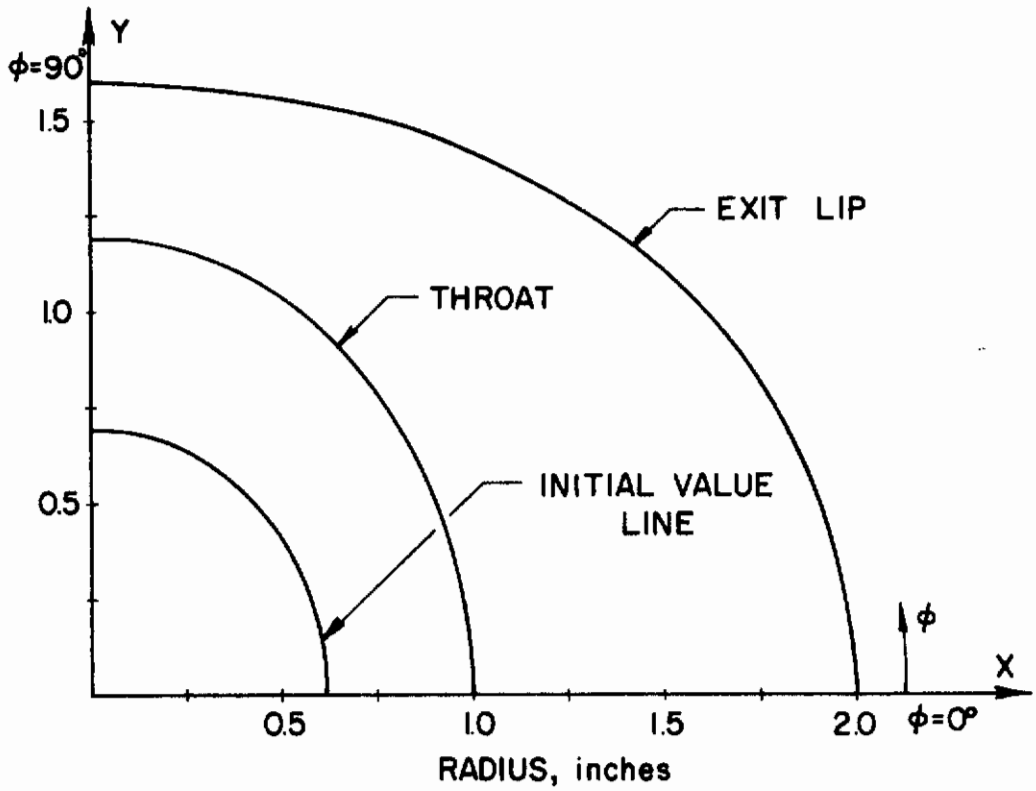

ϕ	Z_{IVL}	θ_{IVL}	M_{IVL}	ψ_{IVL}	Z_e	θ_e	M_e	ψ_e
0.0°	1.89"	12.88°	2.19	0.00°	4.00"	7.67°	2.30	0.00°
15.0	1.89	12.84	2.20	-2.10	3.95	7.67	2.30	0.08
30.0	1.89	12.69	2.20	-3.90	3.85	7.67	2.30	0.05
45.0	1.89	12.50	2.20	-4.61	3.69	7.67	2.30	-0.04
60.0	1.90	12.27	2.21	-4.16	3.53	7.67	2.30	-0.08
75.0	1.90	12.08	2.21	-2.41	3.41	7.67	2.30	-0.13
90.0	1.90	12.02	2.21	0.00	3.38	7.67	2.30	0.00

FIGURE 23. SUMMARY FOR OPTIMAL NOZZLE 4

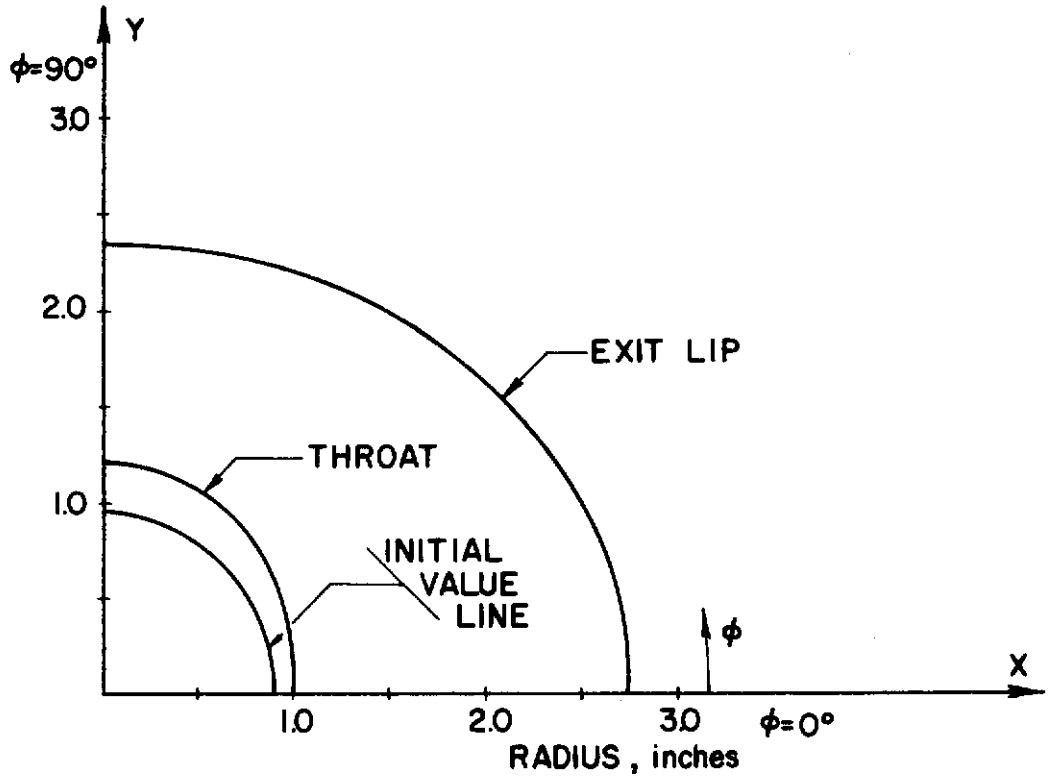

ϕ	Z_{IVL}	Θ_{IVL}	M_{IVL}	Ψ_{IVL}	Z_e	Θ_e	M_e	Ψ_e
0.0°	2.46"	17.52°	2.56	0.00°	5.01"	10.85°	2.65	0.00°
15.0	2.46	17.46	2.56	-1.52	4.96	10.85	2.65	0.17
30.0	2.46	17.28	2.56	-2.85	4.86	10.85	2.65	0.23
45.0	2.46	17.04	2.56	-3.35	4.70	10.85	2.65	0.20
60.0	2.46	16.76	2.56	-2.96	4.56	10.84	2.65	0.16
75.0	2.46	16.55	2.57	-1.85	4.43	10.85	2.65	0.05
90.0	2.46	16.48	2.57	0.00	4.39	10.86	2.65	0.00

FIGURE 24. SUMMARY FOR OPTIMAL NOZZLE 5

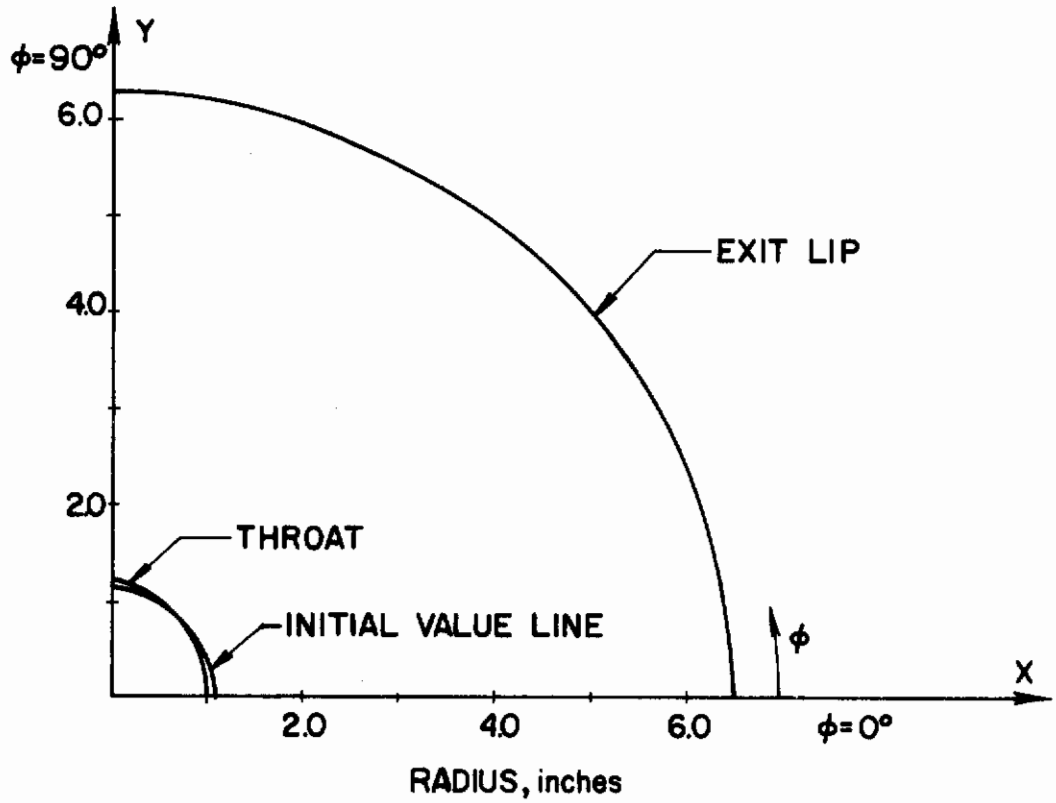

ϕ	Z_{IVL}	θ_{IVL}	M_{IVL}	ψ_{IVL}	Z_e	θ_e	M_e	ψ_e
0.0°	6.75"	10.16°	3.82	0.00°	20.8"	4.62°	3.96	0.00°
15.0	6.75	10.14	3.82	-0.55	20.7	4.62	3.96	0.04
30.0	6.75	10.12	3.82	-0.85	20.6	4.62	3.96	0.05
45.0	6.76	10.06	3.82	-0.97	20.4	4.62	3.96	0.10
60.0	6.76	10.03	3.82	-0.91	20.3	4.62	3.96	0.05
75.0	6.77	10.00	3.82	-0.47	20.2	4.62	3.96	0.05
90.0	6.77	9.99	3.82	0.00	20.2	4.62	3.96	0.00

FIGURE 25. SUMMARY FOR OPTIMAL NOZZLE 6

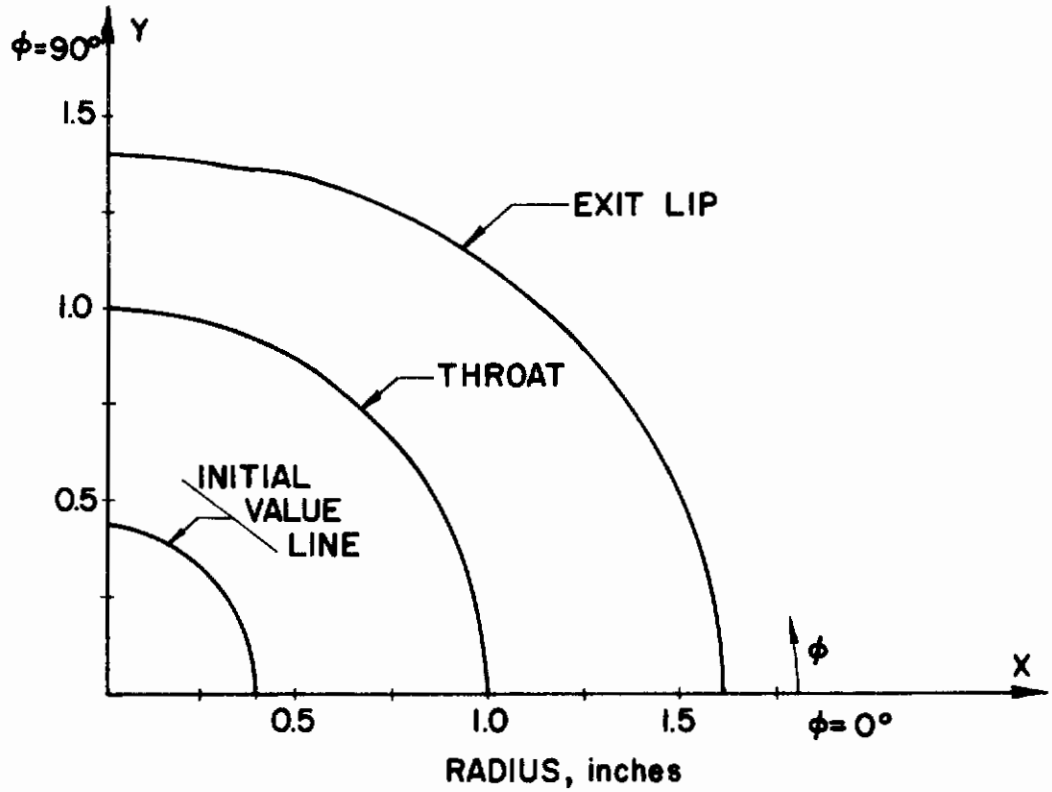

ϕ	Z_{IVL}	Θ_{IVL}	M_{IVL}	Ψ_{IVL}	Z_e	Θ_e	M_e	Ψ_e
0.0°	1.39"	8.95°	1.97	0.00°	3.07"	4.85°	2.07	0.00°
15.0	1.39	8.93	1.97	-1.54	3.05	4.85	2.07	-0.07
30.0	1.39	8.87	1.97	-2.81	2.99	4.85	2.07	-0.13
45.0	1.40	8.79	1.97	-3.37	2.91	4.85	2.07	-0.17
60.0	1.40	8.70	1.97	-2.98	2.83	4.85	2.07	-0.07
75.0	1.40	8.64	1.98	-1.95	2.77	4.85	2.07	-0.06
90.0	1.40	8.60	1.98	0.00	2.75	4.85	2.07	0.00

FIGURE 26. SUMMARY FOR OPTIMAL NOZZLE 7

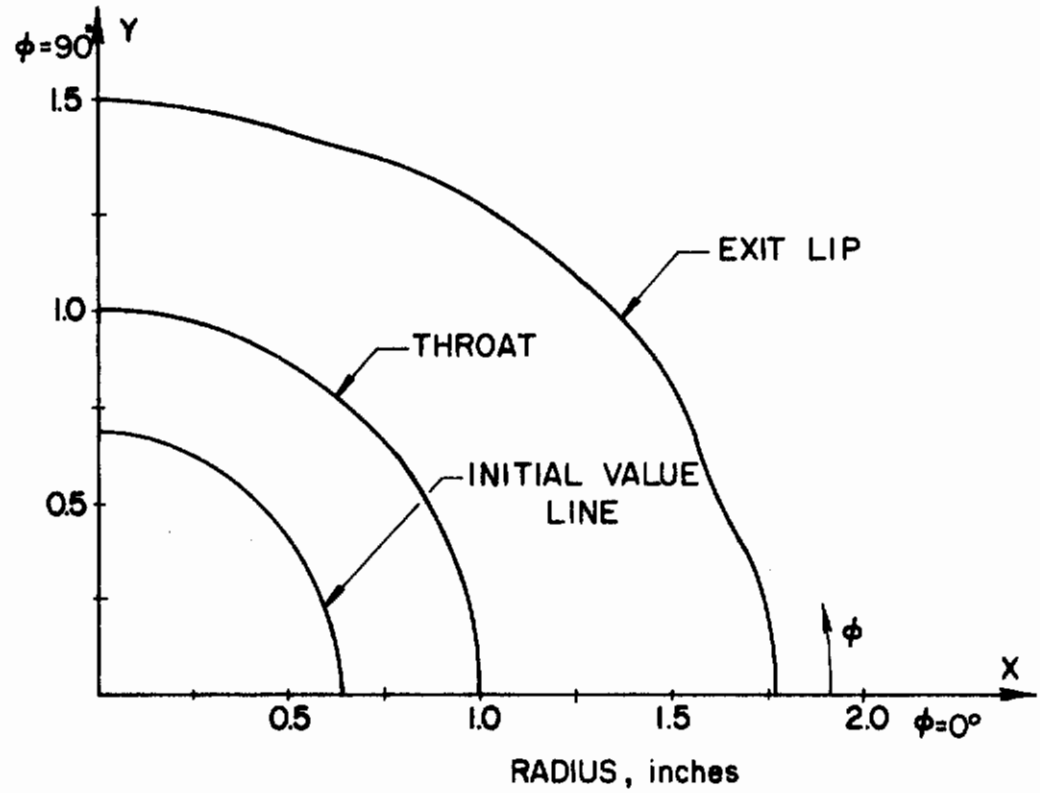

ϕ	Z_{IVL}	θ_{IVL}	M_{IVL}	ψ_{IVL}	Z_e	θ_e	M_e	ψ_e
0.0°	1.39"	14.78°	2.07	0.00°	2.75"	9.73°	2.17	0.00°
15.0	1.39	14.74	2.07	-1.59	2.68	9.74	2.17	0.40
30.0	1.39	14.66	2.07	-2.67	2.67	9.73	2.17	-0.14
45.00	1.40	14.76	2.08	-3.09	2.58	9.73	2.17	-0.17
60.0	1.39	14.40	2.08	-2.71	2.51	9.73	2.17	-0.29
75.0	1.39	14.29	2.08	-1.49	2.47	9.73	2.17	-0.15
90.0	1.39	14.24	2.08	0.00	2.45	9.73	2.17	0.00

FIGURE 27. SUMMARY FOR OPTIMAL NOZZLE 8

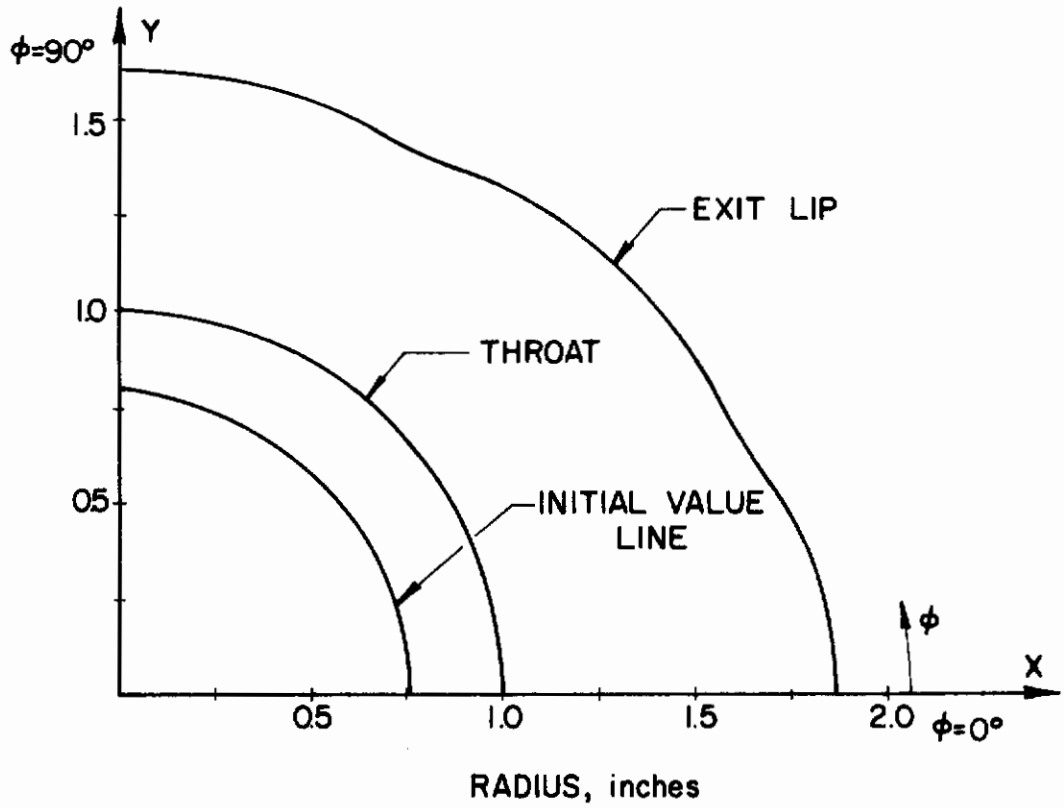

ϕ	Z_{IVL}	θ_{IVL}	M_{IVL}	ψ_{IVL}	Z_e	θ_e	M_e	ψ_e
0.0°	1.39"	17.88°	2.13	0.00°	2.61"	12.43°	2.22	0.00°
15.0	1.39	17.84	2.13	-1.51	2.53	12.41	2.22	0.62
30.0	1.39	17.76	2.14	-2.55	2.47	12.56	2.22	-0.17
45.0	1.39	17.80	2.15	-2.90	2.42	12.51	2.22	-0.19
60.0	1.39	17.45	2.14	-2.47	2.32	12.46	2.22	-1.04
75.0	1.39	17.30	2.14	-1.31	2.35	12.43	2.22	-0.16
90.0	1.39	17.26	2.14	0.00	2.33	12.43	2.22	0.00

FIGURE 28. SUMMARY FOR OPTIMAL NOZZLE 9

SECTION V

SUMMARY

A method has been developed for designing three-dimensional nozzles that produce the maximum axial thrust for the following specific conditions: 1) starting flow conditions, 2) initial expansion contour, 3) length and exit lip shape and 4) ambient pressure. The theoretical development of the optimization design equations, the numerical technique used to solve the design equations and the results from nine sample cases are presented in this work.

The uniqueness of the solution is established by proving that the optimal control surface is a characteristic surface, a result which assures a unique matching of the flow in the kernel with the flow across the control surface. Furthermore, when the flow is constrained to be axially symmetric, the solution reduces to the well known result obtained by Rao (2).

Comparison of the performance of three-dimensional nozzles is difficult since there is no established criteria for comparison. The nozzles discussed here have been compared to two different types of nozzles. First, the thrust coefficients of the optimal three-dimensional nozzles were compared to the thrust coefficients of ideal (perfect) nozzles designed for identical ambient and stagnation conditions. The ratio $C_f/C_{f_{ideal}}$ for the nine optimal three-dimensional nozzles ranged from 0.963 to 0.996. These values are consistent with the results obtained in comparing the performance of optimal axisymmetric nozzles with the performance of comparable ideal nozzles (see Refs. (2) and (28)).

Second, the thrust coefficients of three of the optimal three-dimensional nozzles were compared to the thrust coefficients of non-optimally designed three-dimensional nozzles that had identical initial conditions and comparable overall dimensions. Since the three-dimensional

flow analysis program (23) that was used in this research did not have the capability to handle pressure boundaries, it was only possible to analyze three-dimensional nozzles ending in a plane. The comparison of the thrust coefficients confirms that the performance of the three-dimensional optimal nozzle is significantly better than those three-dimensional comparison nozzles which were analyzed.

Other features of the nine optimal three-dimensional nozzles were also investigated. The results show that two-dimensional or axisymmetric methods are not adequate for designing three-dimensional optimal nozzles. In fact, the results show that for the cases investigated the optimal nozzles with elliptical throats have exits which have an elliptical projection on the $r\phi$-plane but with the orientation of the ellipse rotated by 90 degrees. The results also show that optimal, fixed length, three-dimensional nozzles do not necessarily end in a plane.

APPENDIX A
DERIVATION OF GEOMETRICAL RELATIONSHIPS

1. COORDINATE SYSTEM

Three coordinate values are required to describe the position of a point in three-dimensional space. A r,ϕ,z-cylindrical coordinate system is used throughout this work as the spatial reference. The z-axis is oriented in the principal flow direction with the positive z direction corresponding to the downstream flow direction. The polar angle ϕ is measured in the counterclockwise direction from a stationary reference line in the $r\phi$-plane, and the radius r is measured radially outward from the z-axis. The orientation of the coordinate system is shown in Figure 29.

2. CONTROL SURFACE

A schematic representation of a general three-dimensional nozzle is also shown in Figure 29. The nozzle shown has one plane of symmetry. The zone of influence of the initial contour of the nozzle is denoted as the kernel and is the portion of the supersonic flow for which the flow variables are completely determined by the initial flow conditions upstream of the initial contour and the shape of the initial contour.

The control surface passes through the exit lip contour of the nozzle and intersects the kernel. The control surface can be described parametrically by the equation

$$F'(r,\phi,z) = 0 \tag{81}$$

Equation (81) can be solved for z in terms of r and ϕ to give

$$z = f(r,\phi) \tag{82}$$

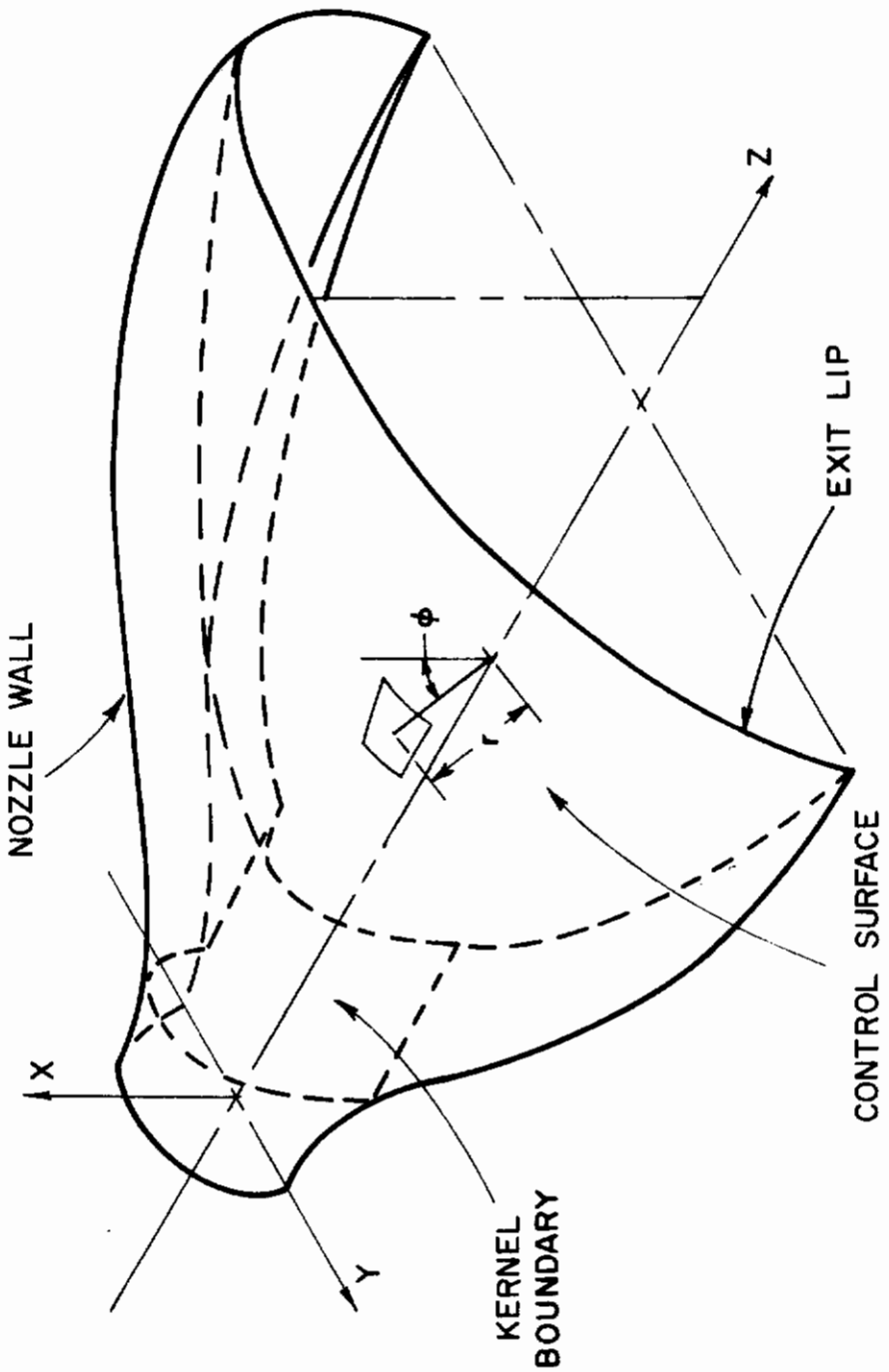

FIGURE 29. THREE-DIMENSIONAL NOZZLE

which describes the control surface when the function $f(r,\phi)$ is known.

The control surface can also be described by the outer unit normal $\bar{n}$ at every point on the control surface. The outer unit normal for an element of the control surface is shown in Figure 30 , and is uniquely specified by two spherical angles α and β. The angle β is defined as the angle between the positive z-axis and the unit outer normal to the control surface, $(0° \leq \beta \leq 180°)$. The angle α is measured counterclockwise from the radial direction to the projection of $\bar{n}$ onto the $r\phi$-plane. Hence, the direction cosines of the unit outer normal to the control surface are

$$n_r = \sin\beta \cos\alpha$$

$$n_\phi = \sin\beta \sin\alpha \tag{83}$$

$$n_z = \cos\beta$$

and $\bar{n}$ can be written as

$$\bar{n} = (\sin\beta \cos\alpha)\bar{i}_r + (\sin\beta \sin\alpha)\bar{i}_\phi + (\cos\beta)\bar{i}_z \tag{84}$$

where $\bar{i}_r$, $\bar{i}_\phi$, and $\bar{i}_z$ are unit vectors in the positive radial, tangential, and axial directions, respectively.

On the control surface, the partial derivatives of f can be expressed in terms of the angles α and β as follows:

$$\frac{\partial f}{\partial r} = - \tan\beta \cos\alpha \tag{85}$$

$$\frac{\partial f}{\partial \phi} = - r\tan\beta \sin\alpha \tag{86}$$

In the formulation, r and ϕ are the independent variables on the control surface. Thus, it is convenient to relate the area of a differential element of the control surface $dA_{c.s.}$ to its projected area on the

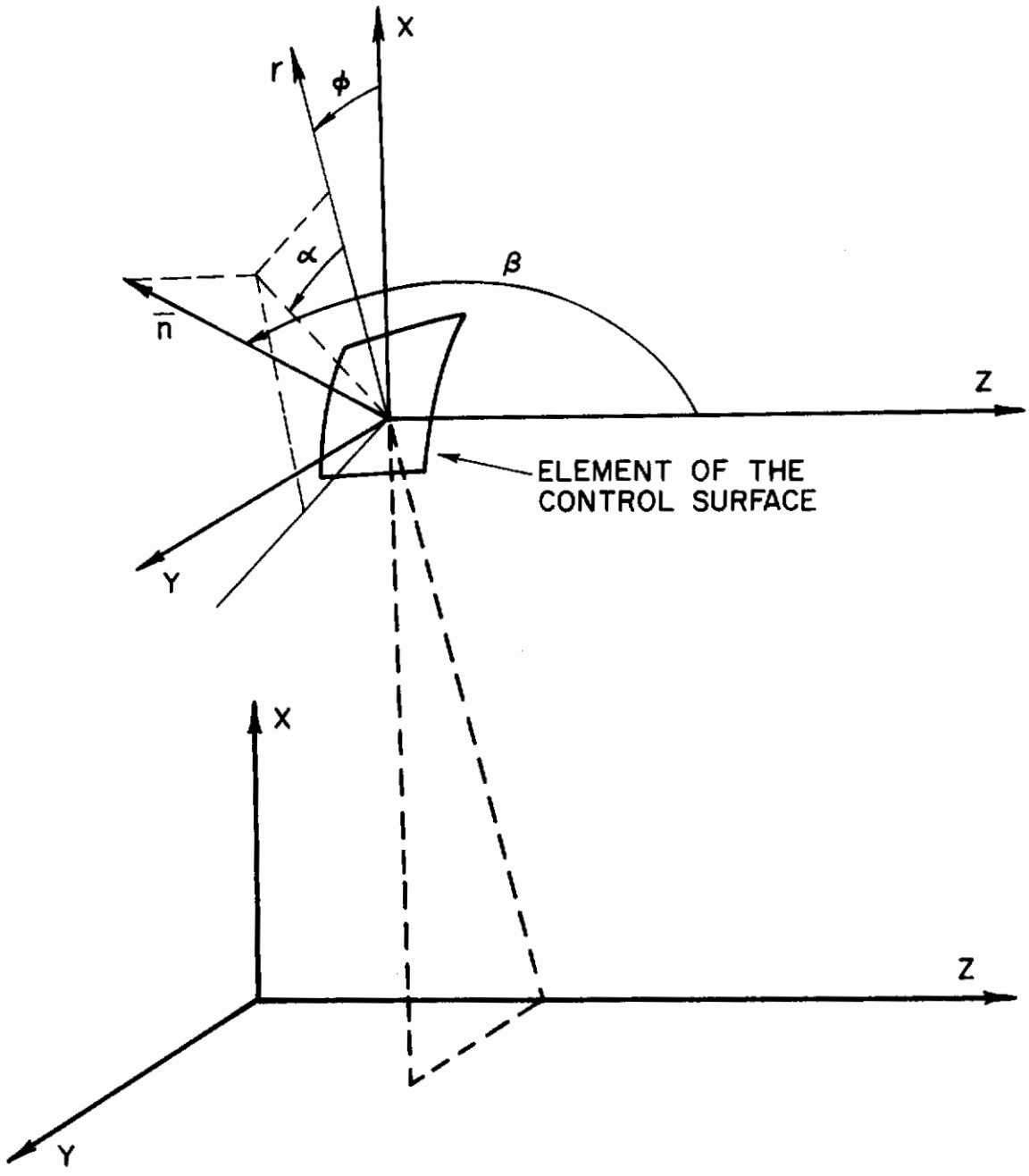

FIGURE 30. UNIT VECTOR NORMAL TO THE CONTROL SURFACE

$r\phi$-plane. By using the vector relationship

$$-(\bar{n} \cdot \bar{i}_z)dA_{c.s.} = rdrd\phi \tag{87}$$

and combining it with Eqs. (83) and (84), the following equation is obtained:

$$dA_{c.s.} = -rdrd\phi/\cos\beta \tag{88}$$

3. VELOCITY VECTOR

The velocity vector $\bar{V}$ at any point in the three-dimensional flow is uniquely determined by its magnitude V and two spherical angles θ and ψ. The angle θ is the angle between the positive z-axis and the velocity vector, $(-90° \leq \theta \leq 90°)$. The angle ψ is measured in the $r\phi$-plane, counterclockwise from the radial direction to the projection of $\bar{V}$ onto the $r\phi$-plane. These angles are illustrated in Figure 31. The direction cosines of $\bar{V}$ are

$$\begin{aligned} V_r &= V \sin\theta \cos\psi \\ V_\phi &= V \sin\theta \sin\psi \\ V_z &= V \cos\theta \end{aligned} \tag{89}$$

Thus, the velocity vector can be written as the following:

$$\bar{V} = V\left((\sin\theta \cos\psi)\bar{i}_r + (\sin\theta \sin\psi)\bar{i}_\phi + (\cos\theta)\bar{i}_z\right) \tag{90}$$

The angle ξ is defined by the following equation:

$$\sin\xi = -(\bar{V} \cdot \bar{n})/V \tag{91}$$

By combining Eqs. (83) and (89) with Eq. (91), the following expression is obtained:

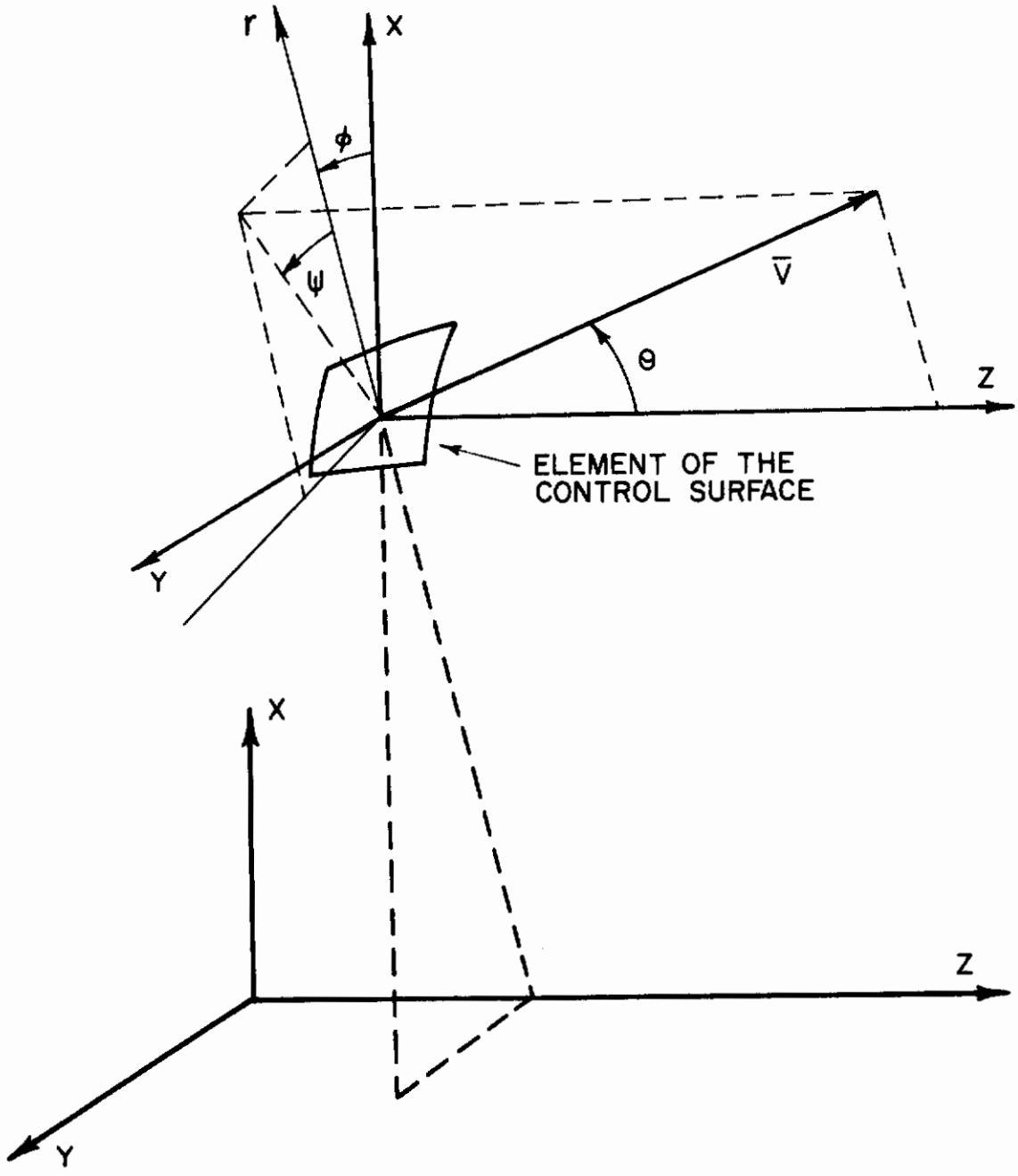

FIGURE 31. VELOCITY VECTOR

$$\sin\xi = -\cos\beta\cos\theta - \sin\beta\sin\theta\cos(\psi - \alpha) \tag{92}$$

When Eqs. (91), (84) and (85) are combined, the expression

$$\frac{\sin\xi}{\cos\beta} = -\cos\theta + \sin\theta\cos\psi\frac{\partial f}{\partial r} + \frac{\sin\theta\sin\psi}{r}\frac{\partial f}{\partial\phi} \tag{93}$$

can be written.

APPENDIX B
DYNAMICS AND THERMODYNAMICS OF THE FLOW

In this appendix the assumptions which constitute the flow model used in this research are presented. The thermodynamic relations governing the flow are combined with the momentum equations to show that the thermodynamic properties p, T and ρ are unique functions of the velocity V, the stagnation conditions p_o and h_o and the constant properties of the flow γ and R. Finally, a number of differential relationships are derived which will be used to introduce the flow model into the formulation and solution of the optimization problem.

The three-dimensional, supersonic flow considered in this work is that of a continuum fluid flowing without friction and without body forces (gravity, electromagnetic, etc.). All stream properties within the flow are assumed to vary continuously in all directions; this implies that shocks are excluded. In addition, the flow is assumed to be steady, homentropic (i.e., the entropy is constant throughout the fluid flow) and isoenergetic (i.e., the stagnation enthalpy h_o is constant throughout the fluid flow). The thermodynamic properties of the flow are assumed to obey the perfect gas relations.

For a homentropic flow of a perfect gas the following equations are valid:

$$T_o/T = 1 + (\gamma - 1)M^2/2 \tag{94}$$

$$p_o/p = (T_o/T)^{\gamma/(\gamma - 1)} \tag{95}$$

$$\rho_o/\rho = (T_o/T)^{1/(\gamma - 1)} \tag{96}$$

$$a^2 = (dp/d\rho)_s = \frac{\gamma p}{\rho} \tag{97}$$

$$h = \gamma RT/(\gamma - 1) \tag{98}$$

where the constants γ and R are the specific heat ratio and the gas constant, respectively. In addition, M is the Mach number where $M \equiv V/a$. The pressure-temperature-density relation of a perfect gas is

$$p = \rho RT \tag{99}$$

For the inviscid flow of a pure substance (e.g. a perfect gas), Crocco's theorem must be satisfied. Crocco's theorem states that

$$T\nabla s - \bar{V} \times (\nabla \times \bar{V}) = \nabla h_o + \partial \bar{V}/\partial t \tag{100}$$

For a steady, isoenergetic, homentropic flow Crocco's theorem is satisfied only if $\bar{V} \times (\nabla \times \bar{V}) = 0$. Thus, the flow is either an irrotational flow or a Beltrami flow (24) (i.e., $\bar{V}$ is parallel to $\nabla \times \bar{V}$).

For a homentropic flow of a perfect gas the following equation is valid:

$$p/\rho^{\gamma} = p_o/\rho_o{}^{\gamma} = K_1 \tag{101}$$

where K_1 is a constant. Since shearing forces and body forces are excluded from this analysis, the only forces acting on the system are the pressure forces. Under these assumptions, Euler's equations of motion are valid. These three equations can be expressed in vector form as

$$\frac{D\bar{V}}{Dt} = -\nabla p/\rho \tag{102}$$

where the symbol D/Dt represents the substantial derivative with respect to time. Reference (16) shows that for a steady, isoenergenetic, homentropic fluid motion the Euler equations of motion, Eq. (102), can be used to derive the following equation:

$$\int_{p_1}^{p_2} \frac{dp}{\rho} + \frac{V^2}{2} = K_2 \qquad (103)$$

where K_2 is constant throughout the flow.

Taking logarithmic differentials of Eq. (101) and combining the resulting equation with Eq. (103) yields the relation

$$V^2/2 + K_1 \gamma \rho^{\gamma-1}/(\gamma-1) = K_3 \qquad (104)$$

where K_3 is a constant. By combining Eqs. (97), (101) and (104) the following equation can be derived:

$$V^2/2 + a^2/(\gamma-1) = a_o^2/(\gamma-1) \qquad (105)$$

Equation (105) relates the velocity V with the sound speed a and the stagnation sound speed a_o which is a constant. Equation (105) can be solved for a^2 so that

$$a^2 = a_o^2 - V^2(\gamma-1)/2 \qquad (106)$$

Equations (97) through (99) can be substituted into Eq. (106) to yield the following equation:

$$M^2 = V^2/a^2 = 1/(h_o(\gamma-1)/V^2 - (\gamma-1)/2) \qquad (107)$$

Therefore, as shown by Eq. (107), the Mach number is an unique function of the flow velocity and the constants γ and h_o. Combining Eq. (107) with Eqs. (94) through (97) yields the following functional relationships:

$$T = T(V, h_o, R, \gamma) \qquad (108)$$

$$p = p(V, p_o, h_o, R, \gamma) \qquad (109)$$

$$\rho = \rho(V, p_0, h_0, R, \gamma) \tag{110}$$

$$a = a(V, p_0, h_0, R, \gamma) \tag{111}$$

The above relationships were derived for a steady, isoenergetic, homentropic flow of a perfect gas. The information in the above equations will be important in the variational problem when deciding what variations are independent. The equations which relate the differentials dp, $d\rho$, da, $d\mu$ and dM to the differential dV will now be derived.

By applying logarithmic differentiation to Eqs. (97), (101), (103) and (105) and combining the resulting equations, the following equations can be derived:

$$dp = - \rho V dV \tag{112}$$

$$d\rho = - \rho V/a^2 dV \tag{113}$$

$$da = - \left(\frac{\gamma - 1}{2}\right) \frac{V}{a} dV \tag{114}$$

By definition, the Mach angle μ is given by the equation

$$\mu = \sin^{-1}(1/M) = \sin^{-1}(a/V) \tag{115}$$

Equations (114) and (115) can be combined so that the differential $d\mu$ can be written in terms of the differential dV as

$$d\mu = \frac{- \left(\frac{\gamma - 1}{2} + \sin^2\mu\right)}{V \sin\mu \cos\mu} dV \tag{116}$$

Furthermore, Eq. (115) can be logarithmically differentiated to yield the following relationship:

$$d\mu = - 1/\left(M(M^2 - 1)^{1/2}\right) dM \tag{117}$$

Equations (116) and (117) can then be combined to obtain the following equation:

$$dM = \left(1 + (\gamma-1)M^2/2\right)/a \; dV \qquad (118)$$

Equations (112) through (114) and (116) through (118) will be used throughout the variational problem to relate the properties of the flow.

APPENDIX C
DERIVATION OF THE INTEGRAL THRUST AND MASS FLOW RATE EQUATIONS

In this appendix expressions for the axial thrust produced by a three-dimensional nozzle and the mass flow rate through a three-dimensional nozzle are derived. The notation used is consistent with that shown in Figure 32. For convenience, the figure is drawn for the axisymmetric case, but the thrust and mass flow rate expressions are for a general three-dimensional nozzle.

In the variational problem the initial expansion contour BC and the flow conditions along a noncharacteristic start surface AB are specified where AB is in a totally supersonic flow region. With this information the flow in the kernel region can be calculated. The surface CIF is the characteristic (wave) surface which is the downstream boundary of the kernel. Therefore, the conditions along the wave surface CIF are known and fixed. In addition, the position of line I is known and fixed. The control surface IE is allowed to seek its optimal shape in the variational problem such that the axial thrust produced by the flow across the surface IF and the control surface IE is a maximum for the specified mass flow rate across these two surfaces. The expressions for the thrust and mass flow rate are written in terms of variables on these two surfaces.

1. INTEGRAL AXIAL THRUST EQUATION

The axial thrust term to be maximized is equal to the gross axial thrust produced by the supersonic nozzle minus the drag force produced by the ambient pressure acting on the projected area of the nozzle. Thus, the axial thrust can be written as

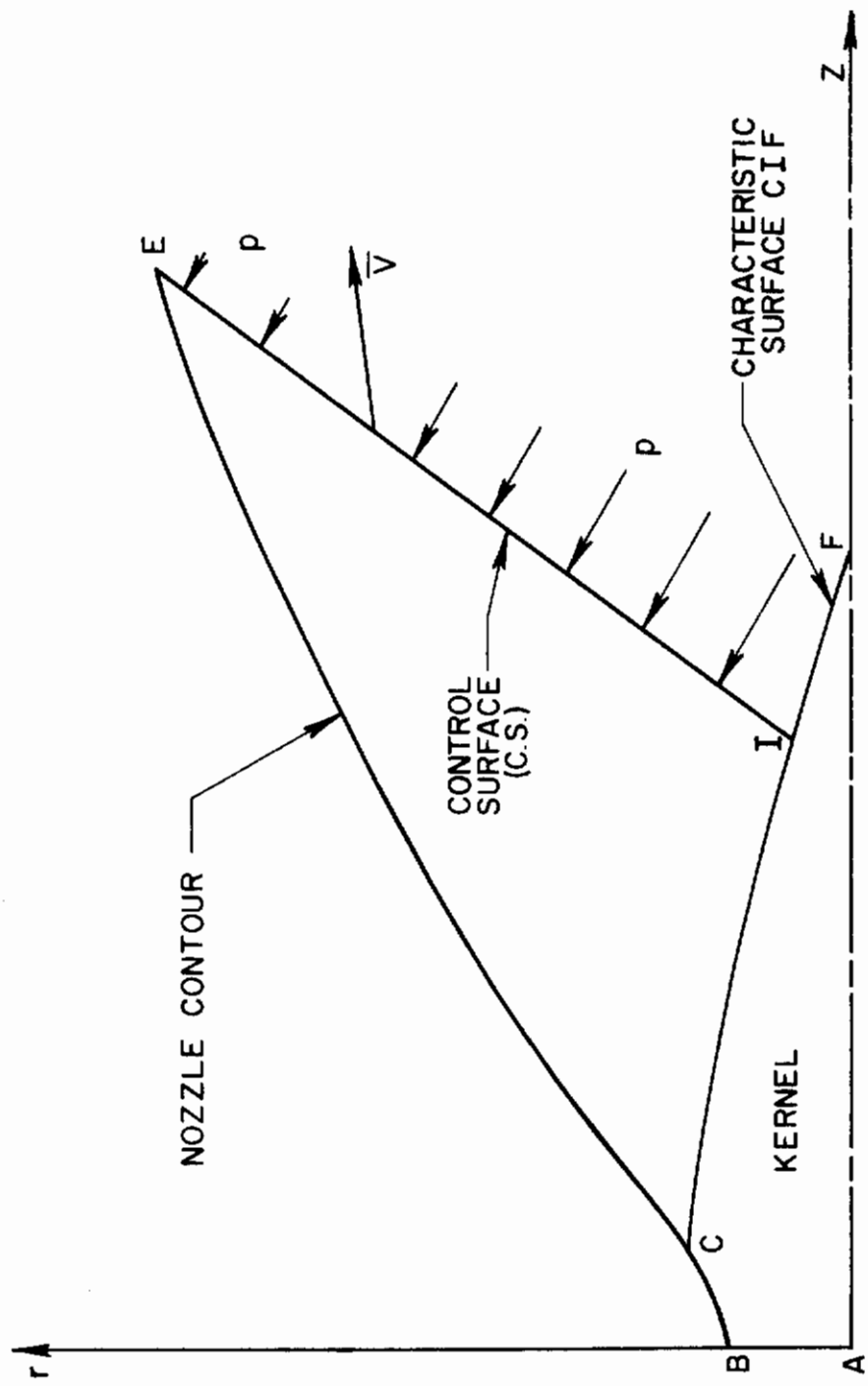

FIGURE 32. CONTROL SURFACE

$$\text{Axial Thrust} = -\iint_{\text{c.s.}} p(\bar{i}_z \cdot \overline{dA}_{\text{c.s.}}) - \iint_{\text{c.s.}} \rho V_z(\bar{V} \cdot \overline{dA}_{\text{c.s.}})$$

$$+ \text{Fixed Axial Thrust}_{IF} - \int_0^{2\pi} \int_0^{r_e(\phi)} rp_a dr d\phi \qquad (119)$$

where the first two terms on the RHS represent the thrust produced by the flow across the control surface, the third term represents the thrust produced by the flow across the characteristic surface IF and the last term represents the ambient pressure force on the frontal area of the nozzle.

In Appendix A the following equations were derived:

$$-(\bar{n} \cdot \bar{i}_z)dA_{\text{c.s.}} = r dr d\phi \qquad (120)$$

$$dA_{\text{c.s.}} = -r dr d\phi / \cos\beta \qquad (121)$$

$$\bar{V} = V((\sin\theta\cos\psi)\bar{i}_r + (\sin\theta\sin\psi)\bar{i}_\phi + (\cos\theta)\bar{i}_z) \qquad (122)$$

$$\sin\xi = -(\bar{V} \cdot \bar{n})/V \qquad (123)$$

where

$$\overline{dA}_{\text{c.s.}} = \bar{n} dA_{\text{c.s.}} \qquad (124)$$

Equations (120), (121) and (124) can be substituted into Eq. (119) to yield the following equation:

$$\text{Axial Thrust} = \int_0^{2\pi} \int_{r_i(\phi)}^{r_e(\phi)} (rp + r\rho V_z(\bar{V} \cdot \bar{n})/\cos\beta)\,dr\,d\phi$$

$$+ \text{Fixed Axial Thrust}_{IF} - \int_0^{2\pi} \int_0^{r_e(\phi)} rp_a\,dr\,d\phi \qquad (125)$$

By combining Eqs. (122) and (123) with Eq. (125) the following equation is obtained:

$$\text{Axial Thrust} = \int_0^{2\pi} \int_{r_i(\phi)}^{r_e(\phi)} (rp - r\rho V^2 \cos\theta \sin\xi/\cos\beta)\,dr\,d\phi$$

$$+ \text{Fixed Axial Thrust}_{IF} - \int_0^{2\pi} \int_0^{r_e(\phi)} rp_a\,dr\,d\phi \qquad (126)$$

The last term in Eq. (126) can be split into two surface integrals and written as

$$\int_0^{2\pi} \int_0^{r_e(\phi)} rp_a\,dr\,d\phi = \int_0^{2\pi} \int_0^{r_i(\phi)} rp_a\,dr\,d\phi + \int_0^{2\pi} \int_{r_i(\phi)}^{r_e(\phi)} rp_a\,dr\,d\phi \qquad (127)$$

where the first term on the RHS is a fixed quantity in the variational problem since $r_i(\phi)$ is known and p_a is a constant. By combining this fixed quantity with the Fixed Axial Thrust_{IF} term, the axial thrust equation can be written as

$$\text{Axial Thrust} = \int_0^{2\pi} \int_{r_i(\phi)}^{r_e(\phi)} (r(p - p_a) - r\rho V^2 \cos\theta \sin\xi/\cos\beta)\,dr\,d\phi$$

$$+ \text{Fixed Axial Thrust}_{IF} \qquad (128)$$

It is the axial thrust as expressed in Eq. (128) that is to be maximized in the variational problem.

2. INTEGRAL MASS FLOW RATE EQUATION

The following expression represents the total mass flow rate through the nozzle:

$$\dot{m}_T = \dot{m}_{c.s.} + \text{Fixed Mass Flow Rate}_{IF} \tag{129}$$

where

$$\dot{m}_{c.s.} = \iint_{c.s.} -\rho(\bar{V} \cdot \overline{dA}_{c.s.}) \tag{130}$$

The Fixed Mass Flow Rate$_{IF}$ term in Eq. (119) is the mass flow rate across the surface IF. By substituting Eqs. (120) through (124) into Eq. (130), it is possible to rewrite Eq. (129) as follows:

$$\dot{m}_T = \int_0^{2\pi} \int_{r_i(\phi)}^{r_e(\phi)} (-r\rho V \sin\xi/\cos\beta)\, dr\, d\phi + \text{Fixed Mass Flow Rate}_{IF} \tag{131}$$

It is the total mass flow rate $\dot{m}_T$ as given by Eq. (131) that is constrained in the analysis to be a constant.

APPENDIX D
APPLICATION OF THE CALCULUS OF VARIATIONS

In this appendix, the necessary conditions which must be satisfied to extremize a generalized functional having the form

$$I = \iint_S F(\phi, r, z_k, p_k, q_k)\,dr\,d\phi \tag{132}$$

are derived. The derivation closely parallels the presentation in Miele (18).

In the surface integral, r and ϕ denote the independent variables, z_k are the dependent variables ($k = 1, \cdots, n$), and

$$p_k \equiv z_{k\phi} \equiv \partial z_k/\partial\phi \tag{133}$$

$$q_k \equiv z_{kr} \equiv \partial z_k/\partial r \tag{134}$$

indicate partial derivatives of z_k with respect to the independent variables. The function F is an arbitrarily specified function of the arguments within the parenthesis, called the fundamental function, and S is the domain of integration.

The value of the functional I depends on the choice of the surface σ, defined by the n functions $z_k(r,\phi)$, whose projection on the $r\phi$-plane is the region S. The boundary of the surface σ is denoted by the symbol τ while the boundary of the planar region S is denoted by the symbol B. Figure 33 illustrates these geometric relationships.

An admissible surface σ is defined as any set of functions $z_k(r,\phi)$ which are continuous, whose derivatives are continuous everywhere except along a finite number of corner lines, and which satisfy the prescribed boundary conditions. The balance of this appendix deals with applying

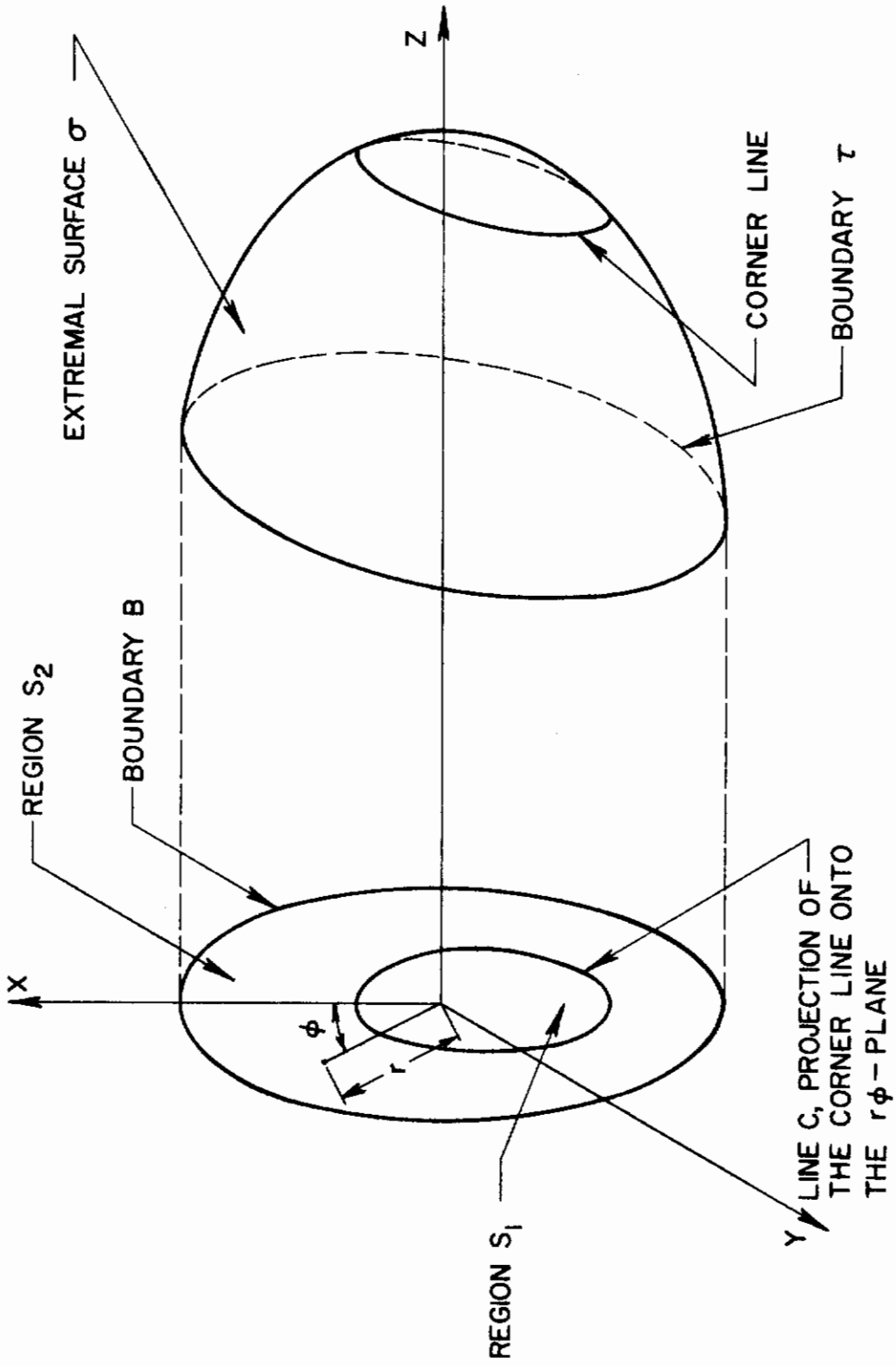

FIGURE 33. EXTREMAL SURFACE

the calculus of variations to the problem of determining that special surface in the class of admissible surfaces which maximizes the functional I in Eq. (132).

For the surface σ to be an extremal surface the set of functions $z_k(r,\phi)$ must be such that the first variation of the functional vanishes identically for every admissible distribution of variations; that is

$$\delta I = 0 \tag{135}$$

The condition expressed in Eq. (135) is a necessary condition for a relative maximum of the functional I. An admissible distribution of variations is defined as any set of functions $\tilde{\delta} z_k(r,\phi)$ which are continuous and consistent with the prescribed boundary conditions.

The first variation of the functional I is given by the expression

$$I = \iint_{S_1} \delta F dr d\phi + \iint_{\delta S_1} F dr d\phi + \iint_{S_2} \delta F dr d\phi + \iint_{\delta S_2} F dr d\phi \tag{136}$$

where the difficulties arising from the presence of discontinuities in the derivatives of the unknown functions are bypassed by dividing the domain of integration for the surface integral into subdomains in which the derivatives are continuous. For simplicity, Eq. (136) is written for the case in which only one corner line is present in the class of surfaces being investigated. The symbol δF denotes the first variation of the fundamental function F calculated at a constant station r and ϕ and is represented by

$$\delta F = \sum_{k=1}^{n} \left(F_{z_k} \tilde{\delta} z_k + F_{p_k} \tilde{\delta} p_k + F_{q_k} \tilde{\delta} q_k \right) \tag{137}$$

with $\tilde{\delta} z_k$, $\tilde{\delta} p_k$, and $\tilde{\delta} q_k$ denoting variations calculated holding the independent variables r and ϕ constant. Because of the continuity requirement for the functions $z_k(r,\phi)$, these variations satisfy the relationships shown below:

$$\tilde{\delta p}_k = \frac{\partial(\tilde{\delta z}_k)}{\partial \phi} \,, (k = 1, \ldots, n) \tag{138}$$

$$\tilde{\delta q}_k = \frac{\partial(\tilde{\delta z}_k)}{\partial r} \,, (k = 1, \ldots, n) \tag{139}$$

In Eq. (136), δS_1 and δS_2 denote the variation of the area of integration resulting from variations of the coordinates of the boundary line τ. For instance, the contour B may be given while the distribution of ordinates is free, or the ordinate z may be required to have a constant value while the contour B is free, or the boundary line τ may be allowed to belong to any surface of three-dimensional space. The latter contains every other problem as a particular case since if a boundary τ is a solution to a problem with an unconstrained boundary, then the same surface σ is an optimal if the boundary is constrained to be this same τ.

Upon combining the above equations, operating on terms by Green's theorem, integrating by parts and rearranging terms as shown in (18), the following optimizing condition is obtained:

$$\begin{aligned}
\delta I = &\iint_{S_1} \sum_{k=1}^{n} \left(F_{z_k} - \frac{\partial}{\partial \phi}(F_{p_k}) - \frac{\partial}{\partial r}(F_{q_k})\right)\tilde{\delta z}_k \, dr d\phi \\
&+ \iint_{S_2} \sum_{k=1}^{n} \left(F_{z_k} - \frac{\partial}{\partial \phi}(F_{p_k}) - \frac{\partial}{\partial r}(F_{q_k})\right)\tilde{\delta z}_k \, dr d\phi \\
&+ \int_B \left(X\delta\phi + Y\delta r + \sum_{k=1}^{n} W_k \delta z_k\right) d\phi \\
&- \int_C \left(\Delta K \delta\phi + \Delta Q \delta r + \sum_{k=1}^{n} \Delta R_k \delta z_k\right) d\phi = 0
\end{aligned} \tag{140}$$

which must be satisfied for every admissible distribution of variations. In these relationships, the functions X, Y, W_k, K, Q and R_k are given by

$$X = \sum_{k=1}^{n} p_k F_{q_k} + \dot{r}(F - \sum_{k=1}^{n} p_k F_{p_k}) \tag{141}$$

$$Y = -(F - \sum_{k=1}^{n} q_k F_{q_k}) - \dot{r} \sum_{k=1}^{n} q_k F_{p_k} \tag{142}$$

$$W_k = -F_{q_k} + \dot{r} F_{p_k}, (k = 1, \ldots, n) \tag{143}$$

$$K = \sum_{k=1}^{n} p_k F_{q_k} + \dot{r}(F - \sum_{k=1}^{n} p_k F_{p_k}) \tag{144}$$

$$Q = -(F - \sum_{k=1}^{n} q_k F_{q_k}) - \dot{r} \sum_{k=1}^{n} q_k F_{p_k} \tag{145}$$

$$R_k = -F_{q_k} + \dot{r} F_{p_k}, (k = 1, \ldots., n) \tag{146}$$

Equation (140) is written with $\Delta(\cdots)$ denoting the difference in the quantity $(\cdots)$ evaluated on the outer side of the corner line and the same quantity evaluated on the inner side.

Equation (140) must be satisfied for every admissible distribution of variations for I to be an extremum.

APPENDIX E
DERIVATION OF THE EQUATIONS FOR AN OPTIMAL CONTROL SURFACE

1. INTRODUCTION

In this appendix the set of equations which will be solved to yield the shape of the optimal control surface and the flow variables V, θ and ψ on the optimal control surface for given initial conditions is derived. Five equations are derived which represent the solution for the five variables $V(r,\phi)$, $\theta(r,\phi)$, $\psi(r,\phi)$, $\alpha(r,\phi)$ and $\beta(r,\phi)$. The shape of the control surface can be determined if $\alpha(r,\phi)$ and $\beta(r,\phi)$ are known.

Four of the five equations result from allowing the variations of the four dependent variables $\tilde{\delta}V$, $\tilde{\delta}\theta$, $\tilde{\delta}\psi$ and $\tilde{\delta}f$ to be arbitrary and independent while applying the calculus of variations to maximize the axial thrust of the nozzle. The fifth equation results from the relationships between α, β and f and the requirement that the derivatives of V, θ, ψ and f be continuous on the optimal control surface except across a finite number of corner lines.

2. EULER EQUATIONS

In Appendix D the necessary conditions which must be satisfied to extremize a generalized functional I having the form

$$I = \iint_S F(r,\phi,z_k,p_k,q_k)\,dr\,d\phi \qquad (147)$$

are presented. In Eq. (147) F is the fundamental function, r and ϕ are the independent variables, z_k (k = 1,..n) represent the n dependent variables, and the terms p_k and q_k are defined as follows:

$$p_k = \partial z_k/\partial\phi = z_{k\phi} \tag{148}$$

$$q_k = \partial z_k/\partial r = z_{kr} \tag{149}$$

A necessary condition for I to be an extremum is that the first variation of I is equal to zero for every admissible distribution of variations. Setting the first variation of I equal to zero results in the following equation:

$$\begin{aligned}\delta I = &\iint_{S_1} \sum_{k=1}^{n} \left(F_{z_k} - \frac{\partial}{\partial\phi}(F_{p_k}) - \frac{\partial}{\partial r}(F_{q_k})\right)\tilde{\delta} z_k \, dr d\phi \\ &+ \iint_{S_2} \sum_{k=1}^{n} \left(F_{z_k} - \frac{\partial}{\partial\phi}(F_{p_k}) - \frac{\partial}{\partial r}(F_{q_k})\right)\tilde{\delta} z_k \, dr d\phi \\ &+ \int_B \left(X\delta\phi + Y\delta r + \sum_{k=1}^{n} W_k \, z_k\right) d\phi \\ &- \int_C \left(\Delta K\delta\phi + \Delta Q\delta r + \sum_{k=1}^{n} \Delta R_k \delta z_k\right) d\phi = 0\end{aligned} \tag{150}$$

where X, Y, W_k, ΔK, ΔQ and ΔR_k are defined by Eqs. (141) through (146). For arbitrary and independent variations of the n dependent variables z_k, Eq. (150) can only be satisfied if the following n equations are valid in the regions S_1 and S_2:

$$F_{z_k} - \frac{\partial}{\partial\phi}(F_{p_k}) - \frac{\partial}{\partial r}(F_{q_k}) = 0 \quad (k = 1,..,n) \tag{151}$$

where

$$F_{p_k} = \partial F/\partial z_{k\phi} \tag{152}$$

$$F_{q_k} = \partial F/\partial z_{kr} \tag{153}$$

The n equations given by Eq. (151) are referred to as the Euler equations.

In this research the functional I to be maximized has the form

$$I = \int_0^{2\pi} \int_{r_i(\phi)}^{r_e(\phi)} F(r,\phi,V,p,\rho,\theta,\psi,\frac{\partial f}{\partial \phi},\frac{\partial f}{\partial r}) dr d\phi \tag{154}$$

where

$$F = r(p-p_a) - r\rho V(V\cos\theta + \lambda_2)(-\cos\theta + \sin\theta\cos\psi \frac{\partial f}{\partial r} + \frac{\sin\theta\sin\psi}{r} \frac{\partial f}{\partial \phi}) \tag{155}$$

In Appendix B it was shown that for steady, inviscid, irrotational, homentropic flow of a perfect gas, the pressure p and density ρ are unique functions of the velocity V, the stagnation pressure p_o and the stagnation enthalpy h_o. Thus, the fundamental function F given by Eq. (155) is only a function of the four dependent variables V, θ, ψ and f. Therefore, to apply the general theory of Appendix D to the functional under consideration, the quantities z_k, p_k and q_k are defined as follows:

$$z_1 = V,\ z_2 = \theta,\ z_3 = \psi,\ z_4 = f \tag{156}$$

$$p_1 = \partial V/\partial\phi,\ p_2 = \partial\theta/\partial\phi,\ p_3 = \partial\psi/\partial\phi,\ p_4 = \partial f/\partial\phi \tag{157}$$

$$q_1 = \partial V/\partial r,\ q_2 = \partial\theta/\partial r,\ q_3 = \partial\psi/\partial r,\ q_4 = \partial f/\partial r \tag{158}$$

Using Eqs. (156) through (158) to expand Eq. (151) results in the following four equations:

$$\frac{\partial F}{\partial V} + \frac{\partial F}{\partial p}\frac{dp}{dV} + \frac{\partial F}{\partial \rho}\frac{d\rho}{dV} - \frac{\partial}{\partial\phi}(\frac{\partial F}{\partial p_1}) - \frac{\partial}{\partial r}(\frac{\partial F}{\partial q_1}) = 0 \tag{159}$$

$$\frac{\partial F}{\partial \theta} - \frac{\partial}{\partial\phi}(\frac{\partial F}{\partial p_2}) - \frac{\partial}{\partial r}(\frac{\partial F}{\partial q_2}) = 0 \tag{160}$$

$$\frac{\partial F}{\partial \psi} - \frac{\partial}{\partial \phi}\left(\frac{\partial F}{\partial p_3}\right) - \frac{\partial}{\partial r}\left(\frac{\partial F}{\partial q_3}\right) = 0 \tag{161}$$

$$\frac{\partial F}{\partial f} - \frac{\partial}{\partial \phi}\left(\frac{\partial F}{\partial p_4}\right) - \frac{\partial}{\partial r}\left(\frac{\partial F}{\partial q_4}\right) = 0 \tag{162}$$

If the above operations are carried out using the fundamental function given in Eq. (155), the four Euler equations, Eqs. (159) through (162), can be rewritten as follows:

$$(V\cos\theta + \lambda_2)(V^2/a^2 - 1)(\sin\xi/\cos\beta) - V(1 + \cos\theta\sin\xi/\cos\beta) = 0 \tag{163}$$

$$V\sin\theta\sin\xi/\cos\beta - (V\cos\theta + \lambda_2)(\sin\theta - \tan\beta\cos\theta + \cos(\psi - \alpha)) = 0 \tag{164}$$

$$(V\cos\theta + \lambda_2)\sin\beta\sin\theta\sin(\psi - \alpha) = 0 \tag{165}$$

$$\frac{\partial}{\partial \phi}(\rho V(V\cos\theta + \lambda_2)\sin\theta\sin\psi) + \frac{\partial}{\partial r}(r\rho V(V\cos\theta + \lambda_2)\sin\theta\cos\psi) = 0 \tag{166}$$

where the three geometric relations

$$\partial f/\partial r = -\tan\beta\cos\alpha \tag{167}$$

$$\partial f/\partial \phi = -r\tan\beta\sin\alpha \tag{168}$$

$$\frac{\sin\xi}{\cos\beta} = -\cos\theta + \sin\theta\cos\psi\,\frac{\partial f}{\partial r} + \frac{\sin\theta\sin\psi}{r}\,\frac{\partial f}{\partial \phi} \tag{169}$$

derived in Appendix A, have been used to simplify the results.

The only acceptable solution to Eq. (165) is that $\alpha = \psi$. The solution $\alpha = \psi + \pi$ is geometrically not acceptable, and the solution $(V\cos\theta + \lambda_2) = 0$ leads to a trivial solution when used in Eqs. (163), (164) and (166). Therefore, on an optimal control surface

$$\alpha = \psi \tag{170}$$

When Eqs. (167) through (170) are combined, the equation

$$\sin\xi = -\cos(\theta + \beta) \tag{171}$$

can be derived. For $\alpha = \psi$ the two Euler equations, Eqs. (163) and (164), can be rewritten in the following forms:

$$\frac{(V\cos\theta + \lambda_2)}{V} = \frac{\sin\theta\sin\xi}{(\sin\theta\cos\beta - \cos\theta\sin\beta)} \tag{172}$$

$$\frac{(V\cos\theta + \lambda_2)}{V} = \frac{\sin^2\mu(\cos\beta + \cos\theta\sin\xi)}{\sin\xi(1 - \sin^2\mu)} \tag{173}$$

where μ is the Mach angle defined by the relationship

$$V/a = M = 1/\sin\mu \tag{174}$$

Setting the RHS of Eq. (172) equal to the RHS of (173) and using Eq. (171) results in the following equation:

$$\sin^2\mu = \sin^2\xi \tag{175}$$

Thus, $\mu = \xi$ since the other solutions to Eq. (175) can be discarded on the basis of geometric considerations.

With this information further simplifications are possible. The relationship $\mu = \xi$ and Eq. (171) can be combined, and the following expression results:

$$\beta = \theta + \mu + \pi/2 \tag{176}$$

By using the fact that $\alpha = \psi$ and $\mu = \xi$, Eq. (172) can be rewritten as

$$\frac{V\cos\theta + \lambda_2}{V} = \frac{\sin\theta\sin\mu}{\sin\theta\cos\beta - \cos\theta\sin\beta} \tag{177}$$

Equation (177) can be further reduced to the following form by using Eq. (30):

$$V\cos\theta + \lambda_2 = - V\sin\theta\tan\mu \tag{178}$$

At this point only one of the original Euler equations has not been utilized. This equation, Eq. (166), can be combined with Eq. (178) to yield the following equation:

$$\frac{\partial}{\partial\phi}\left(\rho V^2\sin^2\theta\tan\mu\sin\psi\right) + \frac{\partial}{\partial r}\left(r\rho V^2\sin^2\theta\tan\mu\cos\psi\right) = 0 \tag{179}$$

In summary, the four Euler equations have been reduced to the four equations:

$$V\cos\theta + \lambda_2 = - V\sin\theta\tan\mu \tag{180}$$

$$\alpha = \psi \tag{181}$$

$$\beta = \theta + \mu + \pi/2 \tag{182}$$

$$\frac{\partial}{\partial\phi}\left(\rho V^2\sin^2\theta\tan\mu\sin\psi\right) + \frac{\partial}{\partial r}\left(r\rho V^2\sin^2\theta\tan\mu\cos\psi\right) = 0 \tag{183}$$

3. EQUATION RESULTING FROM CONTINUOUS DERIVATIVES

In Appendix D the necessary conditions to extremize the general functional I given by Eq. (147) were derived under the assumption that an admissible surface σ was defined as any set of functions z_k (k=1,...,n) which were continuous, had continuous derivatives, and satisfied the prescribed boundary conditions. For the functional I given by Eq. (154), the dependent variables are V, θ, ψ and f. Thus, the functional I is being maximized under the assumption that $V(r,\phi)$, $\theta(r,\phi)$, $\psi(r,\phi)$ and $f(r,\phi)$ are continuous and have continuous derivatives in regions S_1 and S_2. This requirement can be used to obtain a form of the geometric relationships between α, β and f which can be combined with the Euler equations to obtain an additional relationship between V, θ and ψ in regions S_1 and S_2.

As shown in Appendix B, the Mach angle μ is a unique function of V, p_0 and h_0. Thus, when the condition that V, θ and ψ are continuous with continuous first derivatives is combined with Eqs. (181) and (182), it can be concluded that on an optimal control surface the angles α and β must also be continuous and have continuous first derivatives. Furthermore, Eqs. (167) and (168) can be used to show that the derivatives $\partial^2 f/\partial r^2$, $\partial^2 f/\partial \phi^2$, $\partial^2 f/\partial r \partial \phi$ and $\partial^2 f/\partial \phi \partial r$ are continuous since α and β have continuous first derivatives.

As stated in Ref. (19), if all second derivatives of a function are continuous, the order of differentation is immaterial. In other words,

$$\frac{\partial}{\partial \phi}\left(\frac{\partial f}{\partial r}\right) = \frac{\partial}{\partial r}\left(\frac{\partial f}{\partial \phi}\right) \tag{184}$$

Equations (167), (168) and (184) then combine to yield the following expression:

$$\frac{\partial}{\partial \phi}\left(\tan\beta\cos\alpha\right) = \frac{\partial}{\partial r}\left(r\tan\beta\sin\alpha\right) \tag{185}$$

By substituting Eqs. (181) and (182) into Eq. (185), the following equation which must be satisfied on an optimal control surface is derived:

$$\frac{\partial}{\partial\phi}\left(\tan(\theta+\mu+\pi/2)\cos\psi\right)-\frac{\partial}{\partial r}\left(r\tan(\theta+\mu+\pi/2)\sin\psi\right) \quad (186)$$

4. SUMMARY

In summary, the following set of five independent equations which are valid on an optimal control surface has been derived:

$$V\cos\theta+\lambda_2=-V\sin\theta\tan\mu \quad (187)$$

$$\frac{\partial}{\partial\phi}\left(\rho V^2\sin^2\theta\tan\mu\sin\psi\right)+\frac{\partial}{\partial r}\left(r\rho V^2\sin^2\theta\tan\mu\cos\psi\right)=0 \quad (188)$$

$$\frac{\partial}{\partial\phi}\left(\tan(\theta+\mu+\pi/2)\cos\psi\right)-\frac{\partial}{\partial r}\left(r\tan(\theta+\mu+\pi/2)\sin\psi\right)=0 \quad (189)$$

$$\alpha=\psi \quad (190)$$

$$\beta=\theta+\mu+\pi/2 \quad (191)$$

The five dependent variables in the above five equations are $V(r,\phi)$, $\theta(r,\phi)$, $\psi(r,\phi)$, $\alpha(r,\phi)$ and $\beta(r,\phi)$. If $\alpha(r,\phi)$ and $\beta(r,\phi)$ are known, Eqs. (167) and (168) can be used to solve for $f(r,\phi)$.

APPENDIX F
DERIVATION OF THE TRANSVERSALITY EQUATION

The transversality equation is a necessary condition that must be satisfied when variations of the boundaries of the region S are considered. The transversality equation relates the values of the independent and dependent variables on the boundaries of the extremal surface and provides boundary conditions for the Euler equations. In this appendix the transversality equation is derived in a manner consistent with the following constraints: 1) the conditions along the inner boundary of the region S (i.e., the initial value line) are known and can not be varied in the variational problem, and 2) along the outer boundary of the region S (i.e., the nozzle exit lip) the axial position of the boundary is fixed in the variational problem.

The following equation must be satisfied for every set of variations $\delta\phi$, δr and δz_k consistent with the conditions imposed on the location of the boundary line B:

$$\int_B (X\delta\phi + Y\delta r + \sum_{k=1}^{n} W_k \delta z_k) d\phi = 0 \qquad (192)$$

where ϕ has been chosen as the independent variable of the line integral since ϕ has the property of being monotonic everywhere along a boundary. The terms X, Y, W_k and z_k in Eq. (192) are defined as follows:

$$X = \sum_{k=1}^{n} p_k F_{q_k} + \dot{r}(F - \sum_{k=1}^{n} p_k F_{p_k}) \qquad (193)$$

$$Y = -(F - \sum_{k=1}^{n} q_k F_{q_k}) - \dot{r} \sum_{k=1}^{n} q_k F_{p_k} \qquad (194)$$

$$W_k = -F_{q_k} + \dot{r} F_{p_k} \qquad (k = 1,..,4) \qquad (195)$$

where $\dot{r} = dr/d\phi$ and

$$F = r(p-p_a) - r\rho V(V\cos\theta + \lambda_2)(-\cos\theta + \sin\theta\cos\psi \frac{\partial f}{\partial r} + \frac{\sin\theta\sin\psi}{r} \frac{\partial f}{\partial \phi}) \quad (196)$$

$$p_1 = \partial V/\partial\phi,\ p_2 = \partial\theta/\partial\phi,\ p_3 = \partial\psi/\partial\phi,\ p_4 = \partial f/\partial\phi \quad (197)$$

$$q_1 = \partial V/\partial r,\ q_2 = \partial\theta/\partial r,\ q_3 = \partial\psi/\partial r,\ q_4 = \partial f/\partial r \quad (198)$$

For the fundamental function F presented in Eq. (196), Eqs. (192) and (193) through (195) reduce to the following equations:

$$\int_B (X\delta\phi + Y\delta r + W_4\delta f)d\phi = 0 \quad (199)$$

$$X = p_4F_{q_4} + \dot{r}F - \dot{r}p_4F_{p_4} \quad (200)$$

$$Y = -F + q_4F_{q_4} - \dot{r}q_4F_{p_4} \quad (201)$$

$$W_k = 0 \qquad (k = 1,2,3) \quad (202)$$

$$W_4 = -F_{q_4} + \dot{r}F_{p_4} \quad (203)$$

The region S has two boundaries. These are: 1) the projection of the initial value line on the $r\phi$-plane, and 2) the projection of the exit lip of the nozzle on the $r\phi$-plane. The relative locations of these two boundaries is shown in Figure 34.

On the inner boundary of S (i.e., the initial value line) no variations are allowed while applying the calculus of variations to maximize the functional I since the conditions on the initial value line are specified and fixed. Hence, the three variations δf, δr and $\delta\phi$ are each identically zero when evaluated on the inner boundary of the regions. Therefore, Eq. (199) reduces to the following form:

$$\int_{\Gamma_e} (X\delta\phi_e + Y\delta r_e + W_4\delta f_e)d\phi = 0 \quad (204)$$

where Γ_e denotes the outer boundary of the control surface (i.e., the nozzle exit lip). Before any additional information can be obtained

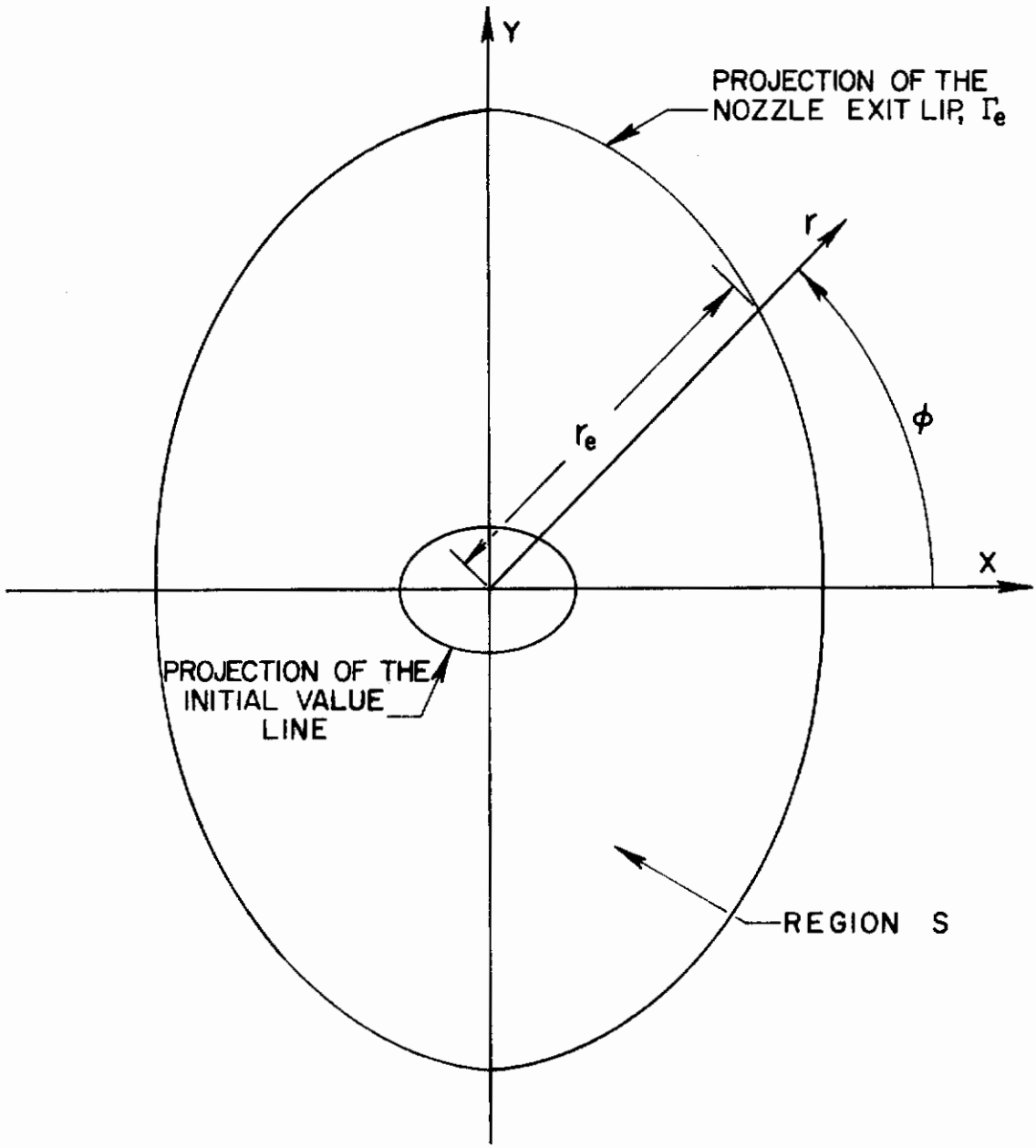

FIGURE 34. CONTROL SURFACE PROJECTION ON THE $r\phi$-PLANE

from Eq. (204), it is necessary to determine how the variations δf_e, δr_e and $\delta \phi_e$ are related. The fixed length constraint can then be imposed on Eq. (204).

As shown by Elsgolc (17), it is possible to write the following expression for the value of f_e in terms of the variational parameter ε:

$$f_e = f_e(\varepsilon) = f_e\left\{\varepsilon,\ r_e(\varepsilon,\ \phi_e(\varepsilon)),\ \phi_e(\varepsilon)\right\} \tag{205}$$

Differentiating f_e with respect to ε yields the following equation:

$$\frac{df_e}{d\varepsilon} = \frac{\partial f_e}{\partial \varepsilon} + \frac{\partial f_e}{\partial r_e}\frac{dr_e}{d\varepsilon} + \frac{\partial f_e}{\partial \phi_e}\frac{d\phi_e}{d\varepsilon} \tag{206}$$

In the limit as $\varepsilon \to 0$ Eq. (206) becomes the following expression:

$$\delta f_e = \tilde{\delta} f_e + \frac{\partial f_e}{\partial r_e}\partial r_e + \frac{\partial f_e}{\partial \phi}\delta\phi \tag{207}$$

where $\tilde{\delta} f_e$ denotes variations of $f_e(\varepsilon, r_e, \phi_e)$ taken while holding the variables r_e and ϕ_e constant, and δf_e denotes variations of $f_e(\varepsilon, r_e, \phi_e)$ with no restrictions on how r_e and ϕ_e can vary.

On the boundary Γ_e, ϕ_e is the sole independent variable, and in the variational problem

$$r_e = r_e(\varepsilon,\ \phi_e(\varepsilon)) \tag{208}$$

From Eq. (208) it follows that

$$\delta r_e = \tilde{\delta} r_e + \dot{r}\delta\phi \tag{209}$$

where $\tilde{\delta} r_e$ denotes variations of $r_e(\varepsilon, \phi_e)$ taken while holding the independent variable ϕ_e constant, and δr_e denotes variations of $r_e(\varepsilon, \phi_e)$ taken with no restrictions on how ϕ_e can vary.

Equation (204) can now be simplified by substituting Eqs. (200) through (203) into Eq. (204) and using Eqs. (207) and (209) to combine terms. These operations result in the following equation:

$$\int_{\Gamma_e} \left(F\tilde{\delta} r_e + (-F_{q_4} + \dot{r}F_{p_4})\tilde{\delta} f_e\right) d\phi = 0 \tag{210}$$

Forming the partial derivatives of F as indicated and substituting Eq. (196) into Eq. (210) yields the following equation:

$$\int_{\Gamma_e} \left\{ \left[r(p-p_a) - r\rho V(V\cos\theta+\lambda_2)\left(-\cos\theta + \sin\theta\cos\psi \frac{\partial f}{\partial r} + \frac{\sin\theta\sin\psi}{r} \frac{\partial f}{\partial \phi}\right)\right] \tilde{\delta} r_e \right.$$

$$\left. + \left[r\rho V \sin\theta (V\cos\theta + \lambda_2)(\cos\psi - \dot{r}\sin\psi/r) \right] \tilde{\delta} f_e \right\} d\phi = 0 \qquad (211)$$

Equation (211) is now evaluated consistent with the constraints on the problem.

The purpose of this research is to design three-dimensional nozzles which are designed for a fixed length (the length may vary with ϕ_e), have a fixed mass flow rate, exhaust to a fixed ambient pressure and produce the maximum axial thrust subject to these conditions. The fixed mass flow rate constraint has already been imposed on the variational problem; however, the fixed length and fixed ambient pressure constraints must be introduced into Eq. (211) in order for the constraints to be satisfied.

Since the length of the nozzle is fixed, the nozzle length f_e can not be varied while applying the calculus of variations to maximize the thrust; therefore, the variation $\tilde{\delta} f_e$ is equal to zero. Since the exit radius r_e is allowed to seek its optimal value and satisfy the ambient pressure constraint, the variation $\tilde{\delta} r_e$ is arbitrary. There is an additional condition which must be true for the fixed length constraint to be satisfied. This condition is that in the variational problem while allowing for variations in r_e the following equations are valid: 1) $\partial f_e/\partial r_e = 0$ and, 2) $\partial f_e/\partial \phi_e = df_e/d\phi_e$. If this condition is not satisfied, the nozzle length f_e can change with variations in r_e. Thus, in the variational problem, the variation $\tilde{\delta} r_e$ is arbitrary and independent, and the following three equations are substituted into Eq. (211) to enforce the fixed length constraint:

$$\tilde{\delta} f_e = 0 \qquad (212)$$

$$\partial f_e/\partial r_e = 0 \qquad (213)$$

$$\partial f_e/\partial \phi_e = df_e/d\phi_e \qquad (214)$$

Substituting Eqs. (212) through (214) into Eq. (211) and requiring that the variation $\tilde{\delta}r_e$ be arbitrary results in the following expression:

$$\left[r(p-p_a) - r\rho V(V\cos\theta + \lambda_2)(-\cos\theta + \frac{\sin\theta\sin\psi}{r_e}\frac{df_e}{d\phi_e})\right]\Bigg|_{\Gamma_e} = 0 \qquad (215)$$

In Appendix E it is shown that on the optimal control surface the following algebraic equation is valid:

$$(V\cos\theta + \lambda_2) = -V\sin\theta\tan\mu \qquad (216)$$

Substituting Eq. (216) into Eq. (215) and dividing by r_e yields the following equation:

$$\left[(p-p_a) + \rho V^2\sin\theta\tan\mu(-\cos\theta + \frac{\sin\theta\sin\psi}{r_e}\frac{df_e}{d\phi_e})\right]\Bigg|_{\Gamma_e} = 0 \qquad (217)$$

Equation (217) is the transversality equation for a fixed length, maximum thrust and constant mass flow rate nozzle where $r_e(\phi)$ has been allowed to seek its optimal value.

The transversality equation for a fixed length constraint can also be derived in a manner analogous to that used by Guderley (3) in the axisymmetric,one independent variable problem. Consider a control surface ending at the exit lip of the nozzle. Since a variation in the nozzle exit radius r_e is permitted, supplement the control surface by an annular surface on which f is only a function of ϕ and which extends between the exit lip of the original nozzle and the exit lip of a new nozzle with a varied contour. The annular surface is illustrated in Figure 35, and the change in radius is $\tilde{\delta}r_e$.

The momentum transferred through this annular surface is given by the following expression:

$$\int_{\Gamma_e}(r(p-p_a) + r\rho V^2\cos\theta(\cos\theta - \frac{\sin\theta\sin\psi}{r}\frac{df_e}{d\phi_e}))\delta r_e d\phi \qquad (218)$$

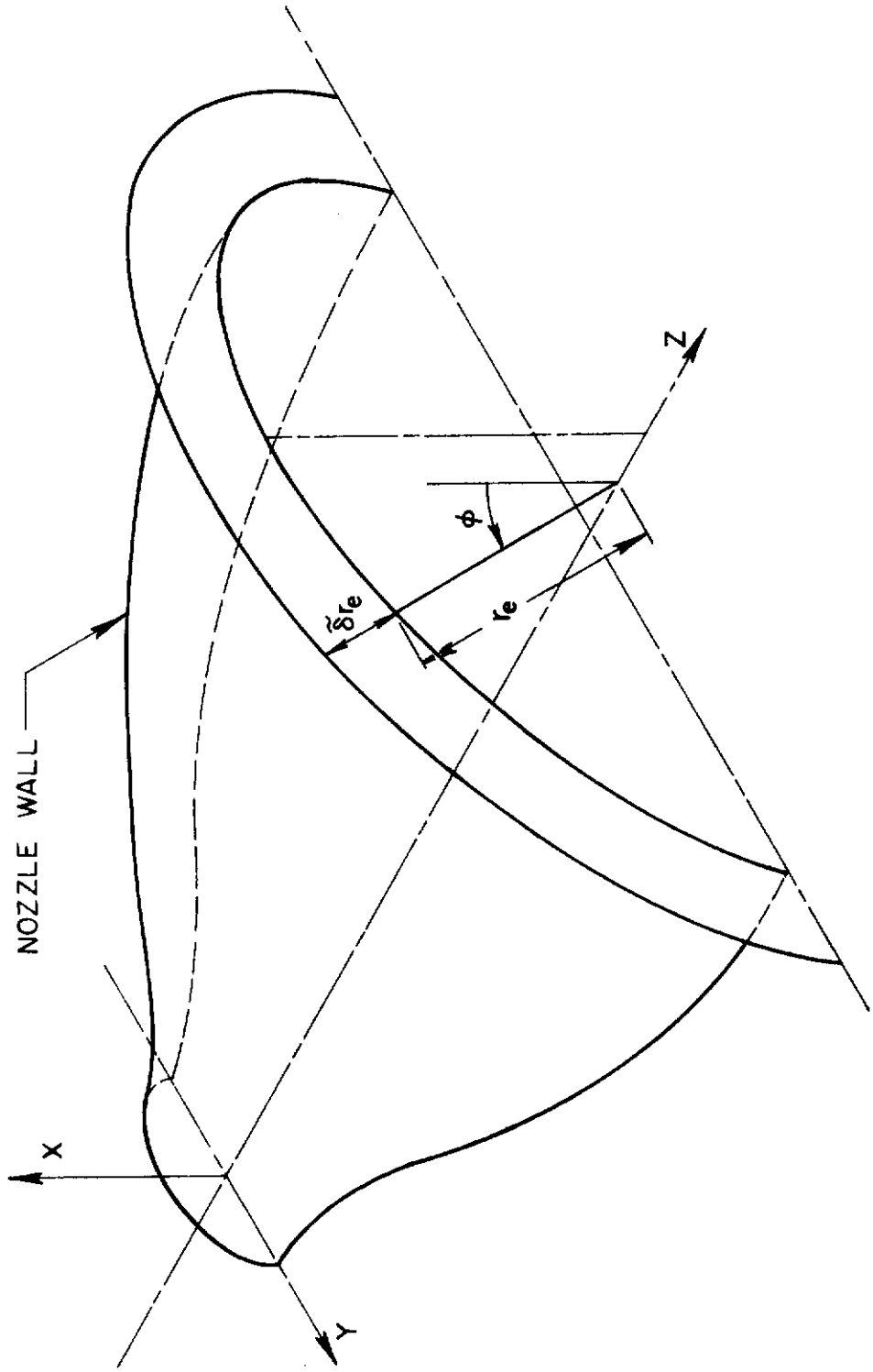

FIGURE 35. ANNULAR SURFACE FOR DERIVING TRANSVERSALITY EQUATION

The mass flow rate through this section is

$$\int_{\Gamma_e} \left(r\rho V\left(\cos\theta - \frac{\sin\theta\sin\psi}{r}\frac{df_e}{d\phi_e}\right)\right)\tilde{\delta}r_e\,d\phi \qquad (219)$$

Therefore, in computing the variation of the fundamental function I, the following additional term appears:

$$\int_{\Gamma_e} \left(r(p-p_a) + r\rho V^2\left(\frac{V\cos\theta + \lambda_2}{V}\right)\left(\cos\theta - \frac{\sin\theta\sin\psi}{r}\frac{df_e}{dr_e}\right)\right)\tilde{\delta}r_e\,d\phi \qquad (220)$$

For arbitrary variations $\tilde{\delta}r_e$, Eq. (220) is satisfied only if

$$\left((p-p_a) + \rho V^2\sin\theta\tan\mu\left(-\cos\theta + \frac{\sin\theta\sin\psi}{r_e}\frac{df_e}{d\phi_e}\right)\right)\Bigg|_{\Gamma_e} = 0 \qquad (221)$$

where Eq. (216) has been used to eliminate λ_2. Equation (221) is identical to the transversality equation, Eq. (217).

APPENDIX G
DERIVATION OF THE CORNER LINE CONDITIONS

In this appendix the Erdmann-Weirstrass corner condition equations for this problem are derived. These equations join subsurfaces of an optimal control surface should there be corner lines on the surface.

An admissible extremal surface σ is defined in Appendix D as any set of functions $z_k(r,\phi)$ which are continuous everywhere except along a finite number of corner lines, and which satisfy the respective boundary conditions. The set of equations which govern the portion of an extremal surface where the derivatives are continuous is derived in Appendix E while the transversality equation which must be satisfied along the boundary of an extremal surface is derived in Appendix F. When a corner line is present on an extremal surface (i.e., the derivatives of the dependent variables z_k are discontinuous across a line on the extremal surface), a mathematical criterion is needed to join the subsurfaces of the extremal surface. This criterion is the Erdmann-Weirstrass corner condition.

The Erdmann-Weirstrass corner condition results from the following expression which must be satisfied in order for δI to equal zero:

$$\oint_C (\Delta K \delta\phi + \Delta Q \delta r + \sum_{k=1}^{n} \Delta R_k \delta z_k) d\phi = 0 \qquad (222)$$

where the line integral is along the corner lines on the extremal surface. In this work no restrictions are placed on the corner lines (i.e., the corner lines are free), and the (n+2) variations $\delta\phi$, δr and δz_k are independent and arbitrary along any corner line. From Eq. (222) it follows that at any point on a corner line the following (n+2) equations must be satisfied:

$$\Delta K = 0 \tag{223}$$

$$\Delta Q = 0 \tag{224}$$

$$\Delta R_k = 0 \qquad (k = 1,..,n) \tag{225}$$

where

$$K = \sum_{k=1}^{n} p_k F_{q_k} + \dot{r}(F - \sum_{k=1}^{n} p_k F_{p_k}) \tag{226}$$

$$Q = -(F - \sum_{k=1}^{n} q_k F_{q_k}) - \dot{r} \sum_{k=1}^{n} q_k F_{p_k} \tag{227}$$

$$R_k = -F_{q_k} + \dot{r}F_{p_k} \qquad (k = 1,..,n) \tag{228}$$

and the symbol $\Delta(\cdots)$ denotes the difference of the quantity $(\cdots)$ evaluated on the outer side of the corner line and the same quantity evaluated on the inner side. Equations (223) through (225) are the Erdmann-Weirstrass corner conditions for the case of the corner lines being free.

For the fundamental function F given by

$$F = r(p - p_a) - r\rho V(V\cos\theta + \lambda_2)(-\cos\theta + \sin\theta\cos\psi \frac{\partial f}{\partial r} + \sin\theta\sin\psi \frac{\partial f}{\partial \phi}) \tag{229}$$

Eqs. (226) through (228) can be rewritten in the following form:

$$K = p_4 F_{q_4} + \dot{r}(F - p_4 F_{p_4}) \tag{230}$$

$$Q = -(F - q_4 F_{q_4}) - \dot{r} q_4 F_{p_4} \tag{231}$$

$$R_k = 0 \qquad (k = 1, 2, 3) \tag{232}$$

$$R_4 = -F_{q_4} + \dot{r}F_{p_4} \tag{233}$$

where

$$F_{q_4} = -r\rho V(V\sin\theta + \lambda_2)\sin\theta\cos\psi \tag{234}$$

$$F_{p_4} = -\rho V(V\sin\theta + \lambda_2)\sin\theta\sin\psi \tag{235}$$

Substituting Eqs. (229) through (235) into Eqs. (223) through (225) results in the following three nonzero corner line conditions:

$$\Delta[-r\rho V(V\cos\theta + \lambda_2)(\sin\theta\cos\psi \frac{\partial f}{\partial \phi} - \dot{r}\cos\theta + \dot{r}\sin\theta\cos\psi \frac{\partial f}{\partial r}) + r\dot{r}(p-p_a)] = 0 \quad (236)$$

$$\Lambda[r\rho V(V\cos\theta + \lambda_2)(-\cos\theta + \frac{\sin\theta\sin\psi}{r} \frac{\partial f}{\partial \phi} - \dot{r} \frac{\sin\theta\sin\psi}{r} \frac{\partial f}{\partial r}) - r(p-p_a)] = 0 \quad (237)$$

$$\Lambda[r\rho V(V\cos\theta + \lambda_2)(\sin\theta\cos\psi - \dot{r} \frac{\sin\theta\sin\psi}{r})] = 0 \quad (238)$$

It has been shown that on an optimal control surface the following equations are valid:

$$V\cos\theta + \lambda_2 = - V\sin\theta\tan\mu \quad (239)$$

$$\partial f/\partial r = - \tan\beta\cos\alpha \quad (240)$$

$$\partial f/\partial \phi = - r\tan\beta\sin\alpha \quad (241)$$

where

$$\alpha = \psi \quad (242)$$

$$\beta = \theta + \mu + \pi/2 \quad (243)$$

Furthermore, on an optimal control surface p_a, r, $\dot{r}$ and the dependent variables V, θ, ψ and f are continuous everywhere. The variables p, ρ and μ are continuous since they are unique functions of V and the stagnation conditions. Since θ, ψ and μ are continuous, Eqs. (242) and (243) show that α and β are also continuous. The continuity of α and β on an optimal control surface in combination with Eqs. (240) and (241) shows that the first derivatives of f are continuous everywhere (i.e., there are no corner lines in the contour of an optimal control surface). The continuity of the RHS of Eq. (239) shows that the quantity $(V\cos\theta + \lambda_2)$ is also continuous. Therefore, in Eqs. (236) through (238), every quantity inside the outer parentheses is continuous, and the three equations are identically satisfied.

In summary, the corner line conditions for this problem have been derived and are identically satisfied by the requirements on the continuity of the dependent variables on the control surface. No additional information is obtained from the Erdmann-Weirstrass corner conditions.

APPENDIX H
PROOF THAT OPTIMAL CONTROL SURFACES ARE WAVE SURFACES

The governing equations for a steady flow of an ideal compressible fluid in three dimensions constitute a system of quasi-linear, first-order, partial differential equations. When the flow velocity exceeds the local velocity of sound, the equations are classed as hyperbolic, and, within the solution space, surfaces exist on which the system reduces to an interior operator (i.e., a linear combination of the equations can be found which involves only directions of differentiation which lie within the surface). These surfaces are called characteristic surfaces, and they are important in the methods of solution of the set of equations.

In (15) it is shown that two infinite families of characteristic surfaces exist for three-dimensional supersonic flow; these are the stream surfaces and the wave surfaces. The family of stream surfaces consists of all surfaces made up of streamlines of the flow. The wave surfaces consist of all surfaces tangent to the local Mach conoid. The system of equations reduces to an interior operator on each surface of both families of characteristic surfaces. The linear combinations of the equations which have the characteristic property are called compatibility relations. Data can not be arbitrarily specified on characteristic surfaces since the compatibility relation must be satisfied.

It is the wave surfaces that are of primary interest here since it will be shown that an optimal control surface is actually a wave surface. The proof that an optimal control surface is a wave surface is an essential step since it establishes the unique character of the control surface. That is, since wave surfaces are unique surfaces in three-dimensional supersonic flow, the proof that optimal control surfaces are wave surfaces is equivalent to a uniqueness proof for the optimization problem.

Each point in a supersonic flow field is associated with a Mach conoid as illustrated in Figure 36. The right circular cone formed by the tangents to the Mach conoid at a point is the Mach cone. The rays of the characteristic cone make the angle μ with the velocity vector, where μ is the Mach angle defined by $\mu = \sin^{-1}(1/M)$.

Associated with each point on a non-characteristic and space-like curve is a Mach conoid. The two surfaces tangent to the Mach conoids and containing the space-like curve are wave surfaces. This geometric condition is also shown in Figure 36. Since a wave surface is tangent to the Mach conoids associated with each point on the wave surface, the velocity vector $\bar{V}$ and the unit outer normal to the wave surface $\bar{m}$ satisfy the following relationship at every point on a wave surface:

$$\bar{V} \cdot \bar{m} = - V \sin\mu \tag{244}$$

In Appendix E it was shown that on the optimum control surface

$$\mu = \xi \tag{245}$$

where the angle ξ is defined by the following equation:

$$\sin\xi = - (\bar{V} \cdot \bar{n})/V \tag{246}$$

and $\bar{n}$ is the unit outer normal to the control surface. Equations through (246) may be combined to show that

$$\bar{n} = \bar{m} \tag{247}$$

and thus, optimal control surfaces are oriented in the same direction as wave surfaces of the flow.

For optimal control surfaces to be wave surfaces it is also necessary that the data on the control surface must satisfy the appropriate compatibility relation. The compatibility relation in a L, N-coordinate system is derived in (20) as the following equation which is valid on wave surfaces in homentropic, irrotational flows:

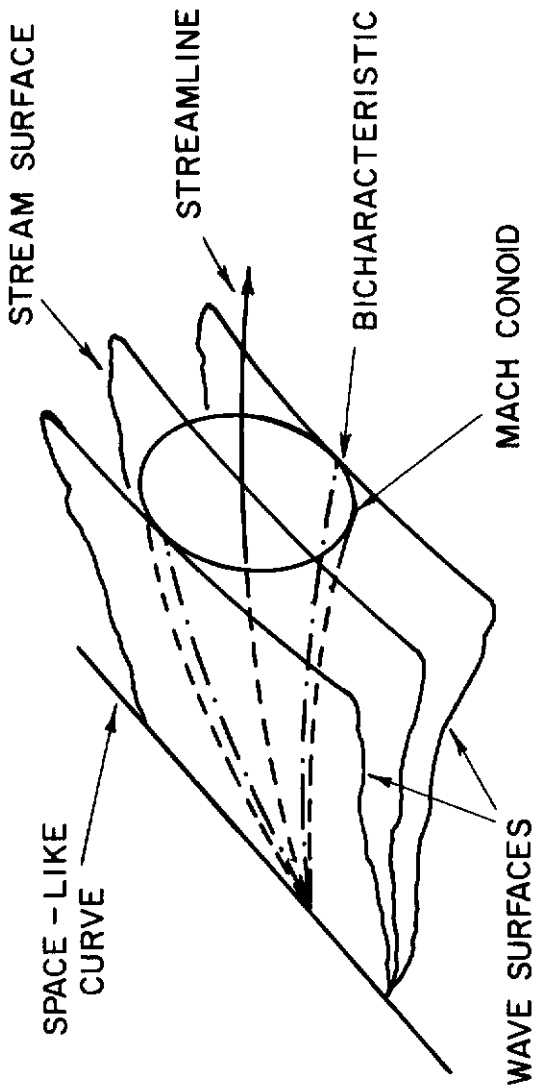

FIGURE 36. CHARACTERISTIC SURFACES

$$\frac{1}{V}\frac{\partial V}{\partial L} - \tan\mu\cos\delta\,\frac{\partial\theta}{\partial L} - \tan\mu\sin\delta\sin\theta\,\frac{(\psi+\phi)}{\partial L}$$
$$- \sin\mu\tan\mu\cos\delta\sin\theta\,\frac{\partial(\psi+\phi)}{\partial N} + \sin\mu\tan\mu\sin\delta\,\frac{\partial\theta}{\partial N} = 0 \qquad (248)$$

where the partial derivatives denote differentiation on the wave surface. Figure 37 illustrates the coordinate system relationships. The direction L is along a bicharacteristic curve (i.e., the intersection of a Mach conoid and a wave surface). The direction N is normal to L and in the tangent plane to the Mach cone at the point Q. Thus, the L, N-coordinates lie on a wave surface. The direction of the velocity vector $\bar{V}$ is described by the angles θ and ψ as defined in the following equation:

$$\begin{aligned} V_r &= V\sin\theta\cos\psi \\ V_\phi &= V\sin\theta\sin\psi \\ V_z &= V\cos\theta \end{aligned} \qquad (249)$$

The angle η is the angle between the $\bar{V}$, z-plane and the $\bar{V}$, L-plane.

The unit vectors in the L and N directions are denoted by $\bar{L}$ and $\bar{N}$ respectively, and the components of $\bar{L}$ and $\bar{N}$ in the r, ϕ and z directions are denoted by L_r, L_ϕ, L_z, N_r, N_ϕ and N_z. The unit vectors $\bar{L}$ and $\bar{N}$ are defined by the following equations:

$$\bar{N} = \frac{\bar{V}\times\bar{n}}{|\bar{V}\times\bar{n}|} \qquad (250)$$

$$\bar{L} = \frac{\bar{n}\times\bar{N}}{|\bar{n}\times\bar{N}|} \qquad (251)$$

Therefore, the following equations can be written:

$$N_r = (n_z V_\phi - n_\phi V_z)/\cos\mu \qquad (252)$$

$$N_\phi = (n_r V_z - n_z V_r)/\cos\mu \qquad (253)$$

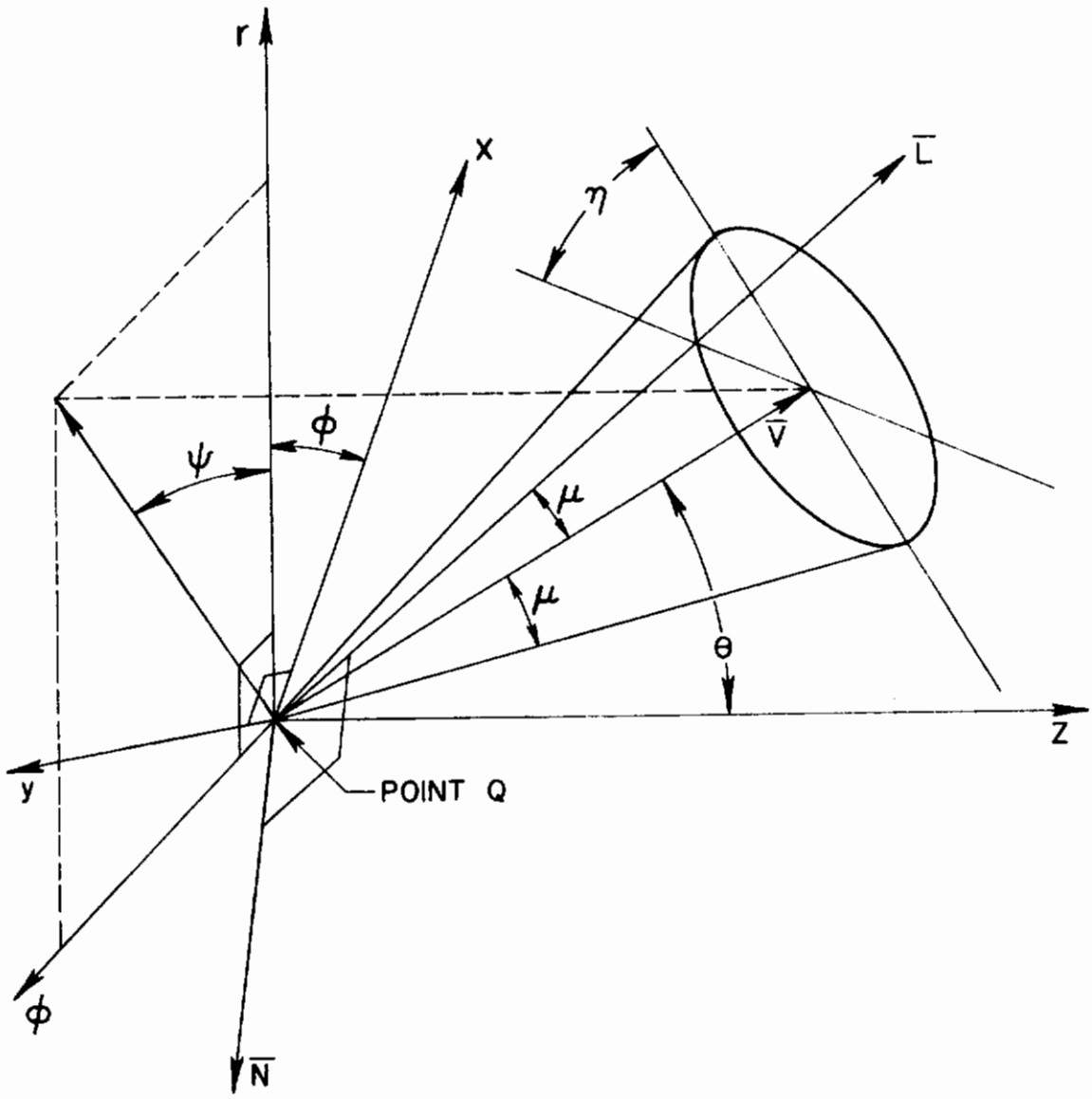

FIGURE 37. COORDINATE SYSTEM FOR WAVE SURFACES

$$N_z = (n_\phi V_r - n_r V_\phi)/\cos\mu \tag{254}$$

$$L_r = (n_r \sin\mu + V_r)/\cos\mu \tag{255}$$

$$L_\phi = (n_\phi \sin\mu + V_\phi)/\cos\mu \tag{256}$$

$$L_z = (n_z \sin\mu + V_z)/\cos\mu \tag{257}$$

The angle η is defined by the following expressions:

$$\cos\eta = \bar{N} \cdot (\bar{i}_z \times \bar{V})/|i_z \times \bar{V}| \tag{258}$$

$$\sin\eta = |\bar{N} \times (\bar{i}_z \times \bar{V})|/|\bar{i}_z \times \bar{V}| \tag{259}$$

Equations (258) and (259) can be expanded and simplified by using Eqs. (249), (252) through (257) and the following equation from Appendix A:

$$\begin{aligned} n_r &= \sin\theta \cos\beta \\ n_\phi &= \sin\theta \sin\beta \\ n_z &= \cos\theta \end{aligned} \tag{260}$$

to yield the expressions

$$\cos\eta = (-\cos\beta\sin\theta + \sin\beta\cos\theta\cos(\psi - \alpha))/\cos\mu \tag{261}$$

$$\sin\eta = -\sin\beta\sin(\psi - \alpha)/\cos\mu \tag{262}$$

If the flow is such that $\alpha = \psi$ on a wave surface, then Eqs. (261) and (262) can be rewritten as

$$\sin\eta = 0 \tag{263}$$

$$\cos\eta = \sin\beta(\cos\theta - \tan\beta\sin\theta)/\cos\mu \tag{264}$$

and the compatibility relation, Eq. (248), can be rewritten in the following form:

$$\frac{1}{V}\frac{\partial V}{\partial L} - \tan\mu\cos\eta\,\frac{\partial\theta}{\partial L} - \sin\mu\tan\mu\cos\eta\sin\theta\,\frac{\partial(\psi + \phi)}{\partial N} = 0 \tag{265}$$

In Appendix E the following equations are derived:

$$V\cos\theta + \lambda_2 = - V\sin\theta\tan\mu \tag{266}$$

$$\frac{\partial}{\partial\phi}\left(\rho V^2\sin^2\theta\tan\mu\sin\psi\right) + \frac{\partial}{\partial r}\left(r\rho V^2\sin^2\theta\tan\mu\cos\psi\right) = 0 \tag{267}$$

$$\frac{\partial}{\partial\phi}\left(\tan(\theta + \mu + \pi/2)\cos\psi\right) - \frac{\partial}{\partial r}\left(r\tan(\theta + \mu + \pi/2)\sin\psi\right) = 0 \tag{268}$$

$$\alpha = \psi \tag{269}$$

$$\beta = \theta + \mu + \pi/2 \tag{270}$$

These equations are the governing equations for an optimal control surface. It will now be shown that Eqs. (266), (267), (269), and (270) can be combined to derive the compatibility relation, Eq. (265).

Expanding Eq. (267) and substituting the differential expressions

$$d\rho = - \rho V/a^2 dV \tag{271}$$

$$d\mu = \frac{-\left(\frac{\gamma - 1}{2} + \sin^2\mu\right)}{V\sin\mu\,\cos\mu}\,dV \tag{272}$$

into the expanded expression yields the following equation:

$$D_1 \frac{\partial V}{\partial r} + D_2 \frac{\partial V}{r\partial \phi} + D_3 \frac{\partial \theta}{\partial r} + D_4 \frac{\partial \theta}{r\partial \phi} + D_5 \frac{\partial \psi}{\partial r} + D_6 \frac{\partial \psi}{r\partial \phi} + D_7 = 0 \qquad (273)$$

where

$$D_1 = - \sin\theta\cos\psi \, (1 + \mathrm{ctn}\theta\tan\mu)/V\tan^2\mu \qquad (274)$$

$$D_2 = D_1 \tan\psi \qquad (275)$$

$$D_3 = \cos\psi(\cos\theta + \sin\theta\,\mathrm{ctn}\mu) \qquad (276)$$

$$D_4 = D_3 \tan\psi \qquad (277)$$

$$D_5 = - \sin\theta\sin\psi \qquad (278)$$

$$D_6 = - D_5 \mathrm{ctn}\psi \qquad (279)$$

$$D_7 = D_6/r \qquad (280)$$

Equation (273) can be transformed to the L, N- coordinate system by the relationships

$$\frac{\partial}{\partial r} = a_1 \frac{\partial}{\partial L} + a_2 \frac{\partial}{\partial N} \qquad (281)$$

$$\frac{\partial}{r\partial \phi} = b_1 \frac{\partial}{\partial L} + b_2 \frac{\partial}{\partial N} \qquad (282)$$

$$a_1 = \frac{\partial L}{\partial r} = L_r + \frac{\partial f}{\partial r} L_z = \cos\psi(\sin\theta - \tan\beta\cos\theta)/\cos\mu \qquad (283)$$

$$a_2 = \frac{\partial N}{\partial r} = N_r + \frac{\partial f}{\partial r} N_z = \cos\beta\tan\psi a_1 \qquad (284)$$

$$b_1 = \frac{\partial L}{r\partial\phi} = L_\phi + \frac{\partial f}{r\partial\phi} L_z = \tan\psi\ a_1 \tag{285}$$

$$b_2 = \frac{\partial N}{r\partial\phi} = N_\phi + \frac{\partial f}{r\partial\phi} N_z = -\cos\beta\ a_1 \tag{286}$$

where Eqs. (248) through (257), Eq. (269) and the equations

$$\partial f/\partial r = -\tan\beta\cos\alpha \tag{287}$$

$$\partial f/\partial\phi = -r\tan\beta\sin\alpha \tag{288}$$

have been used to evaluate the coefficients a_1, a_2, b_1 and b_2. Performing the transformation, Eq. (273) becomes

$$G_1 \frac{\partial V}{\partial L} + G_2 \frac{\partial V}{\partial N} + G_3 \frac{\partial\theta}{\partial L} + G_4 \frac{\partial\theta}{\partial N} + G_5 \frac{\partial(\psi + \phi)}{\partial L} +$$

$$+ G_6 \frac{(\psi + \phi)}{\partial N} + G_7 = 0 \tag{289}$$

where

$$G_1 = a_1 D_1 + b_1 D_2 \tag{290}$$

$$G_2 = a_2 D_1 + b_2 D_2 \tag{291}$$

$$G_3 = a_1 D_3 + b_1 D_4 \tag{292}$$

$$G_4 = a_2 D_3 + b_2 D_4 \tag{293}$$

$$G_5 = a_1 D_5 + b_1 D_6 \tag{294}$$

$$G_6 = a_2 D_5 + b_2 D_6 \tag{295}$$

$$G_7 = D_7 - G_5 \frac{\partial \phi}{\partial L} - G_6 \frac{\partial \phi}{\partial N} \tag{296}$$

Equation (289) reduces to the following equation when Eqs. (269) (270) and (274) through (286) are used to simplify:

$$\frac{1}{V} \frac{\partial V}{\partial L} - \tan\mu\cos\eta \frac{\partial \theta}{\partial L} - \sin\mu\tan\mu\cos\eta\sin\theta \frac{\partial(\psi + \phi)}{\partial N} = 0 \tag{297}$$

where

$$\cos\eta = \sin\beta(\cos\theta - \tan\beta\sin\theta)/\cos\mu \tag{298}$$

Thus, the data on the control surface are specified by Eqs. (266) through (270) in a manner which satisfies the compatibility relation for a wave surface. In summary, the control surface which satisfies Eqs. (266) through (270) is actually a wave surface of a three-dimensional, homentropic, irrotational, supersonic flow, and the control surface is a unique surface.

APPENDIX I
THE AXISYMMETRIC SOLUTION

In this appendix it is shown that for an axisymmetric kernel flow the equations derived in Appendices E and F for optimal three-dimensional nozzles reduce to the equations obtained by Rao (2) and Guderley (3) for optimal axisymmetric nozzles. Also, as an aid to understanding the solution procedure for the design of optimal three-dimensional nozzles, an analogous solution for the design of optimal axisymmetric nozzles is presented.

1. GOVERNING EQUATIONS

The following set of five independent design equations defines the shape of and the flow properties on the control surface (exit characteristic surface) of an optimal three-dimensional nozzle:

$$V\cos\theta + \lambda_2 = - V\sin\theta\tan\mu \tag{299}$$

$$\frac{\partial}{\partial\phi}\left(\rho V^2\sin^2\theta\tan\mu\sin\psi\right) + \frac{\partial}{\partial r}\left(r\rho V^2\sin^2\theta\tan\mu\cos\psi\right) = 0 \tag{300}$$

$$\frac{\partial}{\partial\phi}\left[\tan(\theta + \mu + \pi/2)\cos\psi\right] - \frac{\partial}{\partial r}\left[r\tan(\theta + \mu + \pi/2)\sin\psi\right] = 0 \tag{301}$$

$$\alpha = \psi \tag{302}$$

$$\beta = \theta + \mu + \pi/2 \tag{303}$$

These equations were derived in Appendix E and contain the five dependent variables $V(r,\phi)$, $\theta(r,\phi)$, $\psi(r,\phi)$, $\alpha(r,\phi)$ and $\beta(r,\phi)$.

For an axisymmetric flow $\psi \equiv 0$, and all variables are independent of ϕ (i.e., $\partial(\ )/\partial\phi \equiv 0$). Therefore, for an axisymmetric flow, Eqs. (299) through (303) reduce to the following equations:

$$V\cos\theta + \lambda_2 = - V\sin\theta\tan\mu \tag{304}$$

$$r\rho V^2 \sin^2\theta \tan\mu = -\lambda_3 \tag{305}$$

$$\alpha = \psi \equiv 0 \tag{306}$$

$$\beta = \theta + \mu + \pi/2 \tag{307}$$

where λ_3 is a constant. Equation (301) is identically satisfied since $\psi \equiv 0$ and $\partial(\ )/\partial\phi \equiv 0$. Equations (304), (305) and (307) represent the governing equations for $V(r)$, $\theta(r)$ and $\beta(r)$ on an axisymmetric optimal control surface.

The shape of a nonaxisymmetric control surface is represented by the function $f(r,\phi)$ where

$$\partial f/\partial r = -\tan\beta\cos\alpha \tag{308}$$

$$\partial f/\partial\phi = -r\tan\beta\sin\alpha \tag{309}$$

For an axisymmetric control surface the function f is only a function of r and is given by the solution to the following equation:

$$df/dr = -\tan\beta \tag{310}$$

The transversality equation derived in Appendix F for a three-dimensional, fixed length nozzle has the following form:

$$\left[(p-p_a) + \rho V^2 \sin\theta\tan\mu\left(-\cos\theta + \sin\theta\sin\psi\, df_e/(r_e d\phi_e)\right)\right]\Big|_{\Gamma_e} = 0 \tag{311}$$

For an axisymmetric nozzle $\sin\psi \equiv 0$, and thus Eq. (311) can be rewritten in the following form:

$$\frac{(P_e - P_a)}{\rho_e V_e^2/2} = \sin 2\theta_e \tag{312}$$

Equations (304), (305), (307) and (312) are equivalent to the axisymmetric optimization equations derived by Rao (2) and Guderley (3). Equations (304), (305), (307) and (310) can be rewritten as the following expressions:

$$V\cos(\theta - \mu)/\cos\mu = -\lambda_2 \tag{313}$$

$$r\rho V^2 \sin^2\theta \tan\mu = -\lambda_3 \tag{314}$$

$$\phi' = \theta + \mu \tag{315}$$

$$df/dr = \mathrm{ctn}\phi' \tag{316}$$

where

$$\phi' = \beta - \pi/2 \tag{317}$$

Equations (312) through (316) are identical to the optimization equations derived in (2) and (3). Thus, the optimization equations derived in Appendices E and F for three-dimensional nozzles reduce to the axisymmetric optimization equations for the special case of axisymmetric flow.

2. SOLUTION PROCEDURE

There are several procedures which can be used to design axisymmetric, maximum thrust, fixed length nozzles. All procedures involve the numerical solution of Eqs. (312) through (316), but each approaches the problem in a different manner. Two of the possible approaches have been presented by Rao (2) and Williams* (21). Rao (2) treats the problem as a two point boundary value problem while in Ref. (21), the problem is treated as an initial value problem. When the problem is solved as a two point boundary value problem, a number of iterations are necessary before an optimal control surface is generated which satisfies the conditions at both end points. Treating the problem as an initial value problem makes it possible to calculate an optimal control surface with no iterations and then iterate between optimal solutions to match specific boundary conditions. Also, the solution procedure in Ref. (21) eliminates the sensitive iterative matching procedure used by Rao (2) to match conditions at the kernel.

---

* Williams (21) was not responsible for developing the overall design procedure; however, the procedure is documented in Ref. (21). The design procedure was developed at the NASA Lewis Research Center, Cleveland, Ohio, but it was not documented by the NASA staff.

Both of the approaches are valid; however, the procedure presented in Ref. (21) is more straightforward than Rao's (2) procedure. The overall solution procedure presented in this report for the design of three-dimensional optimal nozzles is similar to the procedure presented in Ref. (21) for axisymmetric optimal nozzles. For this reason the procedure in Ref. (21) for the design of axisymmetric optimal nozzles is now presented.

The following steps which refer to Figure 38 describe the design of a maximum thrust, fixed length, axisymmetric nozzle:

1) Choose an initial expansion contour BC and initial flow conditions along a start line AB.
2) Calculate the supersonic flow field in the portion of the nozzle which is governed by the initial expansion contour (i.e., the kernel).
3) Pick a point I which is on the boundary of the kernel.
4) Numerically solve Eqs. (313) through (316) to construct the optimal control surface which passes through point I.
5) Determine the mass flow rate across CI, and locate point E such that $\dot{m}_{CI} = \dot{m}_{IE}$.
6) Apply Eq. (312) at point E to determine the ambient pressure p_a for which the control surface IE is optimally designed.
7) Calculate the flow field in the region of the nozzle which is bounded by the characteristic surface CI and the characteristic surface IE.
8) Determine the optimal nozzle contour CE by calculating the shape of the streamline which passes through point C and thus also through point E.

These eight steps are now discussed in greater detail.

Assuming that the nozzle designer has complete flexibility in the design of the entire nozzle, he has the choice of the shape of the initial expansion contour BC, the flow conditions along the start line AB in a supersonic flow region, and the position of point I. The nozzle contour upstream of point B is assumed to be known and can be a converging, diverging or constant area section.

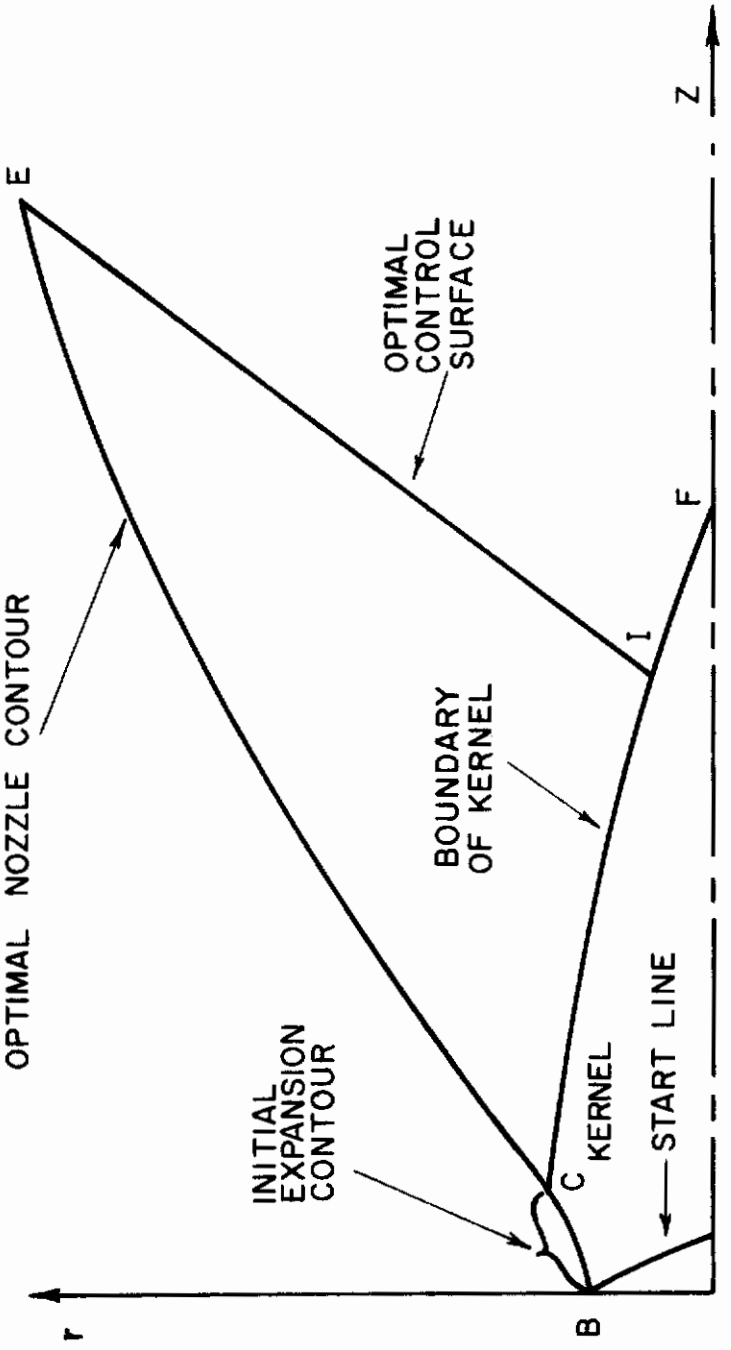

FIGURE 38. AXISYMMETRIC NOZZLE GEOMETRY

If the supersonic nozzle to be designed is a converging-diverging nozzle, then point B is downstream of the throat of the nozzle, and section BC is a suitable initial expansion contour which eliminates sharp corners in the throat region and allows the flow to rapidly expand. In this case, a transonic flow analysis can be used to determine the flow properties along the start line AB which is in a totally supersonic flow region. If the supersonic nozzle to be designed is a nozzle without a sonic throat region (e.g., a nozzle for a scramjet engine), it is assumed that the flow properties are specified along a noncharacteristic start line in a totally supersonic flow region. Again, the initial expansion contour BC is chosen to suitably accelerate the flow. In either case an axisymmetric method of characteristics analysis can be used to calculate the flow region which is dependent only upon the start line AB and the initial expansion contour BC (i.e., the kernel region of the nozzle). The outer boundary of the kernel CIF is the right-running characteristic which emanates from point C.

The next decision to be made is where along the boundary of the kernel (i.e., the right characteristic CF) to position point I. The position of point I and the flow conditions at point I serve as initial conditions in the solution for the shape of and flow conditions on the control surface which produces the maximum axial thrust in a fixed length for a given mass flow rate. For any one choice of the position of point I on a given right characteristic CF a unique optimal nozzle can be designed. This nozzle will be an optimal for a particular exit radius, length and ambient pressure. As point I is chosen farther downstream on a given right characteristic CF the optimum nozzle is longer, has a larger exit radius, and is designed optimally for a lower ambient pressure.

After the position of point I on the characteristic CF has been chosen, Eqs. (313) through (316) are solved to calculate $V(r)$, $\theta(r)$ and $f(r)$. Using the initial conditions at point I the entire solution for the optimal control surface can be generated; however, the position of point E can not be determined until step 5 is completed.

Since the flow properties are known along the start line AB, the magnitude of the total mass flow rate entering the nozzle $\dot{m}_{Total}$ is known and fixed. Also, once the position of point I has been chosen, the mass

flow rate across the line IF, $\dot{m}_{IF}$, can be calculated. Therefore, the mass flow rate across the control surface can be calculated from the following equation:

$$\dot{m}_{IE} = \dot{m}_{Total} - \dot{m}_{IF} \tag{318}$$

By using the following equation for the mass flow rate across the control surface, the position of point E can be determined such that Eq. (318) is satisfied:

$$\dot{m}_{IE} = \int_{r_I}^{r_E} 2\pi r \rho V \sin\mu / \sin(\theta+\mu) dr \tag{319}$$

At this point, the exit radius and length of the maximum thrust nozzle can be determined along with the magnitude of the vacuum thrust produced by the optimal nozzle contour. In step 6 the ambient pressure, for which the nozzle is optimally designed, is determined. The design ambient pressure is calculated using the following form of Eq. (312):

$$p_a = p_e + \rho_e V_e^2 \sin^2\theta_e / (2\cot\mu_e) \tag{320}$$

Since all the flow variables at point E are known, p_a can be evaluated.

In step 7 the flow in the region bounded by the right characteristic CI and the left characteristic IE (i.e., the control surface) is determined. The intermediate flow field is calculated by applying a numerical technique such as the method of characteristics to the equations which govern the irrotational, isentropic, steady flow in the region.

The final step, step 8, consists of determining the path of the streamline which passes through the points C and E. Since the flow properties in the region of the streamline are known from step 7, the streamline can be easily determined. The path of the streamline CE is identical to the contour of the optimal nozzle contour.

If either the length, area ratio or ambient pressure of this optimally designed nozzle does not meet the requirements which the designer has

placed on the problem, then an iteration process is necessary to generate the desired optimal nozzle. Different optimal nozzles are designed by using different starting conditions. During the iteration process, any or all of the following conditions can be changed: 1) the conditions along the start line, 2) the initial expansion contour, and 3) the position of point I.

APPENDIX J
DETAILS OF THE CONSTRUCTION OF INITIAL VALUE LINES

In this appendix the conditions which must be satisfied along an initial value line are presented. Also, the solution technique which is used to generate an initial value line along which these conditions are satisfied is presented.

Throughout this appendix it should be remembered that the overall design problem is being solved by specifying conditions along the inner boundary of the control surface, solving for the corresponding optimal control surface and then determining the length, exit lip shape and ambient pressure for which the nozzle is an optimal. This method of solution is used in place of specifying the length, exit lip shape, ambient pressure and flow conditions on the desired exit lip, solving for the corresponding optimal control surface, and then using an iteration method to match the control surface to some kernel. For this optimization problem, the method of choosing the conditions along the inner boundary of the control surface such that the conditions match an existing three-dimensional supersonic flow and then designing the corresponding optimal nozzle is more advantageous. The method presented in this work yields an optimal nozzle each time the method is applied.

1. EQUATIONS WHICH DEFINE AN INITIAL VALUE LINE

An initial value line (i.e., the intersection of the boundary of the kernel and the optimal control surface) represents the initial conditions for the solution of the design equations derived in Appendix E. Since an initial value line is the inner boundary of an optimal control surface, it must satisfy the same set of design equations that define an optimal control surface. Therefore, the following equations must be satisfied along an initial value line:

$$V\cos\theta + \lambda_2 = - V\sin\theta \tan\mu \tag{321}$$

$$\frac{\partial}{\partial\phi}(\rho V^2\sin^2\theta\tan\mu\sin\psi) + \frac{\partial}{\partial r}(r\rho V^2\sin^2\theta\tan\mu\cos\psi) = 0 \tag{322}$$

$$\frac{\partial}{\partial\phi}\left(\tan(\theta + \mu + \pi/2)\cos\psi\right) - \frac{\partial}{\partial r}\left(r\tan(\theta + \mu + \pi/2)\sin\psi\right) = 0 \tag{323}$$

$$\alpha = \psi \tag{324}$$

$$\beta = \theta + \mu + \pi/2 \tag{325}$$

$$df = (\partial f/\partial r)dr + (\partial f/\partial\phi)d\phi \tag{326}$$

where λ_2 is a constant and

$$\partial f/\partial r = - \tan\beta\cos\alpha \tag{327}$$

$$\partial f/\partial\phi = - r\tan\beta\sin\alpha \tag{328}$$

Equations (322) and (323) do not specify any conditions that must be satisfied along an initial value line (i.e., as will be shown in Appendix K, the characteristic curves of Eqs. (322) and (323) do not coincide with initial value lines; if they did, it would not be possible to use the two equations to solve for optimal control surfaces). On the other hand, Eq. (321) and Eqs. (324) through (328) prescribe relations which must be satisfied along the inner boundary of an optimal control surface. From Eq. (321) the values of V, θ and μ at all points along an initial value line must be such that

$$- V(\cos\theta + \sin\theta\tan\mu) = \lambda_2 \tag{329}$$

where λ_2 has the same constant value at all points. By substituting Eqs. (324), (325), (327) and (328) into Eq. (326), Eq. (326) can be rewritten in the following form:

$$df = - \tan(\theta + \mu + \pi/2)(\cos\psi dr + r\sin\psi d\phi) \qquad (330)$$

By choosing an initial value line to satisfy Eqs. (329) and (330), the initial value line will be compatible with the optimal control surface.

2. DESCRIPTION OF THE DESIGN PROCEDURE

The procedure for generating an initial value line from which an optimal three-dimensional control surface can be constructed consists of the following five steps:

1) Choose an initial expansion contour for a portion of the supersonic nozzle and a noncharacteristic starting surface on which the flow is homentropic, isoenergetic and supersonic, and the perfect gas relations are satisfied.
2) Utilize a three-dimensional supersonic flow analysis program to calculate the homentropic and isoenergetic flow field which is determined by the specified contour and starting surface.
3) Choose a point in the generated flow field (kernel) which will be constrained to lie on the initial value line. This fixes the value of λ_2.
4) On each of several planes of flow data which neighbor the chosen point, determine the shape of the curve along which λ_2 has the chosen value.
5) Determine numerically the shape of the curve which goes through the chosen point, has a constant value of λ_2 and satisfies Eq. (330).

These five steps are now discussed in more detail.

The first step in generating an optimal three-dimensional nozzle is to determine the flow conditions in the kernel region. Thus, it is necessary to have the capability to analyze three-dimensional, supersonic, internal flow fields. A practical and accurate numerical method to calculate three-dimensional, supersonic, internal flow fields was presented by Ransom, Hoffman and Thompson (15). The associated computer program described in (23) is utilized in this research to calculate the three-dimensional flow in the kernel region. The overall design procedure

presented in this appendix is valid for any analysis program; however, since the analysis program (23) uses an integration process which takes place between a series of planes parallel to the starting surface, some parts of the procedure are written to take this into account.

In step 1 the flow properties along a noncharacteristic starting surface are specified so that the analysis program can be used to calculate the resulting internal flow field in which an initial value line can be generated. To use the analysis program, the starting surface must be normal to the z-axis. The values of the flow variables V, θ and ψ must be specified by continuous functions on the starting surface, and to satisfy the isoenergetic and homentropic flow assumptions, the stagnation pressure p_o and the stagnation enthalpy h_o must be constant on the starting surface. Also, the values of V, θ and ψ on the starting surface are specified such that the flow is irrotational.

In addition to specifying the values of the dependent variables on the starting surface, the shape of the boundary (initial expansion contour) must be specified. Since the analysis program (23) uses an integration process which takes place between a series of planes parallel to the starting surface, it is necessary to specify more of the boundary than just the portion upon which the kernel region is dependent. Thus, an entire nozzle contour is specified from the planar starting surface downstream to a planar surface which is certain to be downstream of the position of any desired initial value line.

Step 2 consists of employing the analysis program to calculate the flow field bounded by the starting surface and the specified boundary. The numerical solution of the set of hyperbolic differential equations which governs the homentropic, isoenergetic, supersonic flow field is based on a three-dimensional method of characteristics solution technique. The solution consists of integration along a system of streamlines throughout the flow. The output from the three-dimensional method of characteristics analysis program is the position of a given number of mesh points on each calculational plane and the values of V, θ, μ and ψ at each mesh point.

Figure 39 a shows what the lines of constant λ_2 look like for a representative plane of an axisymmetric flow while Figure 39b shows the

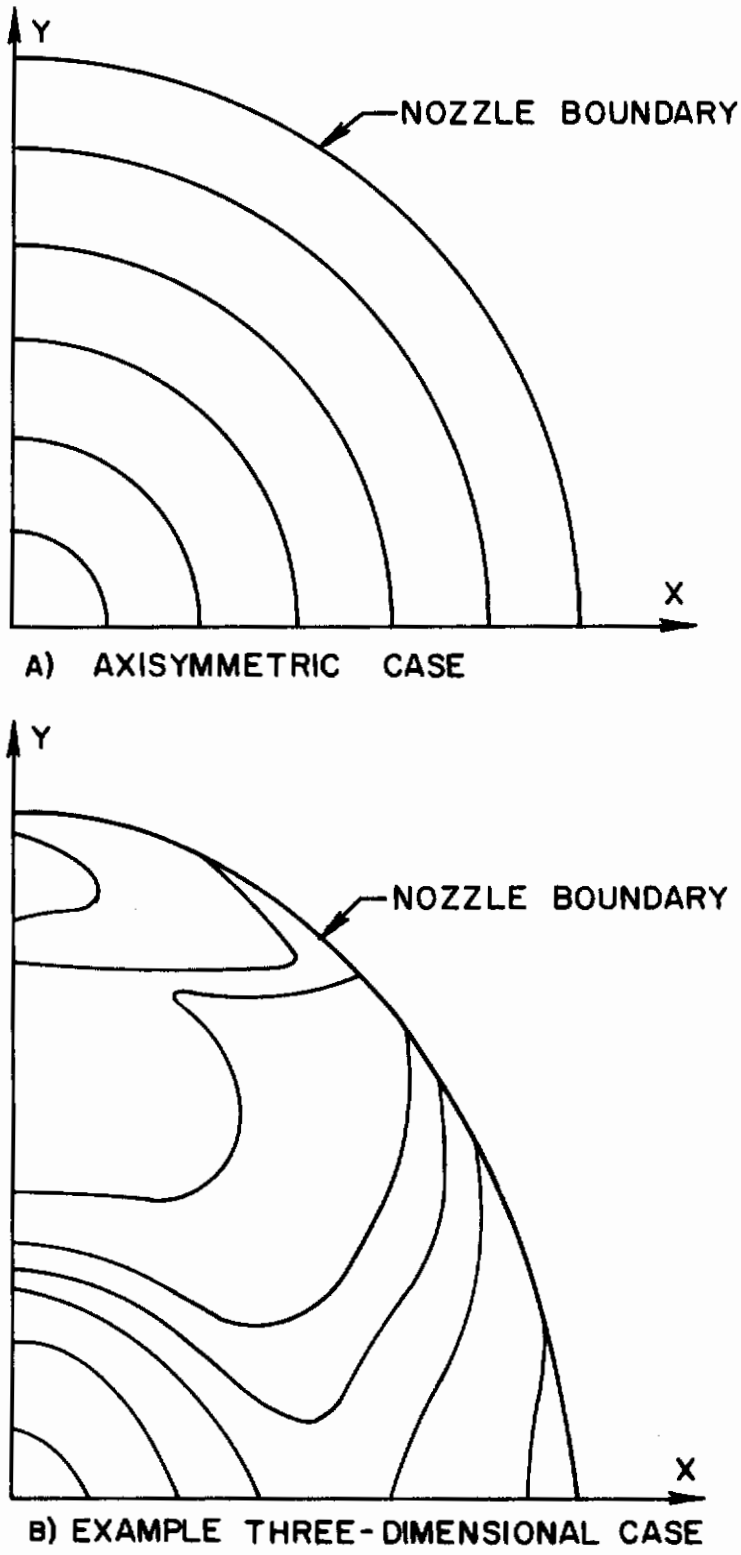

FIGURE 39. LINES OF CONSTANT λ_2

situation which exists on a plane of a representative three-dimensional flow with two planes of symmetry. As illustrated in Figure 39b, the curves of constant λ_2 are not necessarily closed curves for some values of λ_2.

In step 3 a point is selected which will be constrained to lie on the initial value line. This point should be chosen such that it lies on a constant λ_2 curve which is a closed continuous curve. Furthermore, the point should be chosen such that it lies on a characteristic surface which intersects the initial expansion contour downstream of the starting surface. Note that when this point is selected the constant value of λ_2 is then known.

Once a point has been chosen which will be constrained to lie on the initial value line, the next step (step 4) is to examine the flow data on the planes which neighbor the chosen point and determine the curve in each plane along which λ_2 has the known constant value. Equation (328) is satisfied as long as the initial value line consists of a series of points on the generated curves of constant λ_2 or on the interpolated constant λ_2 surface between the planes.

In step 5, Eq. (330) is used to determine the unique initial value line which passes through the chosen point and lies on the constant λ_2 surface which was determined in step 4. To apply Eq. (330) the equation is written in the following finite difference form and applied between neighboring points on the generated constant λ_2 surface:

$$f_2 = f_1 - (r_2 - r_1)\left(\tan(\theta + \mu + \pi/2)\cos\psi\right)\Big|_{\text{average}} - \frac{(r_1 - r_2)}{2}(\phi_2 - \phi_1)\left(\tan(\theta + \mu + \pi/2)\sin\psi\right)\Big|_{\text{average}} \qquad (331)$$

The conditions at point 1 are known while the conditions at point 2 are to be determined. The solution for the position of point 2 is an iterative process which is complete once f_2 is chosen such that the LHS of Eq. (331) is equal to the RHS of Eq. (331). Equation (331) is applied between a series of neighboring points on the constant λ_2 surface until a continuous closed curve has been determined.

Figure 40 illustrates the physical situation where an initial value line has been generated in a three-dimensional flow region with two planes of symmetry. Notice that in general the initial value line will not lie in a plane; however, it must be symmetric with respect to any planes of symmetry. This initial value line which is generated by the above method is a unique line which can serve as the inner boundary of an optimal control surface and matches the flow conditions in a specified kernel.

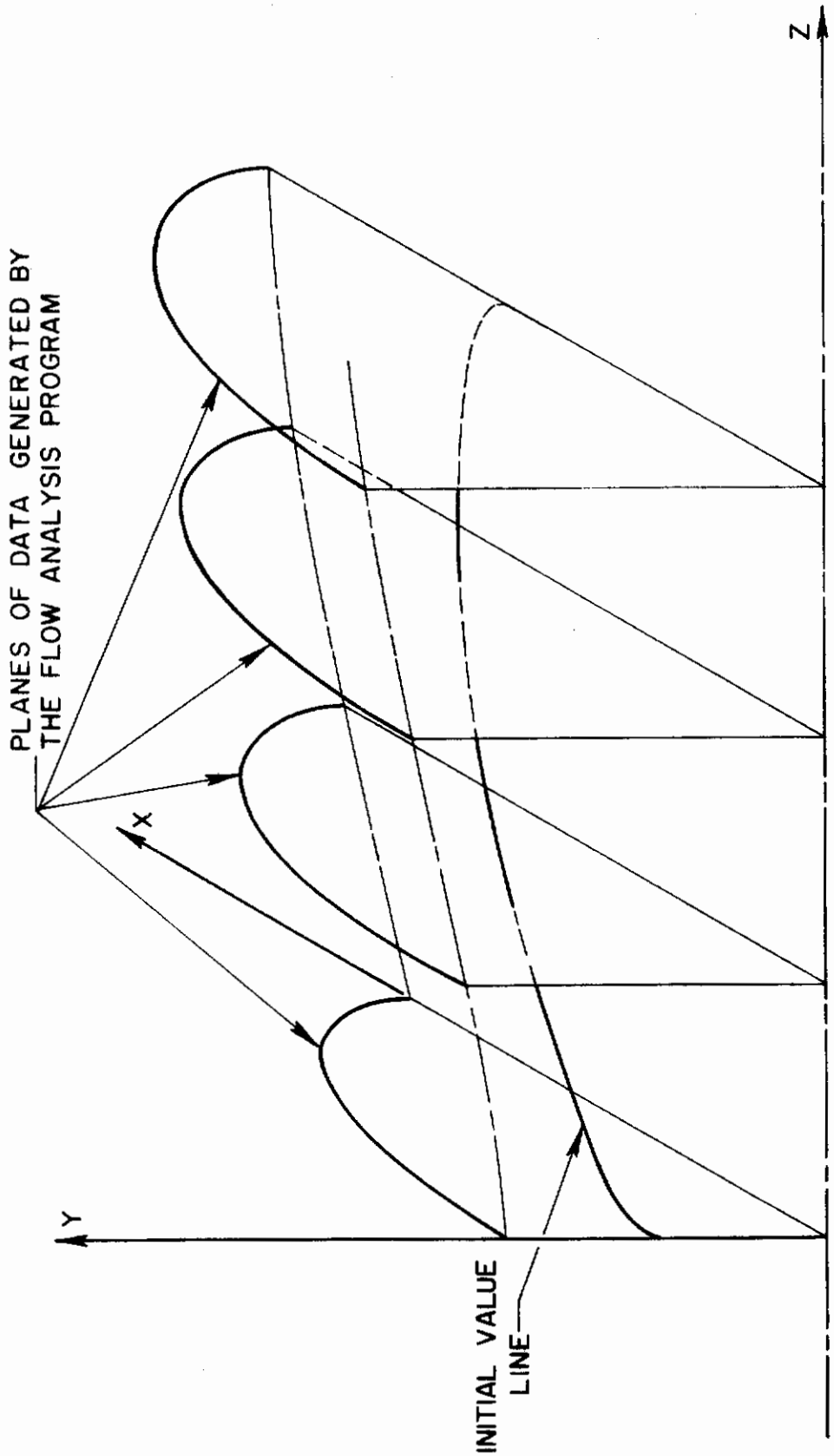

FIGURE 40. INITIAL VALUE LINE

APPENDIX K
DETAILS OF THE CONSTRUCTION OF OPTIMAL CONTROL SURFACES

The equations which describe the shape of the control surface and define the values of V, θ and ψ on the control surface which produces the maximum axial thrust were derived in Appendix E. These design equations are valid for steady, homentropic, isoenergetic flow. In this appendix a method is outlined for solving the design equations to locate the control surface and to determine the values of the flow properties on the control surface.

1. NATURE OF THE DESIGN EQUATIONS

The five design equations for the five unknowns V, θ, ψ, α and β are Eqs. (187) through (191). They are repeated here for convenience.

$$V\cos\theta + \lambda_2 = - V\sin\theta\tan\mu \tag{332}$$

$$\frac{\partial}{\partial\phi}\left(\rho V^2\sin^2\theta\tan\mu\sin\psi\right) + \frac{\partial}{\partial r}\left(r\rho V^2\sin^2\theta\tan\mu\cos\psi\right) = 0 \tag{333}$$

$$\frac{\partial}{\partial\phi}\left[\tan(\theta + \mu + \pi/2)\cos\psi\right] - \frac{\partial}{\partial r}\left[r\tan(\theta + \mu + \pi/2)\sin\psi\right] = 0 \tag{334}$$

$$\alpha = \psi \tag{335}$$

$$\beta = \theta + \mu + \pi/2 \tag{336}$$

In addition, the relationship between α, β and f is given as follows:

$$df = - \tan\beta(\cos\alpha dr + r\sin\alpha d\phi) \tag{337}$$

Notice that Eqs. (332) through (334) contain only the unknowns V, θ, ψ (recall that ρ and μ are functions of V alone). Therefore, the solution for $V(r,\phi)$, $\theta(r,\phi)$ and $\psi(r,\phi)$ is not dependent on the solution for $f(r,\phi)$,

and Eqs. (332) through (334) can be solved independently of Eqs. (335) through (337).

Before attempting to solve Eqs. (332) through (334) it is expedient to determine the nature of the equations (i.e., if the set of equations are elliptic, parabolic or hyperbolic). To do this the three equations is combined so that the two partial differential equations contain only partial derivatives of two dependent variables.

In Appendix H it was shown that Eq. (333) can be rewritten in the following form:

$$D_1 \frac{\partial V}{\partial r} + D_2 \frac{\partial V}{r\partial \phi} + D_3 \frac{\partial \theta}{\partial r} + D_4 \frac{\partial \theta}{r\partial \phi} + D_5 \frac{\partial \psi}{\partial r} + D_6 \frac{\partial \psi}{r\partial \phi} + D_7 = 0 \qquad (338)$$

where

$$D_1 = - \sin\theta\cos\psi \, (1 + \mathrm{ctn}\theta\tan\mu)/V\tan^2\mu \qquad (339)$$

$$D_2 = D_1\tan\psi \qquad (340)$$

$$D_3 = \cos\psi(\cos\theta + \sin\theta\,\mathrm{ctn}\mu) \qquad (341)$$

$$D_4 = D_3\tan\psi \qquad (342)$$

$$D_5 = - \sin\theta\sin\psi \qquad (343)$$

$$D_6 = - D_5\,\mathrm{ctn}\psi \qquad (344)$$

$$D_7 = D_6/r \qquad (345)$$

Also, the following equations were derived in Appendix B:

$$d\mu = - 1/\left(M(M^2 - 1)^{1/2}\right)dM \qquad (346)$$

$$dM = \left(1 + (\gamma-1)M^2/2\right)/a \; dV \qquad (347)$$

When Eq. (332) is differentiated and combined with Eqs. (346) and (347), the following equation is obtained:

$$d\theta = \frac{\dfrac{\left((M^2-1)^{1/2}\cos\theta+\sin\theta\right)}{M\left(1 + (\gamma-1)M^2/2\right)} - \dfrac{M\sin\theta}{(M^2-1)}}{\left((M^2-1)^{1/2}\sin\theta - \cos\theta\right)} dM \qquad (348)$$

By combining Eqs. (338) and (348), Eq. (338) can be rewritten as follows:

$$D_8 \frac{\partial M}{\partial r} + D_9 \frac{\partial M}{r\partial \phi} + D_5 \frac{\partial \psi}{\partial r} + D_6 \frac{\partial \psi}{r\partial \phi} + D_7 = 0 \qquad (349)$$

where

$$D_8 = \left[\frac{-\cos\psi\left((M^2-1)^{1/2}\sin\theta + \cos\theta\right)}{M\left(1 + (\gamma-1)M^2/2\right)}\right]$$

$$\left[(M^2-1)^{1/2} - \frac{\left((M^2-1)^{1/2}\cos\theta + \sin\theta\right)}{\left((M^2-1)^{1/2}\sin\theta - \cos\theta\right)} + \frac{M^2\sin\theta\left(1 + (\gamma-1)M^2/2\right)}{(M^2-1)\left((M^2-1)^{1/2}\sin\theta-\cos\theta\right)}\right] \qquad (350)$$

$$D_9 = D_8 \tan\psi \qquad (351)$$

and D_5, D_6 and D_7 are given by Eqs. (343) through (345).

Expanding Eq. (334) and substituting Eqs. (346) and (348) into the expanded equation results in the following expression:

$$H_1 \frac{\partial M}{\partial r} + H_2 \frac{\partial M}{r\partial \phi} + H_5 \frac{\partial \psi}{\partial r} + H_6 \frac{\partial \psi}{r\partial \phi} + H_7 = 0 \qquad (352)$$

where

$$H_1 = \frac{-M\sin\psi}{\left((M^2-1)^{1/2}\sin\theta+\cos\theta\right)}\left[\frac{-1}{M(M^2-1)^{1/2}} + \frac{1}{\left((M^2-1)^{1/2}\sin\theta-\cos\theta\right)}\right.$$

$$\left.\left[\frac{\left(\sin\theta+(M^2-1)^{1/2}\cos\theta\right)}{M\left(1 + (\gamma-1)M^2/2\right)} - \frac{M\sin\theta}{M^2-1}\right]\right] \qquad (353)$$

$$H_2 = - H_1 \operatorname{ctn}\psi \qquad (354)$$

$$H_5 = \left((M^2-1)^{1/2}\cos\theta - \sin\theta\right)\cos\psi/M \qquad (355)$$

$$H_6 = H_5 \tan\psi \qquad (356)$$

$$H_7 = H_6/r \qquad (357)$$

Equations (349) and (352) are two partial differential equations which are valid on optimal control surfaces and contain derivatives of only the Mach number M and the polar angle ψ. The nature of these two first order, quasi-linear, partial differential equations, Eqs. (349) and (352), can be determined by putting them into a form for a solution by the method of characteristics.

The equations to determine the values of the characteristic directions of Eqs. (349) and (352) are as follows:

$$\sigma_1\left[D_8\frac{\partial M}{\partial r} + D_9\frac{\partial M}{r\partial\phi} + D_5\frac{\partial\psi}{\partial r} + D_6\frac{\partial\psi}{r\partial\phi} + D_7\right] = 0 \tag{358}$$

$$\sigma_2\left[H_1\frac{\partial M}{\partial r} + H_2\frac{\partial M}{r\partial\phi} + H_5\frac{\partial\psi}{\partial r} + H_6\frac{\partial\psi}{r\partial\phi} + H_7\right] = 0 \tag{359}$$

where σ_1 and σ_2 are unknown functions. Adding these two equations and rearranging yields the following equation:

$$(\sigma_1 D_8 + \sigma_2 H_1)\left[\frac{\partial M}{\partial r} + \frac{(\sigma_1 D_9 + \sigma_2 H_2)}{(\sigma_1 D_8 + \sigma_2 H_1)}\frac{\partial M}{r\partial\phi}\right]$$

$$+ (\sigma_1 D_5 + \sigma_2 H_5)\left[\frac{\partial\psi}{\partial r} + \frac{(\sigma_1 D_6 + \sigma_2 H_6)}{(\sigma_1 D_5 + \sigma_2 H_5)}\frac{\partial\psi}{r\partial\phi}\right] + (\sigma_1 D_7 + \sigma_2 H_7) = 0 \tag{360}$$

where the coefficients of the partial derivatives in the r direction of M and ψ have been factored out.

In order to consider Eq. (360) as a directional derivative in a direction in which the partial derivatives of M and ψ both combine to yield total derivatives of M and ψ, the coefficients of the partial derivatives with respect to ϕ must both be set equal to the slope of the desired direction. The slope of the desired direction or characteristic curve is denoted by λ. Thus,

$$\lambda = \frac{r\,d\phi}{dr} = \frac{(\sigma_1 D_9 + \sigma_2 H_2)}{(\sigma_1 D_8 + \sigma_2 H_1)} = \frac{(\sigma_1 D_6 + \sigma_2 H_6)}{(\sigma_1 D_5 + \sigma_2 H_5)} \tag{361}$$

Since M and ψ are assumed to be continuous functions, the following relationships are valid:

$$\frac{dM}{dr} = \frac{\partial M}{\partial r} + \lambda \frac{\partial M}{r\partial \phi} \tag{362}$$

$$\frac{d\psi}{dr} = \frac{\partial \psi}{\partial r} + \lambda \frac{\partial \psi}{r\partial \phi} \tag{363}$$

In view of Eqs. (361) through (363), Eq. (360) becomes

$$(\sigma_1 D_8 + \sigma_2 H_1)dM + (\sigma_1 D_5 + \sigma_2 H_5)d\psi + (\sigma_1 D_7 + \sigma_2 H_7)dr = 0 \tag{364}$$

Equation (364) is a total derivative relationship, called the compatibility equation, which is valid along the characteristic direction λ given by Eq. (361). It remains to eliminate the parameters σ_1 and σ_2 from Eq. (361).

Equation (361) can be considered as two equations for the two unknowns σ_1 and σ_2. These two equations may be written as follows:

$$(D_8\lambda - D_9)\sigma_1 + (H_1\lambda - H_2)\sigma_2 = 0 \tag{365}$$

$$(D_5\lambda - D_6)\sigma_1 + (H_5\lambda - H_6)\sigma_2 = 0 \tag{366}$$

For Eqs. (365) and (366) to have any solution for σ_1 and σ_2 other than the trivial solution, $\sigma_1 = \sigma_2 = 0$, the determinant of the coefficients of σ_1 and σ_2 in Eqs. (365) and (366) must vanish. The following quadratic equation for λ results from setting the determinant equal to zero:

$$(D_8H_5 - D_5H_1)\lambda^2 + (D_5H_2 - D_8H_6 + D_6H_1 - D_9H_5)\lambda + (D_9H_6 - D_6H_2) = 0 \tag{367}$$

Solving Eq. (367) yields the following expression for λ:

$$\lambda_{I,II} = \frac{-c_2 \pm (c_2^2 - 4c_1c_3)^{1/2}}{2c_1} \tag{368}$$

where

$$c_1 = D_8H_5 - D_5H_1 \tag{369}$$

$$c_2 = D_5H_2 - D_8H_6 + D_6H_1 - D_9H_5 \tag{370}$$

$$c_3 = D_9H_6 - D_6H_2 \tag{371}$$

Equation (368) yields two results for λ, denoted by the subscripts I and II corresponding to the positive and negative signs respectively. As discussed in (22), if $c_2^2 - 4c_1c_3 < 0$, then no real solutions for λ exist, and the characteristic curves (directions) are imaginary. Differential equations that result in imaginary characteristics are called elliptic. If $c_2^2 - 4c_1c_3 = 0$, one real characteristic direction exists through each point on the solution surface, and the system of equations is called parabolic. If $c_2^2 - 4c_1c_3 > 0$, two real characteristic directions exist through each point, and the system is called hyperbolic.

The magnitudes of the coefficients c_1, c_2 and c_3 depend on the values of $r(\phi)$, $M(r,\phi)$, $\theta(r,\phi)$ and $\psi(r,\phi)$ on the control surface. At this point, the procedure presented in Appendix J was used to construct a number of initial value lines in the supersonic, homentropic, isoenergetic, three-dimensional flow of a perfect gas. The values of r, M and ψ along these lines were substituted into the equations for D_5, D_6, D_7, D_8, D_9, H_1, H_2, H_5, H_6 and H_7, and the coefficients c_1, c_2 and c_3 were evaluated using Eqs. (369) through (371). In all cases the quantity $c_2^2 - 4c_1c_3$ was positive. Therefore, the set of equations, Eqs. (348), (349) and (352), were assumed to be hyperbolic, and a numerical solution technique based on that assumption was written. The assumption that the set of equations is hyperbolic is checked at every calculational point on the solution surface since λ_I and λ_{II} are calculated at each mesh point by using Eq. (368).

Before the numerical solution is presented, a form of Eq. (364) is derived which does not contain the parameters σ_1 and σ_2. Equation (365) can be solved for σ_2/σ_1 to yield the following equation:

$$\sigma_2/\sigma_1 = -(D_8\lambda - D_9)/(H_1\lambda - H_2) \tag{372}$$

Substituting Eq. (335) into Eq. (364) yields the following result:

$$\left[D_8 - H_1\frac{(D_8\lambda - D_9)}{(H_1\lambda - H_2)}\right]dM + \left[D_5 + H_5\frac{(D_8\lambda - D_9)}{(H_1\lambda - H_2)}\right]d\psi + \left[D_7 + H_7\frac{(D_8 - D_9)}{(H_1 - H_2)}\right]dr = 0 \tag{373}$$

In summary, Eq. (368) defines curves in the $r\phi$-plane along which Eq. (373) is valid. At each point in the $r\phi$-plane there are two

characteristic directions, one with slope $rd\phi/dr = \lambda_I$ and one with slope $rd\phi/dr = \lambda_{II}$. Along the curve with slope λ_I, Eq. (373) is valid with $\lambda = \lambda_I$, and along the curve with slope λ_{II}, Eq. (373) is valid with $\lambda = \lambda_{II}$. Equations (368) and (373) are highly non-linear, total differential equations that can be solved by a finite difference technique.

2. NUMERICAL SOLUTION

It has been noted that Eq. (368) defines two curves through each point on the solution surface, and Eq. (373) specifies one relationship between M and ψ on each curve. In order to obtain two independent relationships between M and ψ at a point, a network can be devised wherein the two families of characteristic curves intersect at a point so that a single relationship between M and ψ on each of the two characteristic curves results in two relationships between M and ψ at the point of intersection. Equation (348) can then be used to solve for the value of θ at the point of intersection. A finite difference solution technique for an interior point on the control surface will now be developed.

An interior point is a point on the solution surface where data at two points (points 1 and 2) can be used to solve for the properties and location of the point determined by the intersection of the characteristic curves through the two known points (point 3). Figures 41a and 41b illustrate the physical situation. Writing Eqs. (368) and (373) for the geometry of Figure 41b yields the following four differential equations:

$$r_I d\phi_I = \lambda_I dr_I \tag{374}$$

$$r_{II} d\phi_{II} = \lambda_{II} dr_{II} \tag{375}$$

$$A'_I dM_I + B'_I d\psi_I + C'_I dr_I = 0 \tag{376}$$

$$A'_{II} dM_{II} + B'_{II} d\psi_{II} + C'_{II} dr_{II} = 0 \tag{377}$$

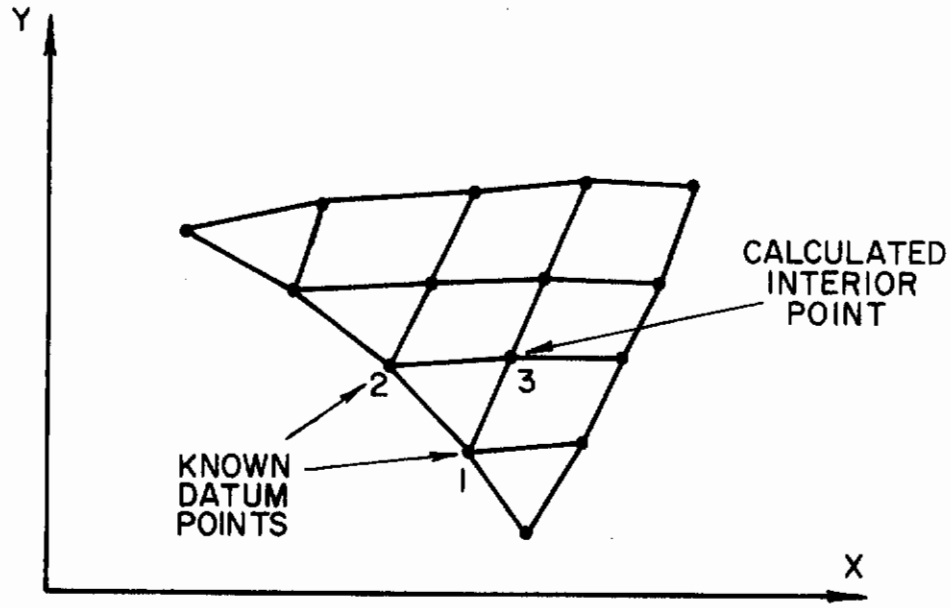

A) MESH POINTS

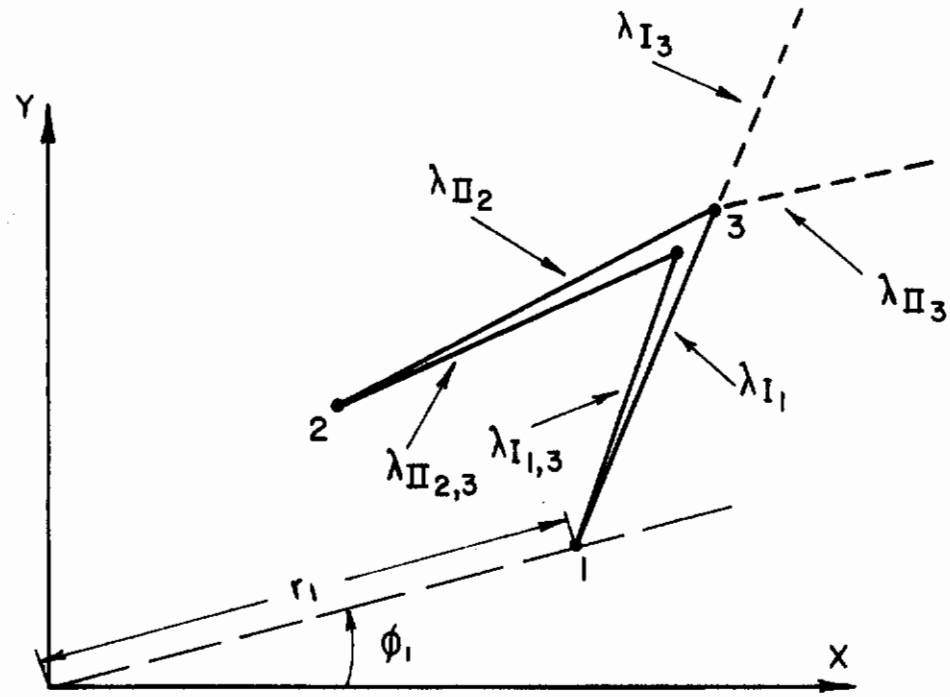

B) UNIT PROCESS

FIGURE 41. MESH POINT NETWORK

where

$$A' = \left[D_1 + H_1 \frac{(D_8\lambda - D_9)}{(H_1\lambda - H_2)}\right] \tag{378}$$

$$B' = \left[D_5 + H_5 \frac{(D_8\lambda - D_9)}{(H_1\lambda - H_2)}\right] \tag{379}$$

and

$$C' = \left[D_7 + H_7 \frac{(D_8\lambda - D_9)}{(H_1\lambda - H_2)}\right] \tag{380}$$

In Eqs. (374) through (377) the differentials are replaced by finite differences resulting in the following algebraic equations:

$$r_I(\phi_3 - \phi_1) = \lambda_I(r_3 - r_1) \tag{381}$$

$$r_{II}(\phi_3 - \phi_2) = \lambda_{II}(r_3 - r_2) \tag{382}$$

$$A'_I(M_3 - M_1) + B'_I(\psi_3 - \psi_1) + C'_I(r_3 - r_1) = 0 \tag{383}$$

$$A'_{II}(M_3 - M_2) + B'_{II}(\psi_3 - \psi_2) + C'_{II}(r_3 - r_2) = 0 \tag{384}$$

There are five unknowns in the above four equations: r_3, ϕ_3, M_3, θ_3 and ψ_3. The value of θ_3 appears in the expressions for A'_I, A'_{II}, B'_I, B'_{II}, C'_I and C'_{II} and the expressions for λ_I and λ_{II}. Thus, an additional equation is needed which will allow one to solve for θ_3 if M_3 is known. Equation (348) can be written in finite difference form and used for this purpose; however, there is a more convenient relationship which can be used. Equation (331) can be rearranged and rewritten in the following form:

$$\theta = \mu \pm \cos^{-1}\left[\left(\frac{-\lambda_2}{a_o}\right)\left(\frac{M^2-1}{M^2}\right)\left(1 + \frac{\gamma-1}{2} M^2\right)^{1/2}\right] \tag{385}$$

where if $\theta > \mu$, the positive sign is correct, and if $\theta < \mu$, the negative sign is correct. Equations (381) through (385) can be solved for the properties and location of point 3 if the points 1 and 2 are known. For a first estimate, all the coefficients in the equations must be evaluated

at the initial points 1 and 2. This results in the classical Euler scheme. Thus,

$$\lambda_I = \lambda_{I_1} \tag{386}$$

$$\lambda_{II} = \lambda_{II_2} \tag{387}$$

$$A'_I = A'_{I_1} \tag{388}$$

$$A'_{II} = A'_{II_2} \tag{389}$$

etc.

Equations (381) and (382) can be solved to yield the equations

$$\phi_3 = \frac{\left(\lambda_{II_2}\lambda_{I_1}(r_1 - r_2) + \lambda_{I_1} r_2\phi_2 - \lambda_{II_2} r_1\phi_1\right)}{\left(\lambda_{I_1} r_2 - \lambda_{II_2} r_1\right)} \tag{390}$$

$$r_3 = r_2 + r_2(\phi_3 - \phi_2)/\lambda_{II_2} \tag{391}$$

which give a first estimate on the location of point 3. Equations (383) and (384) can be solved to yield the equations

$$M_3 = \left(A'_{I_1} B'_{II_2} M_1 - A'_{II_2} B'_{I_1} M_2 + B'_{I_1} B'_{II_2}(\psi_1 - \psi_2)\right.$$

$$\left. + B'_{II_2} C'_{I_1}(r_1 - r_3) + B'_{I_1} C'_{II_2}(r_3 - r_2)\right)/(A'_{I_1} B'_{II_2} - A'_{II_2} B'_{I_1}) \tag{392}$$

and

$$\psi_3 = \left(C'_{I_1}(r_1 - r_3) + A'_{I_1}(M_1 - M_3) + B'_{I_1}\psi_1\right)/B'_{I_1} \tag{393}$$

which can be used to determine a first estimate on M_3 and ψ_3 since first estimates of r_3 and ϕ_3 have been determined.

Equation (385) can then be used to calculate θ_3 by using the first estimate of M_3 if it is known that $\theta_3 > \mu_3$ or that $\theta_3 < \mu_3$. If doubt exists about which is the case, then another approach is used. Such a

doubt exists when μ_1 is very close to the value of θ_1 and μ_2 is very close to being equal to θ_2. For the case of θ_3 approximately equal to μ_3, Eq. (348) can not be used to solve for θ_3 when given M_3 since $d\theta/dM$ approaches infinity as μ_3 approaches θ_3.

The procedure that is used in this case is to switch to using θ and ψ as the dependent variables in the two partial differential equations; Eqs. (349) and (352) can be rewritten as follows:

$$D_{10}\frac{\partial\theta}{\partial r} + D_{11}\frac{\partial\theta}{r\partial\phi} + D_5\frac{\partial\psi}{\partial r} + D_6\frac{\partial\psi}{r\partial\phi} + D_7 = 0 \qquad (394)$$

$$H_{10}\frac{\partial\theta}{\partial r} + H_{11}\frac{\partial\theta}{r\partial\phi} + H_5\frac{\partial\psi}{\partial r} + H_6\frac{\partial\psi}{r\partial\phi} + H_7 = 0 \qquad (395)$$

where

$$D_{10} = D_8(dM/d\theta) \qquad (396)$$

$$D_{11} = D_9(dM/d\theta) \qquad (397)$$

$$H_{10} = H_1(dM/d\theta) \qquad (398)$$

$$H_{11} = H_2(dM/d\theta) \qquad (399)$$

and $dM/d\theta$ is given by Eq. (348). Equations (394) and (395) can be numerically solved in a manner analogous to the solution of Eqs. (349) and (352). Once θ_3 has been estimated, then Eq. (348) can be iteratively solved for M_3. Since the iterative solution of Eq. (348) for M_3 when given θ_3 is not as straightforward as using Eq. (385) to solve for θ_3 given M_3, Eqs. (349), (352) and (385) are used whenever possible.

Once the location and properties at point 3 have been determined based on the Euler scheme, improved values of these parameters can be obtained by evaluating the coefficients of the finite difference equations, Eqs. (381) through (384), using average values of the properties. Such a technique is known as a modified Euler scheme, and its use results in greater accuracy than the standard Euler scheme. Thus, for subsequent trials,

$$\lambda_I = \lambda_{I_{1,3}}(M_{1,3}, \theta_{1,3}, \psi_{1,3}, r_{1,3}) \tag{400}$$

$$\lambda_{II} = \lambda_{II_{2,3}}(M_{2,3}, \theta_{2,3}, \psi_{2,3}, r_{2,3}) \tag{401}$$

$$A'_I = A'_{I_{1,3}}(M_{1,3}, \theta_{1,3}, \psi_{1,3}, r_{1,3}) \tag{402}$$

$$A'_{II} = A'_{II_{2,3}}(M_{2,3}, \theta_{2,3}, \psi_{2,3}, r_{2,3}) \tag{403}$$

where

$$M_{1,3} = (M_1 + M_3)/2 \tag{404}$$

$$M_{2,3} = (M_2 + M_3)/2 \tag{405}$$

etc.

Thus, with the modified Euler scheme, on each succeeding iteration

$$\phi_3 = \frac{(\lambda_I\lambda_{II}(r_2 - r_1) + \lambda_{II}r_{1,2}\phi_1 - \lambda_I r_{2,3}\phi_2)}{(\lambda_{II}r_{1,3} - \lambda_I r_{1,2})} \tag{406}$$

$$r_3 = r_2 + r_{1,2}(\phi_3 - \phi_2)/\lambda_{II} \tag{407}$$

and Eqs. (392) and (393) are combined with Eqs. (400) through (405).

This scheme is repeated as many times as necessary to obtain a desired degree of convergence. Checks for convergence on iteration step (n + 1) are made by checking to see that both of the following conditions are satisfied:

$$\left|(M_3)_{n+1} - (M_3)_n\right| \leq \text{specified value} \tag{408}$$

$$\left|(\psi_3)_{n+1} - (\psi_3)_n\right| \leq \text{specified value} \tag{409}$$

The values of M, θ and ψ for the entire optimal control surface are calculated by repetitively applying the above numerical solution. Figure 42 illustrates the network of mesh points used in the solution technique. The initial value line (J = 1 solution front) is divided into an appropriate number of points (45 points at 2° increments is a practical number; the figure shows 10 points), and then the numerical solution is advanced to the J = 2 solution front. Figure 42 illustrates a case with two planes of symmetry, and thus two mesh points on the J = 2 solution front must be reflected across the planes of symmetry. The solution technique is continued until the optimal exit lip of the nozzle is sure to lie entirely inside the last solution front (fifty solution fronts are generally sufficient). The solution for the optimal exit lip is discussed in Appendix L.

Once the solution for M, θ, ψ, r and ϕ is complete, the value of the function f at each mesh point can be determined by applying Eq. (337) in the following finite difference form:

$$f_2 = f_1 - (r_2-r_1)\left(\tan(\theta+\mu+\pi/2)\cos\psi\right)\Big|_{\text{average}} - \frac{(r_1+r_2)}{2}(\phi_2-\phi_1)\left(\tan(\theta+\mu+\pi/2)\sin\psi\right)\Big|_{\text{average}} \qquad (410)$$

Equation (410) is applied between point 1 where θ, μ, ψ, f, r and ϕ are known and point 2 where θ, μ, ψ, r and ϕ are known but f is unknown. Equation (410) is applied repetitively between mesh points until f is known at all the previously calculated mesh points.

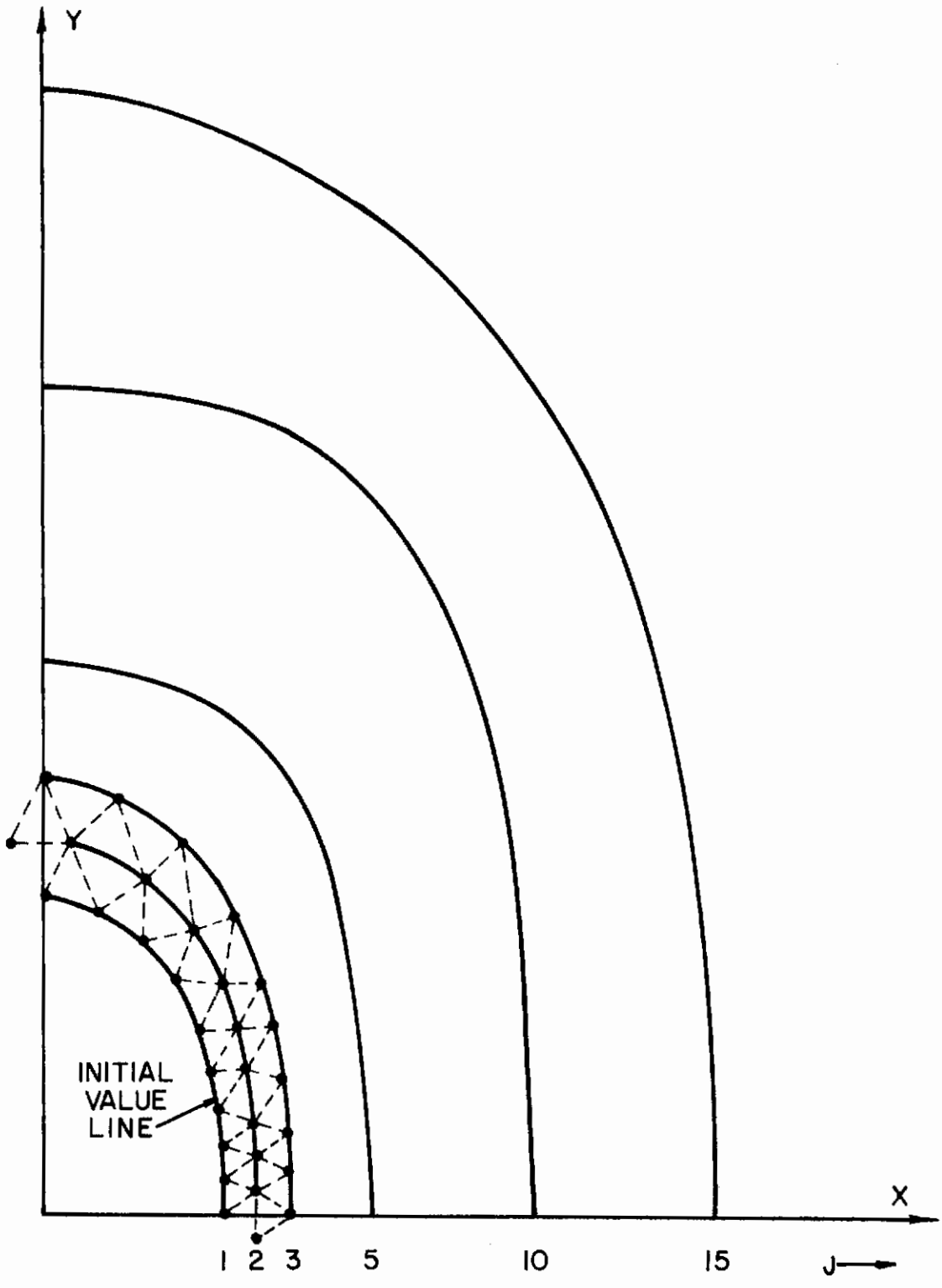

FIGURE 42. OVERALL MESH POINT NETWORK

APPENDIX L
DETAILS OF THE CONSTRUCTION OF OPTIMAL NOZZLE EXIT LIPS

It has been shown that for a particular initial value line a corresponding solution for $V(r,\phi)$, $\theta(r,\phi)$, $\psi(r,\phi)$ and $f(r,\phi)$ can be numerically determined. In this appendix the conditions which define the exit lip of a maximum thrust, fixed length, three-dimensional nozzle are presented. Also, the solution procedure which is used to satisfy these conditions and determine the optimal exit lip for a given initial value line and optimal control surface is described.

1. EQUATIONS WHICH DEFINE AN OPTIMAL EXIT LIP

Two conditions are satisfied by the optimal exit lip which lies on the optimal control surface of a maximum thrust, three-dimensional, supersonic nozzle designed for the restrictions of constant mass flow rate and fixed length. First, the transversality equation derived in Appendix F is satisfied along the exit lip, and second, the exit lip is positioned on the optimal control surface such that the mass flow rate across the control surface satisfies the mass flow rate constraint.

The transversality equation for a maximum thrust, fixed length, constant mass flow rate nozzle is as follows:

$$\left((p-p_a) + \rho V^2 \sin\theta \tan\mu\left(-\cos\theta + \frac{\sin\theta\sin\psi}{r_e}\frac{df_e}{d\phi_e}\right)\right)\Bigg|_{\Gamma_e} = 0 \qquad (411)$$

This equation is satisfied by the variables $p_e(\phi)$, $\rho_e(\phi)$, $V_e(\phi)$, $\theta_e(\phi)$, $\psi_e(\phi)$, $f_e(\phi)$ and $r_e(\phi)$ at all points on an optimal exit lip. The ambient pressure p_a in Eq. (411) is a constant. Since the overall design procedure is based on designing the optimal nozzle for a known kernel and initial value line, the value of p_a for which the nozzle is an optimal

nozzle is part of the solution. The method used to satisfy Eq. (411) is discussed in the next section.

On a plane of symmetry of an optimal control surface $\psi \equiv 0$ and the transversality equation, Eq. (411), reduces to the following form:

$$\left((p-p_a) - \rho V^2 \sin\theta\cos\theta\tan\mu\right)\Big|_{\Gamma_e} = 0 \tag{412}$$

Thus, at the point that an optimal exit lip crosses a plane of symmetry of the control surface, Eq. (412) is valid.

If $\psi_e \neq 0$ and $\theta_e \neq 0$ along the optimal exit lip, Eq. (411) can be rewritten in the following form:

$$\frac{df_e}{r_e d\phi_e} = \left.\left(\frac{\rho V^2 \sin\theta\cos\theta\tan\mu - (p-p_a)}{\rho V^2 \sin^2\theta\tan\mu\sin\psi}\right)\right|_{\Gamma_e} \tag{413}$$

It is in this form that the transversality equation is applied to solve for the optimal exit lip.

Not only is an optimal exit lip located on a control surface such that Eq. (413) is satisfied along Γ_e, but also the mass flow rate across the portion of the control surface bounded by the initial value line and the exit lip is equal to the total mass flow rate through the nozzle minus that portion of the mass flow rate which passes interior to the initial value line. The total mass flow rate $\dot{m}_T$ is known since the conditions on the starting surface are known. The mass flow rate $\dot{m}_{IVL}$ which passes interior to the initial value line is known since the position of the initial value line and the flow conditions in the kernel are known. Therefore, the following condition must be satisfied by the optimal exit lip:

$$\dot{m}_{c.s.} = \dot{m}_T - \dot{m}_{IVL} \tag{414}$$

where

$$\dot{m}_{c.s.} = \int_0^{2\pi} \int_{r_i(\phi)}^{r_e(\phi)} r\rho V \sin\mu/\sin(\theta + \mu)\, dr d\phi \tag{415}$$

The design procedure to satisfy Eqs. (413) and (414) is now presented.

2. DESCRIPTION OF THE DESIGN PROCEDURE

At this point in the numerical solution, the values of $V(r,\phi)$, $\theta(r,\phi)$, $\psi(r,\phi)$ and $f(r,\phi)$ are known on the optimal control surface out to some radius which is greater than the unknown exit lip radius $r_e(\phi)$. The design procedure for determining the position of the optimal exit lip (and therefore, $r_e(\phi)$, $V_e(\phi)$, $\theta_e(\phi)$, $\psi_e(\phi)$ and $f_e(\phi)$) is an iterative type of solution and consists of the following steps:

1) In the $\phi = 0°$ plane (or some other suitable plane) choose an initial point Q which is on the previously determined optimal control surface and is assumed to lie on the exit lip.
2) Choose a reasonable initial value for the ambient pressure p_a.
3) Solve for $f_e(\phi)$ using Eq. (323) in finite difference form.
4) Through an iterative process adjust the value of p_a such that the calculations in step 3 yield a closed curve for the exit lip Γ_e.
5) Determine the mass flow rate across the portion of the optimal control surface bounded by the initial value line and the generated nozzle exit lip.
6) Adjust the position of the point Q chosen in step 1 to satisfy the mass flow constraint, Eq. (414).
7) Repeat steps 2 through 6 until the mass flow rate across the control surface is equal to the required value.

Each step is now explained in more detail.

The first step is to choose some initial point Q on the given control surface. This initial point should be at a radius such that it is a reasonable choice of a point which could lie on the exit lip. Some idea of where to choose Q can come from using Eq. (415) to calculate the mass flow rate which crosses the portion of the optimal control surface bounded by the initial value line and successive solution fronts (see Appendix K); however, in general the solution fronts on the control surface do not correspond to optimal exit lips.

In step 2 a value of p_a is selected so that Eq. (413) can be used to solve for a possible optimal exit lip shape. Unless the initial point Q lies on a plane of symmetry of the optimal control surface, there is no way to determine the correct value of p_a to select. If point Q does lie on a plane of symmetry, then Eq. (412) is used to determine the proper value of p_a to use in Eq. (413).

Once a point Q has been selected and its corresponding p_a value has been selected (or calculated), then Eq. (413) is applied in the following finite difference form to solve for the shape of a possible optimal exit lip:

$$f_2 = f_1 + \left[\frac{r\rho V^2 \sin\theta\cos\theta\tan\mu - r(p-p_a)}{\rho V^2 \sin^2\theta\tan\mu\sin\psi}\right]_{\text{average}} (\phi_2 - \phi_1) \qquad (416)$$

where the exit lip must be a curve on the calculated control surface. The solution of Eq. (416) on an optimal control surface is an iterative process. The position of point 1 is known, and hence, the conditions at point 1 are also known. The value of ϕ_2 is selected so that $(\phi_2 - \phi_1)$ is such that Eq. (416) is an accurate approximation of Eq. (413) ($(\phi_2 - \phi_1) = 2°$ has been found to be suitable). Then the value of f_2 is varied until Eq. (416) is satisfied. This process is applied repetitively for $0° \leq \phi \leq 360°$.

Unless the proper value of p_a at point Q was chosen, the curve which results from step 3 is not a closed curve. In this case, step 4 consists of adjusting the value of p_a at point Q and repeating step 3 until a closed curve is obtained. If point Q is on a plane of symmetry so that Eq. (412) was used to evaluate p_a, a closed curve results from step 3, and no iteration is necessary in step 4.

Not only is the exit lip of an optimal nozzle a closed curve along which Eq. (416) is satisfied, but the exit lip also satisfies Eqs. (414) and (415). The values of $\dot{m}_T$ and $\dot{m}_{IVL}$ are known, and $\dot{m}_{c.s.}$ is determined by numerically integrating Eq. (415) over the control surface using the exit lip calculated in steps 4 and 5 as the outer boundary. In general, the value of $\dot{m}_{c.s.}$ corresponding to the generated exit lip does not satisfy Eq. (414).

If $\dot{m}_{c.s.}$ is such that $\dot{m}_{c.s.} < (\dot{m}_T - \dot{m}_{IVL})$, then the position of the point Q selected in step 1 is moved radially outward some distance, and steps 2 through 6 are repeated until $\dot{m}_{c.s.}$ is the required value. If $\dot{m}_{c.s.} > (\dot{m}_T - \dot{m}_{IVL})$, then the initial point is moved radially inward and steps 2 through 6 are repeated. The entire iteration procedure is complete when a closed curve on the control surface along which Eq. (416) is satisfied and p_a is a constant is found for which $\dot{m}_{c.s.}$ satisfies Eq. (414).

The results for a typical optimal nozzle with two planes of symmetry are shown in Figure 43. The data along the initial value line and the 49 solution fronts are known at the start of the solution for the corresponding optimal exit lip. The first choice of point Q, Q_1, yields an exit lip for which $\dot{m}_{c.s.} > (\dot{m}_T - \dot{m}_{IVL})$ while the first correction point, point Q_2, yields an exit lip for which $\dot{m}_{c.s.} < (\dot{m}_T - \dot{m}_{IVL})$. The final exit lip shape satisfies the mass flow rate constraint as well as satisfying Eq. (416).

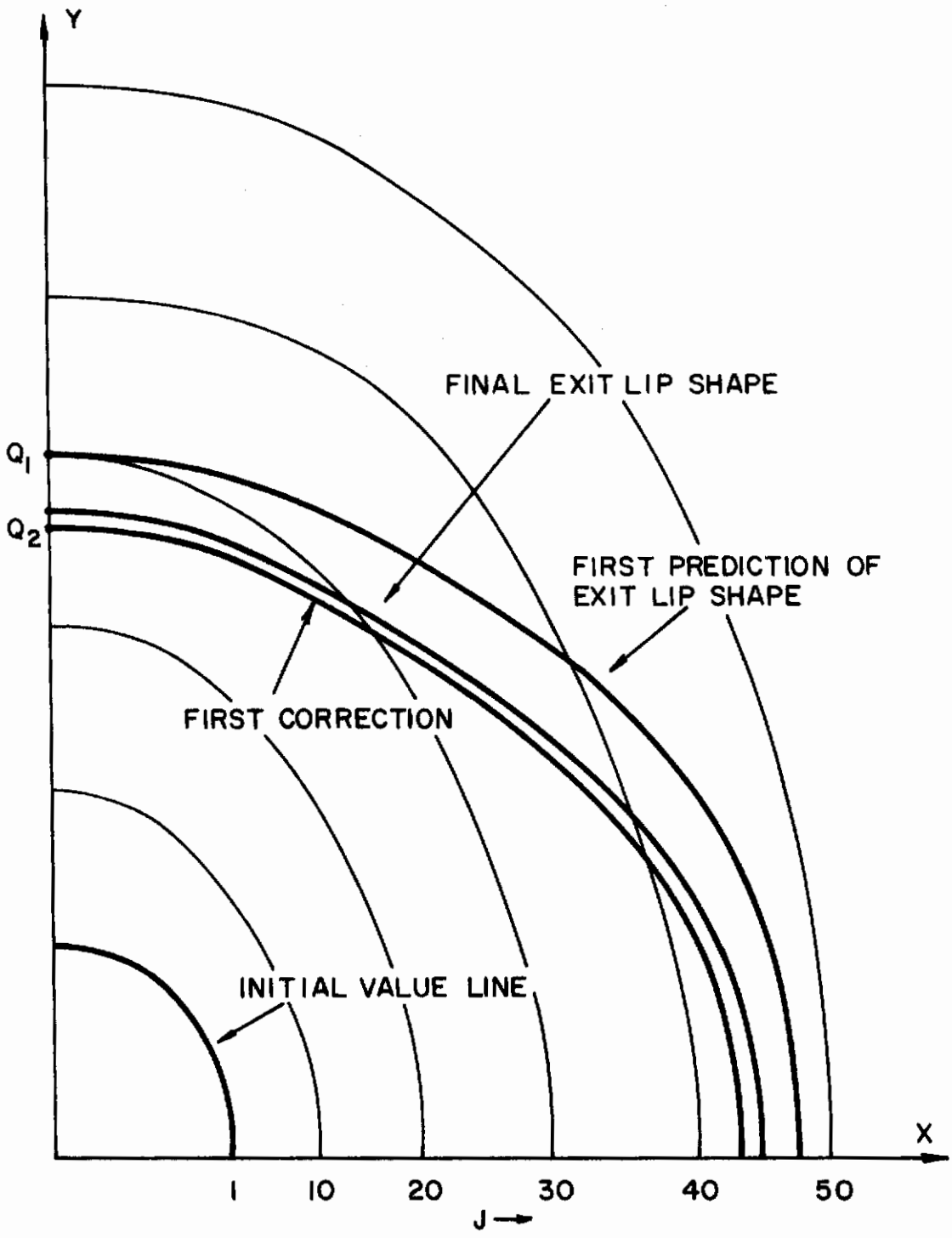

FIGURE 43. SOLUTION FOR OPTIMAL EXIT LIP

LIST OF REFERENCES

1. Guderley, G. and Hantsch, E., "Beste Formen fur Achsensymmetrische Ubershallschubdusen," Zeitschrift fur Flugwissenschaften, Vol. 3, 1955, pp. 305-313.

2. Rao, G. V. R., "Exhaust Nozzle Contour for Optimum Thrust," Jet Propulsion, Vol. 28, 1958, pp. 377-382.

3. Guderley, G., "On Rao's Method for Computation of Exhaust Nozzles," Zeitschrift fur Flugwissenschaften, Vol. 7, 1959, pp. 345-350.

4. Guderley, K. G. and Armitage, J. V., "A General Method for the Determination of Best Supersonic Rocket Nozzles," Paper presented at the Symposium on Extremal Problems in Aerodynamics, Boeing Scientific Research Laboratories, Seattle, Washington, December 3-4, 1962.

5. Guderley, K. G. and Armitage, J. V., "General Approach to Optimum Rocket Nozzles," Chap. 11, Theory of Optimum Aerodynamic Shapes, edited by Angelo Miele, Academic Press, New York, 1965.

6. Hoffman, J. D., "A General Method for Determining Optimum Thrust Nozzle Contours for Chemically Reacting Gas Flows," AIAA Journal, Vol. 5, No. 4, April 1967, pp. 670-676.

7. Scofield, M. P., Thompson, H. D. and Hoffman, J. D., "Thrust Nozzle Optimization Including Boundary Layer Effects," Air Force Aero Propulsion Laboratory, Wright-Patterson Air Force Base, Technical Report No. AFAPL-TR-67-158, December 1967.

8. Hoffman, J. D., Scofield, M. P. and Thompson, H. D., "Thrust Nozzle Optimization for Nonequilibrium, Chemically Reacting Flows Including Boundary Layer Effects," Air Force Aero Propulsion Laboratory, Wright-Patterson Air Force Base, Technical Report No. AFAPL-TR-69-49, April 1969.

9. Scofield, M. P., and Hoffman, J. D., "Maximum Thrust Nozzles for Rotational or Nonequilibrium Simple Dissociating Gas Flows Including Boundary Layer Effects," Air Force Aero Propulsion Laboratory, Wright-Patterson Air Force Base, Technical Report No. AFAPL-TR-69-85, October 1969.

10. Rao, G. V. R., "Spike Nozzle Contour for Optimum Thrust," Ballistic Missile and Space Technology, Vol. II, edited by C. W. Morrow, Pergamon Press, New York, 1961, pp. 92-101.

11. Humphreys, R. P., Thompson, H. D., and Hoffman, J. D., "Design of Maximum Thrust Plug Nozzles for Fixed Inlet Geometry," Air Force Aero Propulsion Laboratory, Wright-Patterson Air Force Base, Technical Report No. AFAPL-TR-70-47, June 1970.

12. Johnson, G. R., "Design of Maximum Thrust Plug Nozzles for Variable Inlet Geometry," Ph.D. Thesis, Purdue University, January 1971.

13. Thompson, H. D., and Murthy, S. N. B., "Design of Optimized Three-Dimensional Thrust Nozzle Contours," Jet Propulsion Center, Purdue University, Report No. TM-65-2, March 1965.

14. Borisov, V. M., "Variational Problem on Three-Dimensional Supersonic Flows," PPM, Vol. 29, No. 1, 1965, pp. 106-113.

15. Ransom, V. H., Hoffman, J. D., and Thompson, H. D., "A Second-Order Numerical Method of Characteristics for Three-Dimensional Supersonic Flow, Volume I, Theoretical Development and Results," Air Force Aero Propulsion Laboratory, Wright-Patterson Air Force Base, Technical Report No. AFAPL-TR-69-98, Vol. I, October 1969.

16. von Mises, R., Mathematical Theory of Compressible Fluid Flow, Academic Press, New York, 1958, pp 17-19 and 65-66.

17. Elsgolc, L. E., Calculus of Variations, Addison-Wesley, Reading, Mass., 1961, pp. 128-147.

18. Miele, A., "Generalized Approach to the Calculus of Variations in Two Independent Variables," Chap. 4, Theory of Optimum Aerodynamic Shapes, edited by Angelo Miele, Academic Press, New York, 1965.

19. Kaplan, W., Advanced Calculus, Addison-Wesley, Reading, Mass., 1952, p. 112.

20. Ferri, A., "The Method of Characteristics," Sec. G, General Theory of High Speed Aerodynamics, edited by W. R. Sears, Vol. VI, Princeton University Press, Princeton, N. J., 1954, pp. 642-646.

21. Williams, T. R., "A Comprehensive Report on the Computer Program for the Design of a Converging-Diverging Rocket Nozzle," TDR 0162-002, Sept. 1961, Allison Division, General Motors Corporation, Indianapolis, Indiana.

22. Courant, R. and Hilbert, D., Methods of Mathematical Physics, Volume II, Interscience Publishers, Inc., New York, 1962, pp. 170-180.

23. Ransom, V. H., Cline, M. C., Hoffman, J. D., and Thompson, H. D., "A Second-Order Numerical Method of Characteristics for Three-Dimensional Supersonic Flow, Volume II, Computer Program Manual," Air Force Aero Propulsion Laboratory, Wright-Patterson Air Force Base, Technical Report AFAPL-TR-69-98, Vol. II, January 1970.

24. Truesdell, C., "Kinematics of Vorticity," Indiana University Publications, Science Series No. 19, 1954, pp. 23-26 and 97-99.

25. Normyle, W. J., "Shuttle Poses Dominant Challenge," Aviation Week and Space Technology, Vol. 92, No. 25, June 22, 1970, pp. 96-121.

26. Shmyglevskii, Yu. D., Some Variational Problems in Gas Dynamics, Moscow, 1963.

27. Kraiko, A. N., "Variational Problems of Gas Dynamics of Nonequilibrium and Equilibrium Flows," PMM, Vol. 28, No. 2, 1964, pp. 285-295.

28. Scofield, M. P., and Hoffman, J. D., "An Analysis of Optimized Conical Thrust Nozzles," Jet Propulsion Center, Purdue University, Report No. TM-66-6, July 1966.

DOCUMENT CONTROL DATA - R & D

(Security classification of title, body of abstract and indexing annotation must be entered when the overall report is classified)

1. ORIGINATING ACTIVITY (Corporate author)
Purdue University
Lafayette, Indiana 47907

2a. REPORT SECURITY CLASSIFICATION
UNCLASSIFIED

2b. GROUP

3. REPORT TITLE
Three-Dimensional Nozzle Design For Maximum Thrust, Vol. I, Theoretical Development of Results

4. DESCRIPTIVE NOTES (Type of report and, inclusive dates)
Technical Report 1 September 1966 to

5. AUTHOR(S) (First name, middle initial, last name)
Lynn E. Snyder and H. Doyle Thompson

6. REPORT DATE	7a. TOTAL NO. OF PAGES	7b. NO. OF REFS
October 1970	179	28

8a. CONTRACT OR GRANT NO.	9a. ORIGINATOR'S REPORT NUMBER(S)
Air Force F33615-67-C-1068	
b. PROJECT NO BPSN: 7(63 301206 6205214)	
c	9b. OTHER REPORT NO(S) (Any other numbers that may be assigned this report) AFAPL-TR-70-77 , Vol. I
d	

10. DISTRIBUTION STATEMENT
This document is subject to special export controls and each transmittal to foreign governments or foreign nationals may be made only with prior approval of the Air Force Aero Propulsion Laboratory, RJT, Wright-Patterson Air Force Base, Ohio 45433.

11. SUPPLEMENTARY NOTES	12. SPONSORING MILITARY ACTIVITY
	Air Force Aero Propulsion Laboratory Air Force Systems Command Wright-Patterson Air Force Base, Ohio

13. ABSTRACT

The problem of designing three-dimensional (nonaxisymmetric) supersonic nozzles which produce the maximum axial thrust for a prescribed upstream flow field, mass flow rate, exit lip shape and position, and ambient pressure has been formulated and numerically solved. The formulation was written to consider a three-dimensional, supersonic, isoenergetic, homentropic flow of a perfect gas. The axial thrust and mass flow rate were written as integrals over a control surface which was constrained to pass through the exit lip of the nozzle. The functional to be maximized was formed by summing the integral equation for the axial thrust and the integral equation for the mass flow rate times a Lagrange multiplier. The fixed length and fixed ambient pressure constraints were imposed by substitution into the variational problem.

The set of partial differential equations and the algebraic equations which resulted from setting the first variation of the functional equal to zero were numerically solved. For a particular set of initial conditions the numerical solution technique generates the characteristic surface which passes through the exit of the resulting optimal nozzle, the position of the exit lip, the magnitude of the axial thrust, and the ambient pressure for which the nozzle is an optimal.

The numerical solution technique was programmed for the CDC 6500 computer. The results for nine sample cases are presented. The results confirm that the three-dimensional optimal nozzles designed using this technique are significantly better than other three-dimensional nozzles that have identical initial conditions and have comparable overall dimensions. Furthermore, the results show that two-dimensional or axisymmetric methods are not adequate for designing three-dimensional optimum nozzles.

14 KEY WORDS	LINK A		LINK B		LINK C	
	ROLE	WT	ROLE	WT	ROLE	WT
Scramjet Technology						
Exhaust Nozzles						
Optimum Nozzle Design						
Calculus of Variations						
Three-Dimensional Flow						